



UNIVERSITY OF  
BIRMINGHAM

MODELLING OF CATALYTIC AFTERTREATMENT OF NO<sub>x</sub>  
EMISSIONS USING HYDROCARBON AS A REDUCTANT

BOONLUE SAWATMONGKHON

A thesis submitted to  
The University of Birmingham  
for the degree of  
DOCTOR OF PHILOSOPHY

School of Mechanical Engineering  
The University of Birmingham  
December 2011

UNIVERSITY OF  
BIRMINGHAM

**University of Birmingham Research Archive**

**e-theses repository**

This unpublished thesis/dissertation is copyright of the author and/or third parties. The intellectual property rights of the author or third parties in respect of this work are as defined by The Copyright Designs and Patents Act 1988 or as modified by any successor legislation.

Any use made of information contained in this thesis/dissertation must be in accordance with that legislation and must be properly acknowledged. Further distribution or reproduction in any format is prohibited without the permission of the copyright holder.

## ABSTRACT

Hydrocarbon selective catalytic reduction (HC-SCR) is emerging as one of the most practical methods for the removal of nitrogen oxides ( $\text{NO}_x$ ) from light-duty-diesel engine exhaust gas. In order to further promote the chemical reactions of  $\text{NO}_x$ -SCR by hydrocarbons, an understanding of the HC-SCR process at the molecular level is necessary. In the present work, a novel surface-reaction mechanism for HC-SCR is set up with emphasis on microkinetic analysis aiming to investigate the chemical behaviour during the process at a molecular level via detailed elementary reaction steps. Propane ( $\text{C}_3\text{H}_8$ ) is chosen as the reductant of HC-SCR. The simulation is designed for a single channel of a monolith, typical for automotive catalytic converters, coated with a silver alumina catalyst ( $\text{Ag}/\text{Al}_2\text{O}_3$ ). The complicated physical and chemical details occurring in the catalytic converter are investigated by using the numerical method of computational fluid dynamics (CFD) coupled with the mechanism. The  $\text{C}_3\text{H}_8$ -SCR reaction mechanism consists of 94 elementary reactions, 24 gas-phase species and 24 adsorbed surface species. The mechanism is optimised by tuning some important reaction parameters against some measurable data from experiments. The optimised mechanism then is validated with another set of experimental data. The numerical simulation shows good agreements between the modelling and the experimental data. Finally, the numerical modelling also provides information that is difficult to measure for example, gas-phase concentration distribution, temperature profiles, wall temperatures and the occupation of adsorbed species on catalyst surface. Consequently, computational modelling can be used as an effective tool to design and/or optimise the catalytic exhaust aftertreatment system.

*“Dedicated to my parents and to my teachers”*

## **ACKNOWLEDGEMENTS**

This thesis would not have been possible without the help, support and contribution of a number of individuals, who I believe deserve special mention and acknowledgement. It is my pleasure to thank them.

I would like to express my sincerest gratitude to my supervisor, Dr Athanasios Tsolakis, for his invaluable advice and guidance throughout the duration of this research. I also thank my co-supervisor, Professor Mirosław L. Wyszynski, for his leadership and knowledge.

I gratefully thank the Royal Thai government for the provision of the Ph.D. scholarship and maintenance grant for the duration of my study at the University of Birmingham, UK.

I am grateful to Dr. Andrew York, Dr. Raj Rajaram, Paul Millington, Mehrdad Ahmadinejad and Paul Collier from Johnson Matthey Technology Centre, Reading, UK, for their useful suggestions, advice and technical expertise.

I am indebted to my many colleagues who have been supportive of my work, namely, Dr. Dale Turner, Dr. Juan Jose Rodríguez-Fernández, Dr. Paul Rounce, Mr. Perry Leung, Dr. Sathaporn Chuepeng and Dr. Simbarashe Sitshebo. A special thank you goes to Dr. Kampanart Theinnoi, whose help and a contribution throughout my study.

Lastly, I would like to thank Associate Professor Dr. Ekachai Juntasaro for his support and encouragement throughout the course of my study.

Boonlue Sawatmongkhon  
December 2011

# TABLE OF CONTENTS

<b>CHAPTER 1 INTRODUCTION.....</b>	<b>1</b>
1.1 Background.....	5
1.2 Objectives and Approaches.....	9
1.3 Thesis Outline .....	10
<b>CHAPTER 2 LITERATURE REVIEW .....</b>	<b>13</b>
2.1 NO <sub>x</sub> from Diesel Engines .....	13
2.2 NO <sub>x</sub> Emissions Control Technologies.....	14
2.2.1 NO <sub>x</sub> Storage Catalyst .....	15
2.2.2 Selective Catalytic Reduction of NO <sub>x</sub> .....	17
2.3 Reductants for Selective Catalytic Reduction of NO <sub>x</sub> .....	18
2.3.1 Ammonia and Urea.....	18
2.3.2 Oxygenated Hydrocarbon.....	20
2.3.3 Hydrocarbon .....	21
2.4 Catalysts for Selective Catalytic Reduction of NO <sub>x</sub> .....	23
2.5 Promotion Effect of Hydrogen on Hydrocarbon-SCR.....	26
2.6 Modelling Approaches .....	30
2.7 Microkinetic Analysis.....	33
2.8 Summary .....	35
<b>CHAPTER 3 EXPERIMENTAL FACILITIES.....</b>	<b>37</b>
3.1 SCR Monolithic Catalyst .....	37
3.2 Experimental Setup.....	38
3.3 Exhaust Gas Analysis and Measuring Equipment .....	39
3.3.1 Gas Analyser.....	39
3.3.2 Gas Chromatograph - Thermal Conductivity Detector (GC-TCD).....	40
3.4 Experimental Conditions .....	40
<b>CHAPTER 4 GOVERNING EQUATIONS AND NUMERICAL METHOD.....</b>	<b>42</b>
4.1 Assumptions .....	42
4.2 Governing Equations .....	43
4.3 Boundary Conditions.....	47
4.4 Numerical Method.....	48

<b>CHAPTER 5 MICROKINETIC MODELLING .....</b>	<b>50</b>
5.1 C <sub>3</sub> H <sub>8</sub> -SCR Microkinetic Mechanism Development .....	51
5.2 Reaction Rate Constant Estimation .....	60
5.3 Heat of Adsorption Calculation .....	63
5.3.1 Metal-Atom Binding.....	64
5.3.2 Weak Binding Molecule .....	64
5.3.3 Strong Binding Molecule .....	65
5.3.4 Medium Binding Molecule .....	65
5.3.5 Weak Binding Symmetric Molecule .....	66
5.3.6 Weak Binding Diatomic Molecule.....	67
5.4 Activation Energy Estimation .....	69
5.5 Heat of Reaction .....	71
<b>CHAPTER 6 MODEL OPTIMISATION.....</b>	<b>73</b>
6.1 Sensitivity Analysis .....	73
6.2 Solution-Mapping Method.....	75
6.3 Optimisation of the Surface Reaction Mechanism .....	80
<b>CHAPTER 7 RESULTS AND DISCUSSION .....</b>	<b>83</b>
7.1 Model Validation .....	83
7.2 Simulations of C <sub>3</sub> H <sub>8</sub> -SCR on the Silver Catalyst.....	86
<b>CHAPTER 8 CONCLUSIONS.....</b>	<b>94</b>
8.1 Concluding Remarks.....	94
8.2 Future Work.....	96
8.2.1 Surface-Reaction Mechanisms for SCR of NO <sub>x</sub> by Using Different Types of Hydrocarbon as a Reducing Agent.....	96
8.2.2 The Effect of Water Vapour on a HC-SCR Process.....	97
8.2.3 The Effect of Hydrogen on a HC-SCR Process .....	97
8.2.4 Deactivation of a HC-SCR Catalyst.....	98
8.2.5 Exhaust Gas Fuel Reforming.....	98
<b>APPENDIX A TRANSPORT AND CHEMICAL PROPERTIES .....</b>	<b>100</b>
<b>APPENDIX B EXAMPLES OF CALCULATION .....</b>	<b>104</b>
<b>APPENDIX C AUTHOR'S PUBLICATIONS .....</b>	<b>107</b>
<b>LIST OF REFERENCES .....</b>	<b>108</b>

## LIST OF ILLUSTRATIONS

<b>Figure 1.1:</b> Comparison of regulated emissions for spark ignited and diesel engines...	1
<b>Figure 1.2:</b> European PM and NO <sub>x</sub> emissions legislation. ....	2
<b>Figure 1.3:</b> Potential energy diagram for a catalytic reaction.....	6
<b>Figure 1.4:</b> Sequence of steps occurring in a heterogeneous catalytic reaction. ....	7
<b>Figure 2.1:</b> NO <sub>x</sub> adsorption and regeneration mechanism. ....	15
<b>Figure 3.1:</b> The simplified schematic of the monolithic reactor system. ....	38
<b>Figure 4.1:</b> Illustration of the structure of the monolithic catalyst and the transport and catalysis phenomena occurring inside a channel. ....	43
<b>Figure 4.2:</b> The actual scale and rectangular structured grids of the single channel....	48
<b>Figure 5.1:</b> Methodology for microkinetic analysis development of propane-SCR on a silver catalyst. ....	51
<b>Figure 5.2:</b> Kinetic reaction pathway of selective catalytic reduction of NO <sub>x</sub> by propane. ....	57
<b>Figure 6.1:</b> Sensitivity analysis. ....	75
<b>Figure 7.1:</b> Comparisons between model predictions and experimental data for the conversion of C <sub>3</sub> H <sub>8</sub> at various operating conditions.....	84
<b>Figure 7.2:</b> Comparisons between model predictions and experimental data for the conversion of NO <sub>x</sub> at various operating conditions. ....	85
<b>Figure 7.3:</b> Comparisons between model predictions and experimental data for the ratio of CO <sub>2</sub> to CO at various operating conditions. ....	86
<b>Figure 7.4:</b> Model prediction of NO <sub>x</sub> conversion as a function of temperature at different inlet concentration of C <sub>3</sub> H <sub>8</sub> and NO.....	87
<b>Figure 7.5:</b> Wall and axial gas temperature profiles at different inlet temperatures. ..	89
<b>Figure 7.6:</b> Simulated surface coverage profiles of surface species, O, OH, CH <sub>3</sub> O, CH <sub>3</sub> COO, NO <sub>3</sub> , CNO and Ag. ....	91
<b>Figure 7.7:</b> Simulated surface coverage of different surface species as a function of inlet temperature. ....	93

## LIST OF TABLES

<b>Table 3.1:</b> The specification of the monolithic automotive catalytic converter.....	37
<b>Table 3.2:</b> Technical data for the Horiba Mexa 7100DEGR analyser.....	39
<b>Table 3.3:</b> Experimental conditions used to optimisation and validation.....	41
<b>Table 5.1:</b> Detailed reaction mechanism for C <sub>3</sub> H <sub>8</sub> -SCR on a silver catalyst with standard enthalpy of reaction, initial values of sticking coefficients or preexponential factors and activation energies.....	58
<b>Table 5.2:</b> Transition state theory estimates of preexponential factor. ....	62
<b>Table 5.3:</b> Schematic illustration of possible adsorbing and binding geometry of surface species. ....	63
<b>Table 5.4:</b> Recommended UBI-QEP values of $Q_{0A}$ for selected adatoms and metals. ....	64
<b>Table 5.5:</b> Heats of adsorption, binding type, bond-energy partitioning or total gas phase energies used to calculate heat of adsorption.....	68
<b>Table 6.1:</b> Minimum and maximum values of sticking coefficient and preexponential factors used to calculate factorial variables.....	76
<b>Table 6.2:</b> Factorial design table for the conversion of C <sub>3</sub> H <sub>8</sub> .....	77
<b>Table 6.3:</b> Factorial design table for the conversion of NO <sub>x</sub> .....	77
<b>Table 6.4:</b> Factorial design table for the ratio of CO <sub>2</sub> to CO .....	79
<b>Table 6.5:</b> Optimised values of active parameters for C <sub>3</sub> H <sub>8</sub> -SCR mechanism on a silver catalyst. ....	82
<b>Table A.1:</b> Chemical formulas, names, molecular weights, standard enthalpies of formation and Lennard-Jones potential parameters. ....	100
<b>Table A.2:</b> Atomic and structural diffusion-volume increments.....	101
<b>Table A.3:</b> Diffusion volumes for simple molecules. ....	101
<b>Table A.4:</b> Polynomial coefficients for mass diffusion coefficient for species $i$ in the mixture of $i$ and nitrogen.....	102
<b>Table A.5:</b> Polynomial coefficients for specific heat capacity.....	103

## LIST OF NOTATIONS

Symbol	Unit	
$A_k$	$s^{-1}$	Preexponential factor of elementary reaction $k$
$C_p$	$J/(kg \cdot K)$	Specific heat capacity at constant pressure
$c_j$	$mole/m^2$	Concentration of species $j$
$D_{AB}$	$kJ/mol$	Bond dissociation energy for an AB molecule
$\mathcal{D}_{AB}$	$kJ/mol$	Bond-energy partitioning for an AB molecule
$\tilde{\mathcal{D}}_{AB}$	$kJ/mol$	Total gas phase energy for an AB molecule
$D_{i,B}$	$m^2/s$	Diffusion coefficient of species $i$ diffusing in the mixture of $i$ and $B$
$E_a$	$kJ/mol$	Activation energy
$E_{a,f}$	$kJ/mol$	Activation energy for forward reaction
$E_{a,r}$	$kJ/mol$	Activation energy for reverse reaction
$\Delta H$	$kJ/mol$	Surface reaction enthalpy
$\Delta H_R$	$kJ/mol$	Enthalpy (or heat) of reaction
$\Delta H_f^o$	$kJ/mol$	Standard enthalpy (or heat) of formation
$\Delta H_R^o$	$kJ/mol$	Standard enthalpy (or heat) of reaction
$h_i$	$kJ/kg$	Enthalpy of species $i$
$J$	$kg/(m^2 \cdot s)$	Diffusive mass flux
$K_s$	dimensionless	Number of surface reactions
$k_k$		Reaction rate constant of elementary reaction $k$
$M_i$	$kg/kmol$	Molecular weight of species $i$
$\bar{M}$	$kg/kmol$	Mean molecular weight
$N_g$	dimensionless	Number of gas-phase species
$N_s$	dimensionless	Number of surface species
$n$	dimensionless	Reaction order
$P$	Pa	Pressure
$Q_{0A}$	$kJ/mol$	Heat of adsorption of an atomic A on an on-top site
$Q_A$	$kJ/mol$	Heat of adsorption of an atom A on a catalyst surface
$Q_{AB}$	$kJ/mol$	Heat of adsorption of an AB molecule
$R$	$kJ/(kmol \cdot K)$	Universal gas constant
$R_i$	$kg/(m^3 \cdot s)$	Net rate of production of species $i$ due to chemical reactions
$r$	m	Radial spatial coordinate
$S_i^0$	dimensionless	Sticking coefficient at vanishing coverage of species $i$
$\dot{s}_i$	$mole/(m^2 \cdot s)$	Net rate of production/depletion of species $i$
$T$	K	Temperature
$v_r$	m/s	Radial velocity
$v_z$	m/s	Axial velocity
$X$	dimensionless	Factorial variable
$Y_i$	$kg/kg$	Mass fraction of species $i$
$z$	m	Axial spatial coordinate
$\beta$	dimensionless	Temperature exponent
$\Gamma$	$kmol/m^2$	Site density

<b>Symbol</b>	<b>Unit</b>	
$\epsilon/k_B$	K	Lennard-Jones energy parameter
$\lambda$	W/(m·K)	Thermal conductivity
$\mu$	Pa·s	Viscosity
$\nu'$	dimensionless	Stoichiometric coefficient for reactants
$\nu''$	dimensionless	Stoichiometric coefficient for products
$\rho$	kg/m <sup>3</sup>	Mass density
$\sigma$	angstrom	Lennard-Jones characteristic length
$v$	dimensionless	Diffusion-volume increment
$\Sigma v$	dimensionless	Diffusion volume
$\Phi$	dimensionless	Objective function

### **Subscript**

$i$	Species number
$k$	Elementary reaction number
$r$	In radial direction
$z$	In axial direction

### **Superscript**

*	Surface species
---	-----------------

## LIST OF ABBREVIATIONS

Ag	Silver
Ag/Al <sub>2</sub> O <sub>3</sub>	Silver/alumina catalyst
Al <sub>2</sub> O <sub>3</sub>	Alumina
Au	Gold
BaO	Barium oxide
C	Atomic carbon
C <sub>3</sub> H <sub>7</sub> O	i-Propoxy radical
C <sub>3</sub> H <sub>7</sub> OH	i-Propanol
C <sub>3</sub> H <sub>8</sub>	Propane
CFD	Computational fluid dynamics
CH <sub>3</sub> CHO	Acetaldehyde
CH <sub>3</sub> CO	Acetyl radical
CH <sub>3</sub> COO	Acetate
CH <sub>3</sub> NO <sub>2</sub>	Nitromethane
CH <sub>2</sub> NO <sub>2</sub>	Nitromethylene
CH <sub>2</sub> NO	Formaldiminoxy
CH <sub>3</sub> O	Methoxy radical
CN	Cyanide
CNO	Nitrile N-oxide
CO	Carbon monoxide
CO <sub>2</sub>	Carbon dioxide
cps	Cells per square inch
Cu	Copper
DRIFT	Diffuse reflectance infrared Fourier transform
GC	Gas chromatography
H	Atomic hydrogen
H <sub>2</sub>	Hydrogen
H <sub>2</sub> O	Water vapour
HC-SCR	Hydrocarbon selective catalytic reduction
HCO	Formyl
HNCO	Isocyanic acid
LHHW	Langmuir Hinshelwood Hougen Watson rate expression
MARI	Most abundant reaction intermediate
N	Atomic nitrogen
N <sub>2</sub>	Nitrogen
N <sub>2</sub> O	Nitrous oxide
NCO	Isocyanate
(NH <sub>2</sub> ) <sub>2</sub> CO	Urea
NH <sub>3</sub>	Ammonia
Ni	Nickel
NO	Nitric oxide
NO <sub>2</sub>	Nitrogen dioxide
NO <sub>3</sub>	Nitrate
NO <sub>x</sub>	Nitrogen oxides

O	Atomic oxygen
O <sub>2</sub>	Oxygen
OH	Hydroxyl
Pd	Palladium
PE	Partial equilibrium
PM	Particulate matter
Pt	Platinum
QSS	Quasi-steady state
RDS	Rate-determining step
SCR	Selective catalytic reduction
SIMPLE	Semi-implicit method for pressure-linked equations
SiO <sub>2</sub>	Silicon dioxide, also known as Silica
THC	Total hydrocarbon
TiO <sub>2</sub>	Titanium dioxide, also known as Titania
TPD	Temperature-programmed desorption
TWC	Three-way catalyst
UBI-QEP	Unity bond index-quadratic exponential potential
ZrO <sub>2</sub>	Zirconium dioxide, also known as Zirconia

# CHAPTER 1

## INTRODUCTION

The use of a diesel engine as a power source in passenger vehicles is steadily increasing because fuel consumption is better than its counterpart, the gasoline engine. In terms of regulated emissions emitted from an internal combustion engine (i.e. carbon monoxide (CO), hydrocarbons (HC), nitrogen oxides (NO<sub>x</sub>) and particulate matter (PM)) emissions of CO and HC from diesel engines are significantly lower than those from gasoline engines (as shown in Figure 1.1). However, comparisons with gasoline engines, diesel engines produce considerably higher emissions of NO<sub>x</sub> and PM.

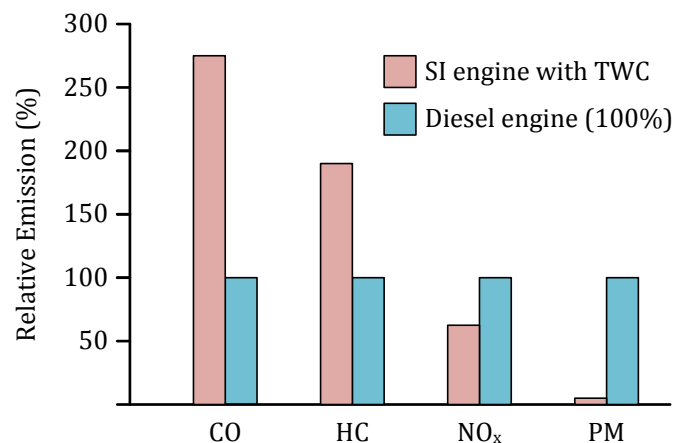


**Figure 1.1:** Comparison of regulated emissions for spark ignited and diesel engines. (after (DieselNet, 2008))

Continuously, the effort to reduce the diesel emissions has been enforced in three major regions, i.e. Europe, the U.S. and Japan. Figure 1.2 shows the trend of stringent automotive emission standards that have been ruled in European countries

since 1992. As a result,  $\text{NO}_x$  and PM control in diesel engines have generated serious concerns to automotive industry.

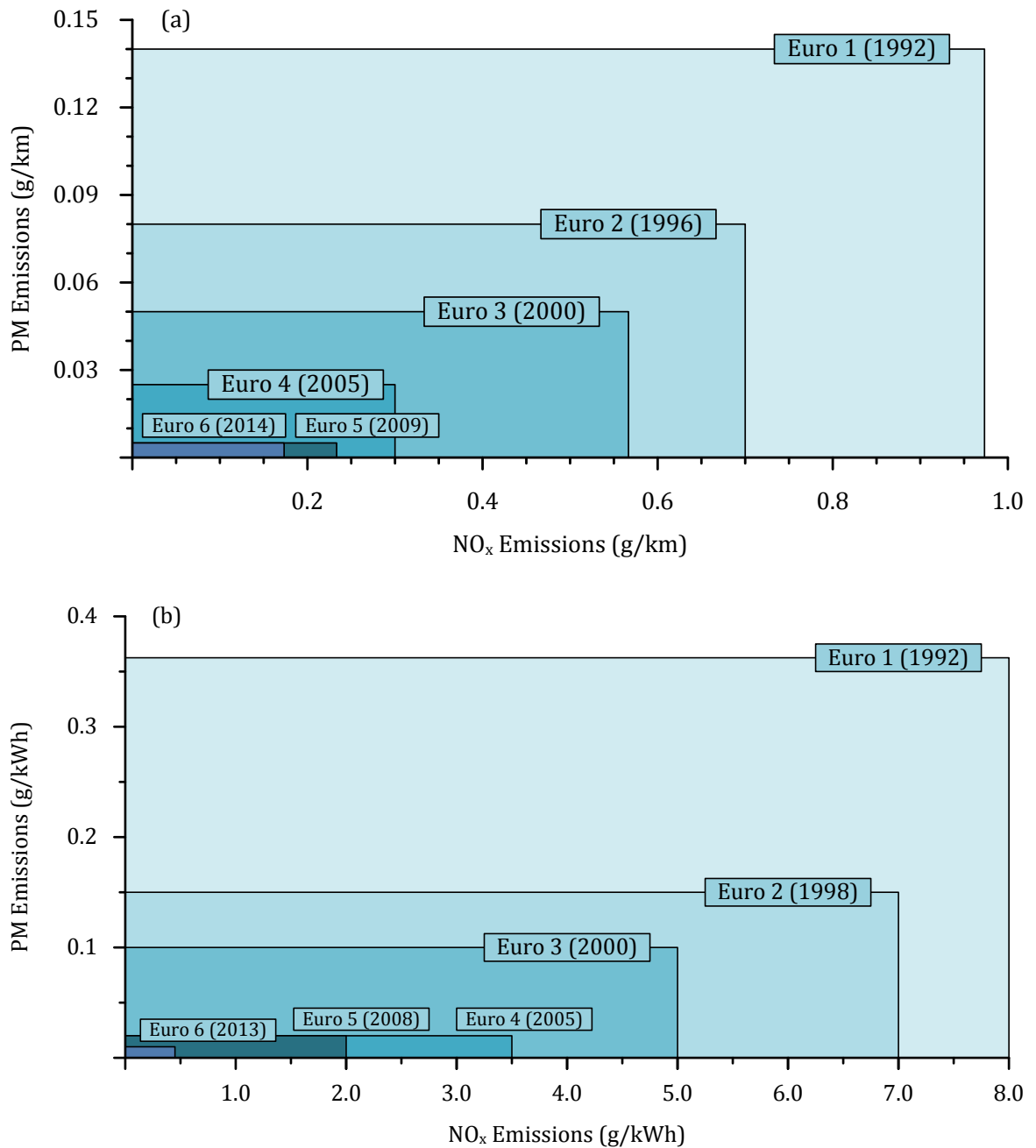


**Figure 1.2:** European PM and  $\text{NO}_x$  emissions legislation.

(a) Light-duty diesel vehicles (g/km). (Taken from reference (Rounce, 2011))

(b) Heavy-duty applications (g/kWh). (Taken from reference (Theinnoi, 2008))

$\text{NO}_x$  plays an important role in the formation of photochemical smog, nitric acid and acid rain. Moreover, emissions of  $\text{NO}_x$  contribute to the greenhouse effect and are ground-level ozone precursors. Therefore, their treatment is of paramount importance from an environmental and biological viewpoint. For the traditional stoichiometric gasoline engine, the conversion from  $\text{NO}_x$  which contain in its exhaust to  $\text{N}_2$  is very effective by using a three-way catalyst (TWC). Nevertheless, the removal of  $\text{NO}_x$  by using the TWC is ineffective for the diesel engine due to lean operation and large oxygen content in the exhaust. Accordingly, several  $\text{NO}_x$  reduction technologies have been developed to solve this problem. Selective catalytic reduction (SCR) which was originally used in thermal power plants by using ammonia as a reducing agent, called ammonia-SCR, is a  $\text{NO}_x$  reduction methodology. Fundamentally,  $\text{NO}_x$  reacts catalytically with ammonia on the surfaces of a catalyst. Different precious metals (e.g. gold, silver, platinum, ruthenium, rhodium and palladium) and base metals (e.g. iron, nickel, lead, zinc and copper) coated on a porous medium in order to increase the chemically active surface have been used as catalysts. Due to high  $\text{NO}_x$  conversion efficiencies seen in stationary applications, ammonia-SCR has also been adapted in transportation where heavy-duty diesel engines are used. Recently, it has also been investigated in light-duty passenger vehicles. However, there are some problems that rise with the using of ammonia-SCR in vehicle. An additional storage tank to contain ammonia or urea is inevitably required. Furthermore, unlike the heavy-duty diesel engine which usually operates at a high and constant operating condition (i.e. engine speed and load), the light-duty diesel engine normally works in a wide range of operating conditions. These operating conditions are changed continually and suddenly. So it is difficult to control the amount of ammonia which is injected into the

exhaust gas for the NO<sub>x</sub> reduction process because this amount varies with operating conditions of the engine. As a result, there has been a worldwide effort to discover more practical technologies for the removal of NO<sub>x</sub> emissions emitted from the light-duty diesel engine. Replacing ammonia or urea with hydrocarbons, a method that is known as hydrocarbon SCR (HC-SCR) is the most convenient. A wide variety of hydrocarbons (e.g. oxygenated hydrocarbon, light hydrocarbon, traditional diesel fuel, biodiesel fuel and synthetic diesel fuel) has been studied in both laboratory-scale experiments and full-scale tests to discover the appropriate hydrocarbon used as the reducing agent. Moreover, several catalytic substances have been screened to determine the suitable catalyst for HC-SCR.

Due to the growth in the potential of computer processing, mathematical modelling together with numerical analysis techniques, for example, computational fluid dynamics (CFD), has been developed over the past few decades. It will be continually improved as an effective tool which is to be able to reliably solve engineering problems, such as fluid flow, heat transfer and chemical reactions in complex systems. Computer-based simulations can be applied to simulate systems in which experiments are difficult, dangerous, expensive or impractical to perform. In addition, since numerical modelling is cheaper and easier to setup than experiments, it has been employed in the situation which a large volume of results is demanded (e.g. parametric studies). Once a modelling is established and produces accurate results, the modelling can be adapted to predict relative situations.

## 1.1 Background

A catalyst is a substance that affects the rate of a chemical reaction but is not one of the initial reactants or finishing products, i.e. it is not consumed or produced in the reaction (Fogler, 2006). Catalysts have been widely used in chemical production and petroleum refining. Moreover, they also have been used as environmental catalysts (i.e. aftertreatment systems) in order to convert harmful components in engine exhaust gases into harmless substances. The development of sophisticated catalysts is immensely important to increase product yield by promoting the desired chemical reaction pathways and to simultaneously reduce unwanted products by suppressing undesired pathways.

In order to transform the original reactants to the final products, reactants need at least the minimum energy required to overcome an energy barrier (activation energy). When this minimum reaction energy is reached, it is able to carry on spontaneously. The role of the catalyst is to provide an alternate reaction pathway between reactants and products by lowering the activation energy of the reaction, as shown in Figure 1.3. A catalyst changes only the rate of a reaction; it does not change the energies of the initial and final states, nor the equilibrium itself. Thus, the heat of reaction (also called the enthalpy of reaction) ( $\Delta H$ ), reaction free energy ( $\Delta G$ ) and the equilibrium constant ( $K_e$ ) are not affected by the presence of a catalyst.

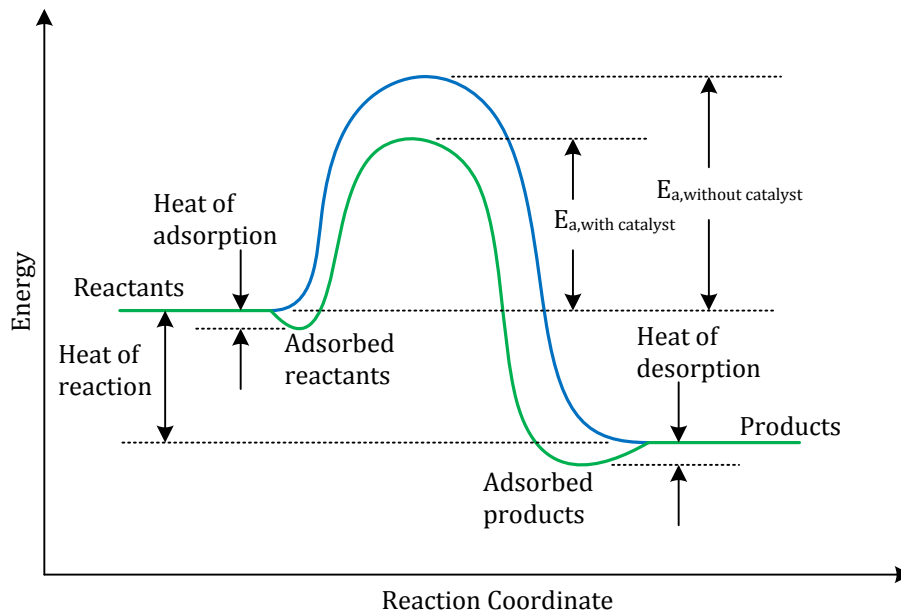


**Figure 1.3:** Potential energy diagram for a catalytic reaction. (after (Hayes and Kolaczkowski, 1997))

A catalytic process can be classified into two categories: i) a homogeneous catalytic process and ii) a heterogeneous catalytic process. In the homogeneous catalytic process, the catalyst operates in the same phase as the reductants. On the other hand, the catalyst is in a different phase from the reactants or products for the heterogeneous catalytic process. Usually, the catalyst is a solid and the reactants and products are in liquid or gaseous form (Fogler, 2006). In an aftertreatment application, the heterogeneous catalyst has been widely used. Since the heterogeneous catalytic reaction occurs at the fluid-solid interface, a large interfacial area is necessary to maximise the catalytic reaction rate. To accomplish this, a catalytic substance (e.g. silver, platinum and palladium) is typically dispersed on a porous structure (known as washcoat). The washcoat, such as  $\text{Al}_2\text{O}_3$ , contains huge numbers of pores which provides the enormous area required for the high rate of reactions (Hayes and Kolaczkowski, 1997).

The conversion of a reactant  $A$  to a product  $B$  in a heterogeneous catalytic process consists of the following physical and chemical steps, shown schematically in Figure 1.4:

- 1) Diffusion (mass transfer) of the reactant throughout a boundary layer from the bulk fluid to the external surface of the catalyst.
- 2) Diffusion of the reactant into the porous catalyst.
- 3) Adsorption of the reactant onto the surface of the catalyst.
- 4) Reaction on the catalyst surface to transform the adsorbed reactant to the adsorbed product.
- 5) Desorption of the adsorbed product from the surface.
- 6) Diffusion of the product from the catalyst surface through the catalyst pores to the external surface.
- 7) Mass transfer of the product from the external catalyst surface through the boundary layer into the bulk fluid.

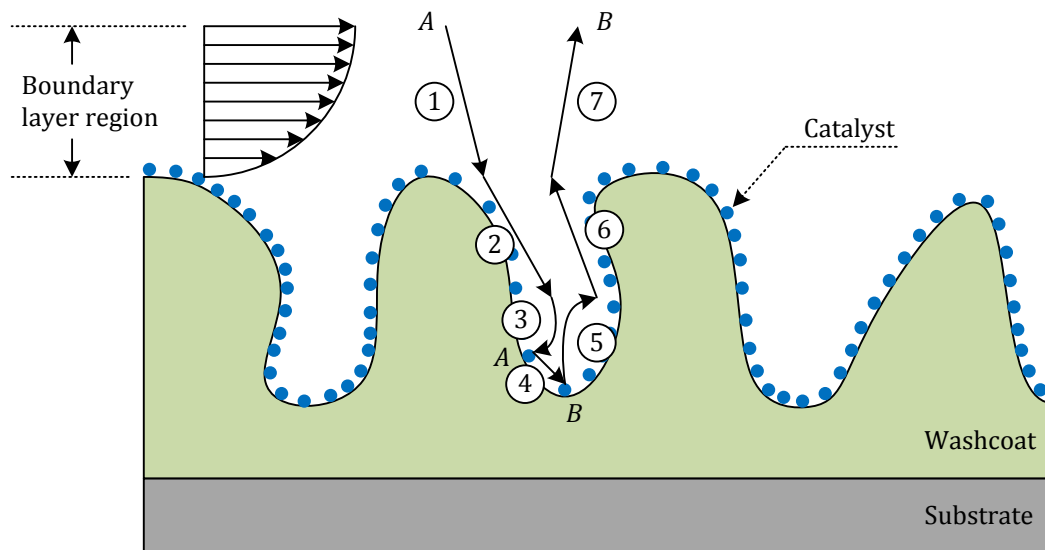


**Figure 1.4:** Sequence of steps occurring in a heterogeneous catalytic reaction. (Adapted from reference (Fogler, 2006).)

For a catalytic reaction to occur, at least one and frequently all of the reactants must become attached to the catalyst surface. This attachment process (known as adsorption) takes place by two different processes: physical adsorption and chemical adsorption (usually referred to as chemisorption). Physical adsorption is caused primarily by van der Waals forces. These are relatively low strength forces and physical adsorption is similar in principle to condensation. Physical adsorption is exothermic and the heat of adsorption is relatively small (usually the same order of magnitude as the heat of condensation). On the other hand, the type of adsorption that affects the rate of a chemical reaction is chemisorption. A rearrangement of an electronic structure (valence electrons) of both adsorbed atoms or molecules and catalyst surface (called the active site) makes them enormously reactive. As a result, the heats of adsorption for chemisorption are usually higher than those for physical adsorption (Hayes and Kolaczkowski, 1997). The heats of adsorption for chemisorption are generally of the same order of magnitude as the heat of a chemical reaction (Fogler, 2006). Once molecules are on the surface, they react with some other surface or gas-phase species, forming intermediate species then producing final products. Hundred of intermediate species can be formed during the surface reaction process. Finally, adsorbed products or intermediate species can be released from the catalyst surface during the desorption process. The free catalyst sites that were occupied previously are available for new coming processes of adsorptions and surface reactions.

## 1.2 Objectives and Approaches

This dissertation focuses on the numerical simulation of the selective catalytic reduction of  $\text{NO}_x$  on a silver based catalyst by using hydrocarbons, propane in this case, as a reductant. This  $\text{C}_3\text{H}_8$ -SCR process consists of a combination of physical and chemical phenomena. The objectives of this research are to:

- a) Create a catalytic reaction mechanism for  $\text{C}_3\text{H}_8$ -SCR on a silver based catalyst in order to explain at the molecular level the chemistry occurring on the surface of the catalyst. To accomplish this task, reaction pathways and detailed elementary reactions are carefully formulated from literature. Then, the parameters for these elementary reactions are estimated by using theories of chemical bonding.
- b) Model the transport phenomena that take place during the SCR process with the purpose of providing physical properties that are difficult to experimentally measure, for instance, temperature, velocity and concentration profiles. To achieve this objective, the laws of conservation (i.e. conservation of mass, momentum, energy and species) together with appropriate assumptions are applied to transform the physical and chemical problem into a numerically resolvable system of mathematical equations. From this a numerical method is applied to solve these governing equations.
- c) Predict the effect of operating conditions, such as, operating temperatures and concentrations of reactants (i.e.  $\text{C}_3\text{H}_8$  and  $\text{NO}_x$ ), on the conversion of  $\text{NO}_x$  to  $\text{N}_2$ .
- d) Investigate the effect of chemical properties, for example intermediate species, on the  $\text{NO}_x$  conversion.

- e) Demonstrate the effect of the state of catalyst surface, e.g. the surface occupation by adsorbed species and free active sites, on the NO<sub>x</sub> conversion.

### **1.3 Thesis Outline**

An introduction to the selective catalytic reduction of NO<sub>x</sub> by using hydrocarbon as the reducing agent has been presented. However, the remainder of the thesis is systematically arranged as follows:

#### **Chapter 2: Literature Review**

This chapter reviews the formation of NO<sub>x</sub> emissions in diesel engines. Technologies for NO<sub>x</sub> control in lean burn engines (i.e. Diesel), such as, NO<sub>x</sub> storage catalysts and selective catalytic reduction of NO<sub>x</sub> (NO<sub>x</sub>-SCR), are also presented. Furthermore, an overview of the available reducing agents and catalytic materials utilised in NO<sub>x</sub>-SCR is provided. The role of hydrogen in promoting the NO<sub>x</sub>-SCR by hydrocarbons is also reviewed. Approaches that are frequently applied for numerical modelling are briefly discussed. Finally the microkinetic analysis, which is adopted in this work in order to explain the chemistry during HC-SCR of NO<sub>x</sub>, at the molecular level, is presented.

#### **Chapter 3: Experimental Facilities**

This chapter describes the details of experimental facilities that consist of the specification of monolithic catalysts, experimental setup and equipment used for emissions measurement. The experimental conditions created for model optimisation and validation purposes are also presented.

#### **Chapter 4: Governing Equations and Numerical Method**

In this chapter assumptions that are imposed on the physical problem, in order to mathematically simplify it, are provided. Transport and chemical phenomena that rule the NO<sub>x</sub> reduction activities are written in systems of mathematical equations, called governing equations. Numerical methods and boundary conditions that are applied to numerically solve these governing equations are explained.

#### **Chapter 5: Microkinetic Modelling**

This chapter is the heart of this dissertation. It provides the methodology for establishing the surface reaction mechanism of C<sub>3</sub>H<sub>8</sub>-SCR of NO<sub>x</sub> on a silver based catalyst. To represent various chemical processes occurring during C<sub>3</sub>H<sub>8</sub>-SCR, the mechanism contains a number of elementary chemical reactions. The estimation of reaction rate constants and activation energies for these elementary reactions is explained in detail.

#### **Chapter 6: Model Optimisation**

In this chapter the procedures for optimising the catalytic NO<sub>x</sub> reduction mechanism which has been created in the prior chapter are illustrated. Sensitivity analysis is applied to identify some essential reactions that virtually control the NO<sub>x</sub> reduction processes. Solution mapping, the method used to find out the optimum reaction parameters, is also discussed.

#### **Chapter 7: Results and Discussion**

Simulated results produced by using the fundamentals appearing in previous chapters are presented and discussed in this chapter. The effects on NO<sub>x</sub> reduction activities of the different concentrations of reducing agent (propane in this case) and

NO<sub>x</sub> are predicted by using numerical simulation. Moreover, information that is complicated or unfeasible to measure, such as, profiles of concentration and temperature inside the reacting channel and wall temperatures is presented. Furthermore, details about the state of catalyst surface, for instance, the variation with temperature of adsorbed species, abundant surface intermediates and free active site, are investigated by modelling.

### **Chapter 8: Conclusions**

The conclusions of the thesis are discussed and the potential related areas for further research are outlined.

### **Appendices**

Transport and chemical properties for gas-phase and surface species used in this dissertation and not given in main chapters are presented in Appendix A. Appendix B shows examples of how chemical parameters appearing mainly in Chapter 5 are calculated. The papers written by the author during the research project are listed in Appendix C.

## CHAPTER 2

### LITERATURE REVIEW

In this chapter, the harmful emission ( $\text{NO}_x$ ) emitted from diesel engines, is discussed in terms of its formation and environmental effects. In addition, related technologies used to control these emissions are also examined. The explanations for modelling the HC-SCR of  $\text{NO}_x$  are also presented.

#### 2.1 $\text{NO}_x$ from Diesel Engines

Nitrogen oxides ( $\text{NO}_x$ ) are considered as one of the most critical pollutants produced from diesel engines along with particulate matter (PM). In the automotive aftertreatment,  $\text{NO}_x$  is the abbreviation to represent nitric oxide (NO) and nitrogen dioxide ( $\text{NO}_2$ ). While NO is a colourless and odourless gas,  $\text{NO}_2$  is a reddish-brown colour and strong odour. The formation of  $\text{NO}_x$  in internal combustion engines consists of three primary mechanisms: i) the thermal  $\text{NO}_x$  mechanism — the reaction at high temperatures of nitrogen found in combustion air and oxygen during combustion processes; ii) the fuel  $\text{NO}_x$  mechanism — the oxidation of nitrogen contained in the fuel and iii) the prompt  $\text{NO}_x$  mechanism — the reaction of atmospheric nitrogen with radicals derived from fuel.

The thermal  $\text{NO}_x$  mechanism is generally considered as the main source of  $\text{NO}_x$  formation. It can be explained via the extended Zeldovich mechanism (Heywood, 1988):



The corresponding NO can be converted forward to NO<sub>2</sub> or back to NO via:



Concentrations of NO<sub>x</sub> in diesel exhaust are typically between 100 and 1000 ppm (Burch et al., 2002).

## **2.2 NO<sub>x</sub> Emissions Control Technologies**

Successful NO<sub>x</sub> removal technology for exhaust gas from engines operated in the stoichiometric condition (e.g. gasoline engines) has already established by using a three-way catalyst. Harmful NO<sub>x</sub> is catalytically converted to benign N<sub>2</sub> by unburned hydrocarbons (HCs), CO and H<sub>2</sub> on supported precious metals including Pt, Rh and Pd. Simultaneously, remaining HCs and CO are oxidised to CO<sub>2</sub> and H<sub>2</sub>O. However, the TWC is not effective for lean-burn engines (e.g. diesel engines) because unburned HCs prefer to unfavourably oxidise with excess oxygen rather than reduce NO<sub>x</sub> to N<sub>2</sub>. In addition, in contrast with gasoline engines, the amount of CO and H<sub>2</sub> from diesel operation is usually low. To keep HCs from undesired consumption by excess oxygen and promote these HCs for the conversion of NO<sub>x</sub> to N<sub>2</sub>, new catalysis technologies based on novel catalyst are really desired.

### 2.2.1 NO<sub>x</sub> Storage Catalyst

Unfortunately, the three-way catalyst is inactive when excess oxygen is present in the exhaust gas. The new concept for the removal of NO<sub>x</sub> from a lean-burn engine calls the NO<sub>x</sub> storage catalyst. This technology involves NO<sub>x</sub> adsorption during lean conditions and, then, NO<sub>x</sub> reduction (also referred to as the regeneration) when the engine is turned to rich modes for a short period. The NO<sub>x</sub> storage catalyst consists of three key components: i) an oxidation catalyst (e.g. Pt), ii) a NO<sub>x</sub> storage medium (e.g. barium oxide (BaO)) and iii) a reduction catalyst (e.g. Rh). The overall fundamentals of NO<sub>x</sub> adsorption and reduction processes are illustrated in Figure 2.1. These sequential mechanisms are described by the following steps (Majewski, 2007):

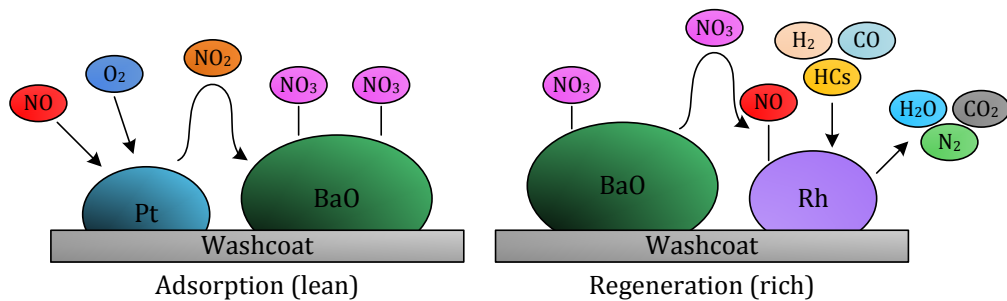
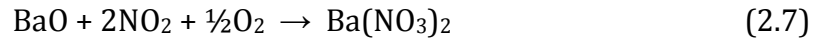


**Figure 2.1:** NO<sub>x</sub> adsorption and regeneration mechanism.  
(Adapted from reference (Majewski, 2007))

- 1) *NO oxidation to nitrogen dioxide.* Nitric oxide, the main component of NO<sub>x</sub>, reacts with oxygen on the active oxidation catalyst site (Pt) to form NO<sub>2</sub>, described by Reaction (2.6).

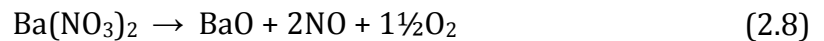


- 2) *NO<sub>2</sub> storage.* The adsorbed NO<sub>2</sub> migrates from the Pt site to the NO<sub>x</sub> storage medium (BaO) and, then, accumulates in the form of inorganic nitrates, according to Reaction (2.7).



3) *Reductant evolution.* The exhaust is turned into the rich condition by switching the engine to the rich mode. Oxygen is replaced by reducing species, i.e., HCs, CO and H<sub>2</sub>.

4) *Nitrates release from the storage medium.* Under rich conditions, the nitrate species become thermodynamically unstable. They are decomposed to form NO which, next, is removed onto the Rh site. One of the possible reduction paths is described by Reaction (2.8).



5) *NO reduction to nitrogen.* Finally, NO is catalytically reduced by HCs, CO and H<sub>2</sub> to produce N<sub>2</sub> on the reduction catalyst, in a process which takes place on the conventional three-way catalyst. Reaction (2.9) represents the potential process of NO reduction.



The NO<sub>x</sub> storage catalyst can make traditional TWC active properly for lean-burn operation engines; however, there are a number of other possible problems reported in the literature. Sulphur compounds that are present in the exhaust react with a NO<sub>x</sub> storage medium to form sulphates which accumulate gradually on the active catalyst surface during lean conditions. This makes the NO<sub>x</sub> storage medium saturated with sulphates and lost active sites for NO<sub>x</sub> adsorption. Although sulphates can be thermally decomposed, high temperatures (>600 °C) are required to desulphate under rich conditions because they are more stable than corresponding nitrates on the storage medium (Blakeman et al., 2003).

### **2.2.2 Selective Catalytic Reduction of NO<sub>x</sub>**

By using the method of selective catalytic reduction, NO<sub>x</sub> contained in the exhaust gas can be converted to N<sub>2</sub> when it reacts catalytically with a reductant (e.g. ammonia, urea, oxygenated hydrocarbon and hydrocarbon) in the presence of a catalyst. Unlike the NO<sub>x</sub> storage catalyst, SCR removes NO<sub>x</sub> continuously through the active reductant on the catalyst surface. The removal of NO<sub>x</sub> by SCR was first established for the thermal power plant in Japan in the late 1970s. It has since been applied to industrial stationary applications. Originally, ammonia was used as the reducing agent in these SCR systems. Later, SCR technology has been customised for automotive applications. It has been employed in heavy-duty diesel engines. Now, it is being developed for light-duty passenger vehicles. Owing to safety reasons, ammonia has been ruled out and replaced by urea. Other reductants, also, have been screened to substitute ammonia. Oxygenated hydrocarbons, later, have been discovered as another potential reductant. The alternative choice, recently, is hydrocarbons which is gaining more attention from researchers. Due to the existence of hydrocarbon in the exhaust gas (passive mode) or in the injected fuel itself (active mode), it is a relatively simple to apply to the passenger vehicles.

As reported by many researchers, the advantage of SCR over the NO<sub>x</sub> storage catalyst is that it is effective in the different kinds of reductants (e.g. urea, oxygenated hydrocarbons and hydrocarbons), catalyst materials (e.g. ion-exchanged zeolites, Cu, Pt and Ag) and catalyst supports (e.g. Al<sub>2</sub>O<sub>3</sub>, SiO<sub>2</sub>, ZrO<sub>2</sub> and TiO<sub>2</sub>) (Shimizu and Satsuma, 2006). Moreover, the SCR has been reported to have moderate tolerance to poisoning from sulphur (Meunier and Ross, 2000, Houel et al., 2005).

## 2.3 Reductants for Selective Catalytic Reduction of NO<sub>x</sub>

In the SCR process, the reducing agent is competitively consumed by two main pathways, i.e., the completed oxidation by oxygen and the selective reduction by NO<sub>x</sub>. The former is the undesired reaction, while the latter is the favourable mechanism. A lot of investigative research has been devoted to discover the appropriate reductants and catalyst materials for the SCR system. The details of reductants used in SCR of NO<sub>x</sub> are presented in this section, while the information about catalyst materials applied is provided in next section.

### 2.3.1 Ammonia and Urea

Ammonia has been used as a reductant for control of NO<sub>x</sub> in thermal power plants and industrial stationary applications. However, the use of ammonia in automotive vehicles is unsuitable because it is hazardous and toxic. In addition, its high vapour pressure makes it challenging to store and on-board transport safely. To prevent these problems, ammonia is chemically transformed to non-toxic urea. Urea is an organic compound with the chemical formula (NH<sub>2</sub>)<sub>2</sub>CO. It is solid, colourless, odourless and highly soluble in water. The urea-SCR for NO<sub>x</sub> reduction involves the following steps (Koebel et al., 2000).

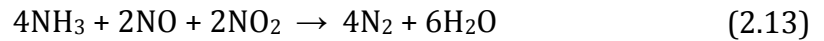
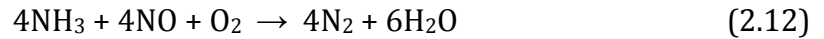
1. Heating liquid urea in the hot exhaust causing endothermic decomposition to form ammonia and isocyanic acid (so called thermolysis process):



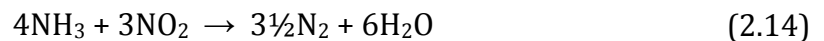
2. Isocyanic acid reacts further with water (contained in the exhaust) by an exothermic hydrolysis reaction yielding ammonia and carbon dioxide:



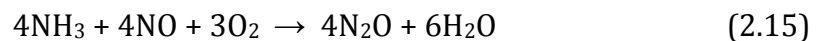
3.  $\text{NO}_x$  is selectively reduced by ammonia to generate nitrogen and water according to the following reactions:



Reaction (2.12) and (2.13) are called the standard SCR and fast SCR reactions respectively. Usually,  $\text{NO}_x$  in exhaust from a diesel engine is composed of NO more than 90% (Koebel et al., 2000); accordingly, the standard SCR is the main reaction for ammonia-SCR. On the other hand, the reaction rate of the fast SCR reaction is much faster than that of the standard SCR reaction. So, to promote the performance of  $\text{NO}_x$  reduction, the fraction of  $\text{NO}_2$  in the exhaust is deliberately increased by placing an oxidation catalyst before the SCR catalyst. Nonetheless, the fraction of  $\text{NO}_2$  to NO should not exceed 1:1 because the reduction of  $\text{NO}_2$  without NO, as shown in Reaction (2.14), is much slower than Reaction (2.12) and (2.13) (Koebel et al., 2000, Chatterjee et al., 2008).



Moreover, it was reported by Koebel et al. that nitrous oxide was found at high temperature ( $>400$  °C) (Koebel et al., 2001), as shown in Reaction (2.15). Nitrous oxide is one of greenhouse gases.



Due to high selectivity and reactivity, urea has been considered as the promising reductant for the SCR of  $\text{NO}_x$  presented in diesel exhaust. However, there are some further problems coming with urea-SCR. The amount of injected urea needs to be precise to maintain the high  $\text{NO}_x$  conversion. If the injection of urea is too high,

excess toxic ammonia produced from urea is released to the atmosphere, known as ammonia slip. Unfortunately, in a light duty engine, load and engine speed vary often and abruptly. To minimise ammonia slip, thus, the sophisticated strategy of urea injection, such as a closed feedback control, is required. Furthermore, a short distance between urea injector and the SCR catalyst leads to short residence times for urea to create ammonia by thermolysis and hydrolysis. Moreover, the high freezing point of the aqueous urea solution ( $\approx 11$  °C) makes its use in winter difficult.

### 2.3.2 Oxygenated Hydrocarbon

As selective reduction agents, oxygenated hydrocarbons such as ethanol, acetone, and propanol provide high conversions of  $\text{NO}_x$  (above 80%) at 250-400 °C even in the presence of 10% water vapour (Miyadera, 1993). By using an alumina-supported silver catalyst, the conversion of NO was in the order of 2-propanol > acetone > ethanol > 1-propanol >> methanol at 350 °C (Miyadera, 1993). Although oxygenated hydrocarbons (i.e. diethyl ether and ethanol) showed higher  $\text{SO}_2$  tolerance than alkanes (i.e. propane) over the alumina-supported silver catalyst (Shimizu et al., 2007b). However, there was a significant formation of undesirable by-products such as nitrous oxide ( $\text{N}_2\text{O}$ ), ammonia ( $\text{NH}_3$ ), acetonitrile ( $\text{CH}_3\text{CN}$ ) and hydrogen cyanide (HCN) (Miyadera, 1997). After studying various oxygenated hydrocarbons as the reductant for  $\text{NO}_x$ -SCR, He et al. concluded that enolic on  $\text{Ag}/\text{Al}_2\text{O}_3$  catalyst was highly active with  $\text{NO} + \text{O}_2$ , resulting in the formation of isocyanate which was the key intermediate species in the SCR of  $\text{NO}_x$ . They also presented that the conversion of  $\text{NO}_x$  to  $\text{N}_2$  by using oxygenated hydrocarbons as the reducing agent was higher than that by using alkanes because surface enolic was

formulated only from the partial oxidation of oxygenated hydrocarbons (Yu et al., 2003, Yu et al., 2004, He and Yu, 2005).

### **2.3.3 Hydrocarbon**

There are difficulties in using urea and oxygenated hydrocarbons in automotive SCR systems, although they have been reported as being highly effective reductants. However, additional on-board reductant storage is inevitable. Furthermore, there is a necessity to build new infrastructures for supplying these reductants. Accordingly, hydrocarbons have been thought to be an alternative reducing agent for the SCR of NO<sub>x</sub> in lean burn engine exhaust. The idea of using hydrocarbons as the reductant is feasible since Iwamoto et al. (Iwamoto, 1990, Iwamoto et al., 1991) and Held et al. (Held et al., 1990) have independently reported that NO<sub>x</sub> reduction under excess oxygen were quite effective on cation-exchange zeolites (e.g. Cu-ZSM-5). Diesel-type fuels (e.g. diesel, synthetic diesel and biodiesel) are considered as the source of active hydrocarbons. So, it is not essential to install an extra tank for containing the reductant. Due to the diesel fuel consisting of a range of hydrocarbons, the systematic investigation into the effect of different hydrocarbons on the SCR activities have been extensively studied. Light hydrocarbons (i.e. propene and propane) have been broadly studied to establish the mechanistic fundamentals of HC-SCR (Meunier et al., 1999, Shimizu et al., 1999, Kameoka et al., 2000, Shimizu et al., 2000a, Shimizu et al., 2001a, Yu et al., 2007, Tamm et al., 2008). Derived from hydrocarbons, intermediate species, such as acetate, nitromethane and isocyanate, have been accepted as the key species for HC-SCR. Nonetheless, when the diesel fuel is employed as the reducing agent, the catalysts are expected to provide high

efficiency by using long-chain hydrocarbons that are already contained in the diesel fuel. Subsequently, heavy hydrocarbons have been considered as the challenged reductants for HC-SCR. Burch and Millington reviewed the performance of supported platinum-group metals for the SCR of NO<sub>x</sub> by hydrocarbons under oxidising conditions (Burch and Millington, 1995). They reported that in general, NO<sub>x</sub> reduction activity increases with an increase in the carbon number of hydrocarbons. Moreover, at the equivalent carbon number, the SCR efficiency increases in the order i-paraffins (alkanes) < aromatics < n-paraffins < olefins (alkenes) ≈ alcohols. Later, the direct variation of the SCR efficiency on the carbon number was advocated by Shimizu et al. (Shimizu et al., 2000b) and Čapek et al. (Čapek et al., 2005). Shimizu, after conducting some kinetic studies of HC-SCR on alumina-supported silver catalysts, reported that the de-NO<sub>x</sub> activity and water tolerance are noticeably increased as the carbon number of alkanes increases. They also proposed that the water vapour, injected to the exhaust, markedly promotes NO<sub>x</sub> reduction because it inhibits the unselective oxidation of hydrocarbons and suppresses the poisoning effect caused by carboxylate and carbonate species. Čapek et al. used an in-situ FTIR technique to compare the effects of decane, propane and propene on the SCR activity. They found that when decane and propene are used as the reactants, the NO<sub>x</sub> reduction activity is increased under increasing concentration of water vapour, while propane gives a lower SCR efficiency. They concluded that decane cracks to low-chain olefins (alkenes) that preferably take part in the SCR of NO<sub>x</sub>.

## **2.4 Catalysts for Selective Catalytic Reduction of NO<sub>x</sub>**

Numerous types of catalysts have been studied to discover the practical HC-SCR catalyst in relation to activity, durability and stability. Ion-exchanged zeolite catalysts (e.g. Cu-ZSM-5) show high performance on the reduction of NO<sub>x</sub> by hydrocarbons in the presence of excess oxygen. In addition, the relatively wide temperature window makes them more attractive. Moreover, in contrast to silver oxide catalysts, the ion-exchanged zeolite gives relatively high NO<sub>x</sub> conversion and this efficiency is not significantly affected by the nature of the reducing agent. Furthermore, it shows high tolerance to catalyst deactivation caused by both sulphur poisoning and coke deposition (Houel et al., 2005). However, their instability under hydrothermal conditions is the most serious problem (Matsumoto, 1996). The reversible loss of the activity under these situations is attributed to the occupation of water on active catalyst sites, resulting in insufficient active sites left for gaseous reactants to be adsorbed (Liu and Woo, 2006). Moreover, the permanent deactivation of the catalyst is due to either metal sintering or zeolite dealumination (Houel et al., 2005). Since the hydrothermal condition is always existent in aftertreatment applications, therefore, the ion-exchanged zeolite is probably unsuitable for the realistic SCR of NO<sub>x</sub> from diesel engines.

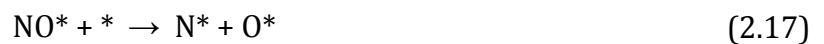
Copper-aluminum oxide catalysts have been tested for the HC-SCR of NO<sub>x</sub>. Shimizu et al. studied various transition metals as the catalyst substance. The Cu-Al<sub>2</sub>O<sub>3</sub> with 16 wt.% Cu content exhibited higher activity than Cu-ZSM-5 at low temperature. Furthermore, the Cu-Al<sub>2</sub>O<sub>3</sub> showed higher hydrothermal stability than Cu-ZSM-5 (Shimizu et al., 1998). After conducting a comparative study of Cu-Al<sub>2</sub>O<sub>3</sub>

and Ag/Al<sub>2</sub>O<sub>3</sub> catalyst for C<sub>3</sub>H<sub>6</sub>-SCR of NO<sub>x</sub>, He et al. discovered that Ag/Al<sub>2</sub>O<sub>3</sub> showed high activity for NO<sub>x</sub> reduction but Cu-Al<sub>2</sub>O<sub>3</sub> showed high activity for unfavourable C<sub>3</sub>H<sub>6</sub> oxidation. They also suggested that the formation of enolic species (the highly active intermediate for HC-SCR) was promoted by silver sites (He et al., 2004).

Platinum-based catalysts have been known as an excellent metal group for NO<sub>x</sub> reduction at low temperature and stability in water and sulphur. Nevertheless, one of their well-known disadvantages is the formation of nitrous oxide, the extremely active greenhouse gas. The formation of N<sub>2</sub>O rather than N<sub>2</sub> (the product derived from NO) varies by the range of 25-80% dependant on the operating condition (Burch and Millington, 1995). The selectivity of NO to N<sub>2</sub>O increases when the inlet NO concentration is increased (Lionta et al., 1996). Moreover, a narrow temperature window for NO<sub>x</sub> reduction, another drawback of the platinum group, makes this catalyst inappropriate for use in light-duty diesel engines where the exhaust temperature varies usually between 200 and 400 °C. Normally, the platinum group metal catalysts show NO<sub>x</sub> reduction activity in the temperature range 200-250 °C (Burch and Millington, 1995, Burch and Ottery, 1997).

Recently, supported silver oxide-based catalysts have been reported as having a high potential ability for HC-SCR of NO<sub>x</sub>. Miyadera first reported alumina-supported silver catalysts giving high performance for SCR of NO<sub>x</sub> when propene and oxygen-containing organic compounds (e.g. ethanol, acetone, 1-propanol and 2-propanol) were used as the reducing agent. Moreover, in the presence of water vapour, the Ag/Al<sub>2</sub>O<sub>3</sub> catalyst also showed high activity, while the conversion of NO<sub>x</sub> to N<sub>2</sub> on Co/Al<sub>2</sub>O<sub>3</sub> and Al<sub>2</sub>O<sub>3</sub> catalysts was considerably decreased (Miyadera, 1993). After studying the influence on C<sub>3</sub>H<sub>6</sub>-SCR performance of silver content in Ag/γ-Al<sub>2</sub>O<sub>3</sub>

catalysts, Meunier et al. reported that the formation of NO<sub>2</sub> and N<sub>2</sub>O and the unselective oxidation of C<sub>3</sub>H<sub>6</sub> were promoted by silver loading (Meunier et al., 1999). They also suggested in detail that the dissociation of NO and recombination of nitrogen adatom with another give N<sub>2</sub> or with surface NO give N<sub>2</sub>O. This NO decomposition-type mechanism is described below:



After the screening of different silver/alumina catalysts for HC-SCR applications, Lindfors et al. concluded that the highest NO to N<sub>2</sub> activity was discovered over catalysts having a silver loading slightly above 2 wt% (Lindfors et al., 2004).

In terms of the effect of sulphur on the activity of silver/alumina catalyst, Meunier and Ross studied the SCR of NO<sub>x</sub> by using C<sub>3</sub>H<sub>6</sub> and NO<sub>2</sub> as the reducing agents and found that when C<sub>3</sub>H<sub>6</sub> was used, the catalyst was rapidly and permanently deactivated by adding SO<sub>2</sub>, while the catalyst deactivation did not observe when NO<sub>2</sub> was employed. Moreover, by using the DRIFTS technique, they reported that aluminium and silver sulphates (formed by chemical reactions of SO<sub>2</sub> with alumina and silver sites, respectively) have been detected on the catalyst surface. The silver sulphate deteriorated the C<sub>3</sub>H<sub>6</sub>-SCR by inhibiting the oxidation of NO (occurring on silver sites) to form ad-NO<sub>x</sub> species (Meunier and Ross, 2000). Later, Satokawa et al. confirmed that silver sulphate was extremely harmful to the C<sub>3</sub>H<sub>8</sub>-SCR activity on the Ag/Al<sub>2</sub>O<sub>3</sub> catalyst (Satokawa et al., 2001). To improve the tolerance of sulphur, it was reported that the Ag/Al<sub>2</sub>O<sub>3</sub> catalyst could be partially regenerated by thermal

decomposition at temperatures higher than 550 °C (Satokawa et al., 2001). Sulphate species could be entirely removed from silver site by calcining the catalyst in 10% H<sub>2</sub>/Ar at 650 °C for 2 hours; so, most of the activity of the fresh catalyst was recovered (Meunier and Ross, 2000). Recently, Shimizu et al. studied the effect of H<sub>2</sub> addition and silver loading on the SO<sub>2</sub> tolerance and de-NO<sub>x</sub> performance of Ag/Al<sub>2</sub>O<sub>3</sub> for the C<sub>3</sub>H<sub>8</sub>-SCR reaction and found that the presence of silver sulphate inhibited the formation of NCO (the crucial intermediate species of HC-SCR) on silver sites, resulting in a decrease in NO<sub>x</sub> reduction efficiency. Furthermore, they proposed that sulphates which are normally adsorbed on silver sites were removed from the catalyst surface by a flow of a H<sub>2</sub>-containing mixture, resulting in the formation of gas-phase SO<sub>2</sub> or migration of the sulphates from silver to alumina sites. Therefore, they concluded that SO<sub>2</sub> tolerance of Ag/Al<sub>2</sub>O<sub>3</sub> for the C<sub>3</sub>H<sub>8</sub>-SCR was improved by H<sub>2</sub> co-feeding and Ag loading increasing (Shimizu et al., 2006a).

In terms of the promotion effect of hydrogen which the mechanistic details will be presented later in Section 2.5, among the silver-based catalyst, Ag/Al<sub>2</sub>O<sub>3</sub> clearly showed a significant increase (from 0 to 36%) in the conversion of NO to N<sub>2</sub> at relatively low temperature (573 K). Interestingly, the promotion effect of hydrogen was not observed over the other Ag-based catalysts (i.e. Ag/TiO<sub>2</sub>, Ag/ZrO<sub>2</sub>, Ag/SiO<sub>2</sub> and Ag/Ga<sub>2</sub>O<sub>3</sub>). Moreover, Co/Al<sub>2</sub>O<sub>3</sub> and Pt/Al<sub>2</sub>O<sub>3</sub> catalysts did not show such a hydrogen effect (Satokawa et al., 2003).

## 2.5 Promotion Effect of Hydrogen on Hydrocarbon-SCR

Hydrogen is widely considered as an ideal co-feeder gas in active mode (i.e. injected HCs) HC-SCR operation in order to decrease the minimum temperature

needed to drive the NO<sub>x</sub>-reducing reactions. Shimizu et al. proposed that the hydrogen effect on hydrocarbon-SCR promotes several processes (Shimizu et al., 2006b, Shimizu et al., 2007a): (1) oxidation of NO to nitrate (Satokawa et al., 2003, Shibata et al., 2003, Sazama et al., 2005); (2) oxidation of NO to NO<sub>2</sub> (Satokawa et al., 2003, Shibata et al., 2003, Sazama et al., 2005, Houel et al., 2007); (3) partial oxidation of hydrocarbon to acetate (Satokawa et al., 2003, Shibata et al., 2003, Sazama et al., 2005); (4) oxidation of hydrocarbon to CO<sub>x</sub> (Shimizu et al., 2006b); (5) oxidation of acetate with NO + O<sub>2</sub> mixture (Satokawa et al., 2003, Shibata et al., 2003); (6) enhancement of rate-determining step (Shibata et al., 2003, Sazama et al., 2005) and (7) prevention active sites from strongly adsorbed species (e.g. nitrates) at low temperature (Shimizu et al., 2006b, Houel et al., 2007, Creaser et al., 2009). Shibata et al. found that the addition of hydrogen resulted in the promotion of hydrocarbon to mainly surface acetate, which is the rate-determining step of hydrocarbon-SCR in the absence of hydrogen (Shibata et al., 2003). Later, Shimizu et al., after conducting some kinetic studies, reported that hydrogen addition results in a decreased activation energy for NO<sub>x</sub> reduction (i.e. the temperature window was shifted towards lower values) (Shimizu et al., 2006b). They also showed that the addition of hydrogen can retard nitrate poisoning by reducing the concentration of nitrates on the catalyst surface, therefore enhancing the HC-SCR reaction dramatically, results that are also supported by Creaser et al. (Creaser et al., 2009). Sazama et al. studied the enhancement of decane-SCR of NO<sub>x</sub> over a silver/alumina catalyst by hydrogen. They published that transformation of intermediate cyanide species (bound on Ag<sup>+</sup> site) into isocyanate (bound on Al site) and oxidation of decane to formate are the surface reaction steps that are enhanced most by the addition of hydrogen to the SCR-NO<sub>x</sub>

reduction (Sazama et al., 2005). By the use of an in-situ UV-vis spectroscopic analysis, the addition of hydrogen was shown to reduce  $\text{Ag}^+$  ions (normally observed in the absence of hydrogen) and produce moderate agglomerated  $\text{Ag}_n^{\delta+}$  clusters that promote the  $\text{NO}_x$  reduction activity generally through the activation of the hydrocarbon (Satokawa et al., 2003, Sazama et al., 2005). Shimizu et al. reasonably assumed that the addition of hydrogen resulted in the formation of hydride on silver clusters, which may react with oxygen to form a reactive oxidant, such as hydroperoxy radical ( $\text{HO}_2$ ), peroxide ( $\text{O}_2^{2-}$ ) or superoxide ions ( $\text{O}_2^-$ ) (Shimizu et al., 2006b). Houel et al. suggested that the addition of hydrogen promotes the formation of  $\text{NO}_2$  over the  $\text{Ag}/\text{Al}_2\text{O}_3$  catalyst, which is very effective in oxidising carbon-rich species formed over the catalyst when diesel fuel or long chain hydrocarbons ( $>\text{C}_{12}$ ) are used as the reductant, thus preventing catalyst deactivation at low temperatures and the high  $\text{NO}_x$  conversion to  $\text{N}_2$  can be maintained (Houel et al., 2007). In the presence of  $\text{H}_2$ , Zhang et al. found gas-phase acetaldehyde and acrolein as partial oxidation products of  $\text{C}_3\text{H}_6$  and gas-phase nitrogen-containing products such as nitromethane. However, these gas-phase products were not detected in the absence of  $\text{H}_2$  (Zhang et al., 2007).

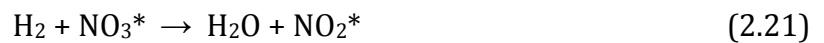
On the one hand, as explained above, hydrogen promotes indirectly the SCR- $\text{NO}_x$  reduction through the changes in some states of the active catalyst but hydrogen itself is not active as it is neither a reducing agent nor an intermediate species. On the other hand, Wichterlová et al. studied the effect of  $\text{H}_2$  and  $\text{CO}$  during the SCR of  $\text{NO}_x$  over a silver/alumina catalyst by using in-situ UV-vis and FTIR spectroscopy techniques. They found that the formation of  $\text{Ag}_n^{\delta+}$  clusters was observed in both  $\text{H}_2$  and  $\text{CO}$  as the co-reductant but the promotion of  $\text{NO}_x$  reduction was found only in the

case of H<sub>2</sub>. They concluded that the promotional effect of H<sub>2</sub> on the NO<sub>x</sub> reduction activity at low temperature did not relate to the formation of Ag<sub>n</sub><sup>δ+</sup> clusters. However, they also suggested that hydrogen itself participates in the NO<sub>x</sub> reduction processes with a chemical function resulting in the acceleration of critical SCR-NO<sub>x</sub> reaction steps (Wichterlová et al., 2005).

The positive effects of hydrogen are generally accepted; however, the mechanistic detail of it for HC-SCR of NO<sub>x</sub> is still ambiguous. From literature, the chemical mechanisms for the SCR of NO<sub>x</sub> in presence of hydrogen were different and based on a range of assumptions. Mhadeshwar et al. incorporated the promotion effect of hydrogen in their microkinetic mechanism via an elementary reaction: formations of adsorbed atomic nitrogen and hydroxyl from surface nitrogen oxide and atomic hydrogen (Mhadeshwar et al., 2009).



Creaser et al. indicated that adsorbed nitrate species poisons the catalytic sites. They proposed the catalytic mechanism by integrating the promotion effect of hydrogen through a chemical transformation from poisonous surface nitrate to highly active nitrogen dioxide (Creaser et al., 2009):



In this work, a detailed multi-step reaction mechanism for HC-SCR is designed under the hypothesis that the presence of hydrogen changes the state of the Ag/Al<sub>2</sub>O<sub>3</sub> catalyst, and so does not chemically react with any other gas-phases or surface species. The mechanism has been validated and optimised by comparison with experimental data.

## **2.6 Modelling Approaches**

Besides experimental studies, theoretical modelling studies can be used as an effective tool to provide knowledge about heterogeneous combustion. Normally, experimental studies are very expensive, while modelling studies need only a proper model formulation and adequate physicochemical data (Canu and Vecchi, 2002). The basic information (e.g. temperatures and gas composition distributions) determined from the modelling is extremely useful in sizing the reactor, understanding its behaviour in operation and predicting the effect of changing operating conditions. Modelling studies have been employed to assist in research and development in the aftertreatment area. Ansell et al. formulated a kinetic model from steady state kinetics data in order to predict diesel lean NO<sub>x</sub> catalyst performance. The numerical modelling shows good agreement between experimental data and simulation results in terms of both hydrocarbon oxidation and NO<sub>x</sub> reduction. Finally, the authors summarised that modelling could be used to optimise hydrocarbon injection strategies with the purpose of maximising NO<sub>x</sub> reduction and minimising fuel penalties (Ansell et al., 1996).

To design a model of a chemical reaction, first, governing equations based on appropriate assumptions are formed to mathematically represent the physical and chemical system. Governing equations are systems of mathematical equations which describes the relationship between the physical and chemical properties controlling the behaviour of a process. In the field of catalytic reactions, these equations are established from the conservation of mass, momentum, species and energy laws as well as from the relationships between the physical and chemical properties.

Governing equations, then, are solved by using computers through a numerical method. In the area of the modelling of catalytic combustion inside a monolith structure, although a monolith channel is in a three-dimensional configuration, the governing equations are generally set up in a form of one-dimensional (1D) or two-dimensional (2D) model (Hayes and Kolaczkowski, 1997). Due to the complication of the model and the requirements of high computer power, three-dimensional (3D) model is infrequently found in practice.

In a 1D model (also known as a plug flow model), fluid properties (e.g. velocity, temperature and concentration) are assumed to be uniform over the channel cross-section. Thus, the gradients of these properties in the radial and angular directions are neglected; the properties are varied only in the axial direction. Since the catalytic reactions take place on the catalyst surface, there is a depletion of reactants, formation of products and consumption/generation of heat at the reacting wall. Due to lack of the variation in radial direction, the transfers of mass and heat between the wall and bulk fluid in such direction are incorporated via mass and heat transfer coefficients, respectively. However, these coefficients are formulated from experimental data combined with theories of mass and heat transfer. Therefore, correlations of mass and heat coefficients found in literature are often inconsistent (Hayes and Kolaczkowski, 1999, Salomons et al., 2004, Dalle Nogare et al., 2008, Santos and Costa, 2009, Creaser et al., 2009).

In contrast to a 1D model, a 2D model integrates the variation effect in the radial direction into its model. As a result, mass and heat transfer coefficients are not required to link the physical and chemical properties between catalyst surface and bulk fluid. Transport phenomena between a reacting wall and bulk fluid can be

carried out autonomously through a boundary layer occurring over such a wall (Hayes and Kolaczowski, 1997).

After conducting comparative studies of three alternate models (i.e. the Navier-Stokes, boundary-layer and plug-flow models) for catalytic combustion in a monolith, Raja et al. reported that the 2D Navier-Stokes model needs very few assumptions and is thus valid in the most general setting; however, this model is computationally expensive. The boundary layer model is a form of two-dimensional governing equations that are formulated to simplify the Navier-Stokes model. Based on the assumption that diffusive transport in an axial direction is ignored, the boundary layer model is significantly simpler than the Navier-Stokes model. The accuracy and computational cost of the boundary layer model are acceptable. The validity of this model is acceptable to high Reynolds numbers ( $Re_d > 20$ ). The plug-flow model is computationally inexpensive but their range of validity is limited to low Reynolds numbers ( $0.02 \ll Re_d \ll 50$ ) (Raja et al., 2000). To formulate the rate expressions and optimise the preexponential factors, however, the catalytic combustion problem has to be solved repeatedly. Due to the short computational time, therefore, the plug-flow model is generally preferable (Westerberg et al., 2003, Tronconi et al., 2005, Mhadeshwar and Vlachos, 2005a, Wurzenberger and Wanker, 2005). Under assumptions that convection is mainly directed parallel to the surface and the diffusive transport, in perpendicular direction, dominates (i.e. high Reynolds numbers), the boundary-layer model can be effectively employed (Koop and Deutschmann, 2009, Hartmann et al., 2010). Although the Navier-Stokes model requires tremendous computational power, it is applied in order to understand in

depth the details of aftertreatment applications because of its robustness (Mladenov et al., 2010).

## **2.7 Microkinetic Analysis**

Commonly in the aftertreatment applications, chemical reactions generally occur on the catalyst surface (called catalytic or heterogeneous reactions) via adsorption, surface reaction and desorption processes. Thermodynamics gives data about the state of the system before and after a reaction, it does not however, provide information about the rate at which a chemical process takes place (Hayes and Kolaczkowski, 1997). A rate of reaction can be shown as an expression which relates the properties of the system, usually temperatures and reactant concentrations, and two or more constants to the reaction. A power law rate expression has regularly been used in a gas phase reaction, also called a homogeneous reaction, as well as a catalytic reaction (Ansell et al., 1996, Wanker et al., 2000, Westerberg et al., 2003, Wurzenberger and Wanker, 2005, Liu et al., 2007). Constant values appearing in this rate expression are normally extracted from experimental data. Since the catalytic reaction occurs on the limited catalyst surface, the rate of reaction is decreased when free active sites are low. However, the rate expression formed by the power law does not include the effect of the catalyst active sites availability on the rate of reaction, resulting in validity over a limited range of operating conditions. Moreover, the power law rate expression needs a lot of experiments to determine constant values. To capture the effect of catalyst surface state, the Langmuir Hinshelwood Hougen Watson (LHHW) rate expression originally based on Langmuir adsorption has been systematically developed and successfully implemented in many catalytic reaction

applications. LHHW kinetic rate expressions are frequently used to model catalytic processes for three-way catalyst (Voltz et al., 1973, Santos and Costa, 2009). Nevertheless, LHHW reaction models require a few assumptions such as a rate-determining step (RDS), most abundant reaction intermediate (MARI), quasi-steady state (QSS) and partial equilibrium (PE). In many applications that involve catalytic reactions, the rate-determining step changes when the operating condition is changed. Therefore, the validity of these assumptions cannot be verified. Like the power law rate expression, the LHHW method requires the input of several data from experiments for model discrimination and parameter estimation (Tufano and Turco, 1993, Hayes et al., 2001).

Microkinetic analysis is the examination of catalytic reactions in terms of elementary chemical reactions that occur on the catalyst surface and their relationship during a catalytic cycle (Dumesic et al., 1993). The aim of the microkinetic approach to a gas/solid catalytic reaction is to correlate the kinetic parameters from both experimental data and theoretical principles for surface elementary steps (adsorption, desorption, Langmuir-Hinshelwood steps) involved in a plausible mechanism of the reaction (Dumesic et al., 1993). Microkinetic analysis has been successfully used by many researchers in an assortment of catalytic combustion applications. Vlachos' research group used microkinetic analysis to establish a variety of catalytic mechanisms such as the oxidation of hydrogen on platinum (Park et al., 1999, Aghalayam et al., 2000), oxidation of methane on platinum (Mhadeshwar et al., 2002, Aghalayam et al., 2003), partial oxidation and reforming of methane on rhodium (Mhadeshwar and Vlachos, 2005a), oxidation of carbon monoxide on platinum (Mhadeshwar and Vlachos, 2005c), water-gas shift

(Mhadeshwar and Vlachos, 2005b) and selective catalytic reduction of  $\text{NO}_x$  on silver (Mhadeshwar et al., 2009). Deutschmann et al. implemented microkinetic analysis to many catalytic processes using a range of hydrocarbons and catalysts (Deutschmann et al., 2000, Chatterjee et al., 2001, Quiceno et al., 2006, Schädel et al., 2009). Storsæter et al. (Storsæter et al., 2006) proposed microkinetic modelling of Fischer-Tropsch synthesis over a cobalt catalyst. In comparison with LHHW rate expressions, microkinetic modelling is valid over a wide range of operating conditions; it does not require assumptions that are necessary for the method of LHHW. Moreover, the rate parameters (i.e. preexponential factor and activation energy) can be independently extracted from experiments or estimated by theories of chemical bonding rather than fitted from experimental data (Dumesic et al., 1993).

## **2.8 Summary**

There are currently two main alternative catalyst concepts for lean  $\text{NO}_x$  reduction:  $\text{NO}_x$  storage catalyst and selective catalytic reduction. SCR of  $\text{NO}_x$  can be classified into three categories by the type of reductant, i.e., ammonia-SCR, oxygenate hydrocarbon-SCR and hydrocarbon-SCR. Of these alternatives, hydrocarbon-SCR is the least efficient but has practical advantages in terms of implementation, engine operation, cost and sometimes durability. A number of catalysts have been tested in the HC-SCR; however, to date no catalyst seems to be suitable for the reduction of  $\text{NO}_x$  from diesel engines (Shimizu and Satsuma, 2006). Under diesel engine operating conditions, the catalysts are necessitated to be stable hydrothermally in the presence of  $\text{SO}_x$  and water vapour and active at a range of temperatures.  $\text{NO}_x$  storage catalysts are unlikely to be suitable as an automotive application due to its instability under

hydrothermal condition. Pt-based catalysts appear to offer the best low temperature activity and are resistant to water and SO<sub>x</sub> poisoning. However, the formation of N<sub>2</sub>O and a narrow temperature region for NO reduction are two major disadvantages. Alumina-supported silver catalysts, which have been reported to have moderate tolerance to water and SO<sub>2</sub>, are considered to be another candidate for practical use. Several reports on engine bench tests demonstrated the potential of Ag/Al<sub>2</sub>O<sub>3</sub> in practical applications. Nevertheless, one of important problems of Ag/Al<sub>2</sub>O<sub>3</sub> is that high temperatures are required to maintain high NO<sub>x</sub> reduction activity. To overcome this problem, hydrogen used with SCR of NO<sub>x</sub> as the co-feeding reductant in order to shift the operating temperature to a lower region. The HC-SCR performance of supported silver catalysts is known to be very sensitive to the reaction conditions, especially the type of hydrocarbons and the addition of H<sub>2</sub>. So, the control of reaction conditions would be crucial for practical use (Shimizu and Satsuma, 2006).

## CHAPTER 3

### EXPERIMENTAL FACILITIES

The experimental facility used for optimising and validating the modelling is introduced in this chapter. This includes the SCR catalyst specification, the experimental setup and the exhaust gas analysis and measuring equipment. A detail of how experimental conditions were set up during the experiments is also presented.

#### 3.1 SCR Monolithic Catalyst

A silver catalyst 2 wt.% (supplied by Johnson Matthey Plc) was prepared by impregnating  $\gamma$ -alumina (surface area  $\sim 150 \text{ m}^2/\text{g}$ ) with aqueous  $\text{AgNO}_3$  before drying and calcining in air for 2 hours at  $500 \text{ }^\circ\text{C}$ . The catalyst was made into an aqueous suspension, which was then uniformly coated onto ceramic monolith substrates with cell density 400 cpsi. The dimensions, given as diameter  $\times$  length, of the catalyst used for the experiments were  $24 \text{ mm} \times 25 \text{ mm}$  with a wall thickness  $0.152 \text{ mm}$ . The specifications of monolith are summarised in Table 3.1.

**Table 3.1:** The specification of the monolithic automotive catalytic converter.

Parameter	Unit	Value
Diameter	mm	24
Length	mm	25
Support		Cordierite
Cell shape		Square
Cell density	cpsi	400
Wall thickness	mm	0.152
Washcoat thickness	mm	0.025
Hydraulic diameter	mm	1.068
Open frontal area	%	70.72
Geometric surface area	$\text{m}^2\text{m}^{-3}$	2649

### 3.2 Experimental Setup

The schematic system which was used in order to provide the experimental data for optimisation and validation purposes is shown in Figure 3.1. Simulated engine exhaust gas compositions were generated from bottled gases. The specification of each bottled gas was: 20% propane in nitrogen, 1% nitric oxide in nitrogen, high purity hydrogen (>99%), 93% oxygen in nitrogen and high purity nitrogen as a balance gas. Due to the small amount of propane, nitric oxide and hydrogen in simulated exhaust, the quantities of these gases were controlled through high precision metering valves.

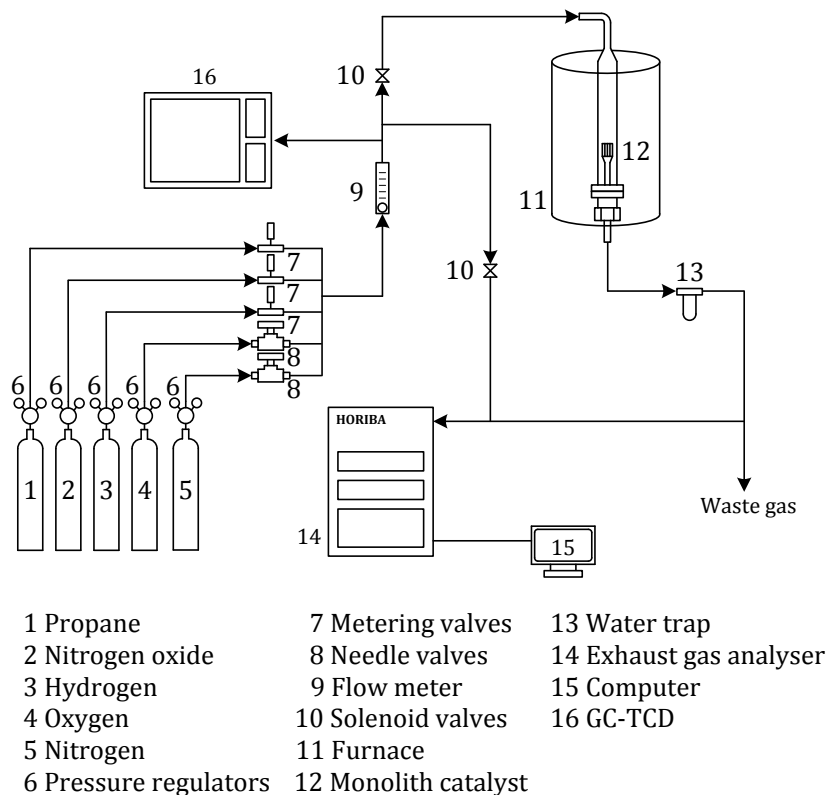


**Figure 3.1:** The simplified schematic of the monolithic reactor system.

The monolithic catalyst was installed in a quartz-tube reactor; then, heated using a tubular furnace. Its temperature was set to simulate the engine-out exhaust at

different loads and speeds and monitored through a K-type thermocouple positioned at the inlet of the reactor, 5 mm upstream of the catalyst bed.

### 3.3 Exhaust Gas Analysis and Measuring Equipment

A special technique and analyser was used to measure gaseous components. The exhaust gas analysers used in the experimental phase are presented below detailing the method they were used to measure.

#### 3.3.1 Gas Analyser

A Horiba Mexa 7100DEGR analyser was employed to measure the concentrations of NO<sub>x</sub> (NO + NO<sub>2</sub>) by heated vacuum-type chemiluminescence detection (CLD); CO and CO<sub>2</sub> by non-dispersive infrared (NDIR); O<sub>2</sub> by a magneto-pneumatic detection (MPD) method and C<sub>1</sub> hydrocarbons (HCs) by flame ionization detection (FID). The measuring range, resolution and accuracy of the equipment are listed in Table 3.2.

**Table 3.2:** Technical data for the Horiba Mexa 7100DEGR analyser

Species	Range	Resolution	Noise <sup>a</sup>
CO	Min. range 0 – 100 ppm	1 ppm	± 1% FS <sup>b</sup>
	Max. range 0 – 12% vol	0.01%	
CO <sub>2</sub>	Min. range 0 – 5000 ppm	1 ppm	± 1% FS
	Max. range 0 – 20% vol	0.01%	
THC	Min. range 0 – 10 ppm C <sub>1</sub>	1 ppm	± 1% FS
	Max. range 0 – 50000 ppm C <sub>1</sub>		
O <sub>2</sub>	Min. range 0 – 5% vol	0.01%	± 1% FS for zero
	Max. range 0 – 25% vol		± 1.5% FS in measurement
NO/NO <sub>x</sub>	Min. range 0 – 10 ppm	1 ppm	< 20 ppm: ± 1.5% FS
	Max. range 0 – 10000 ppm		> 20 ppm: ± 1% FS

<sup>a</sup> Peak to peak width in 5 min

<sup>b</sup> Full scale measurement

### **3.3.2 Gas Chromatograph - Thermal Conductivity Detector (GC-TCD)**

The concentration of hydrogen in ppm were measured before the monolithic SCR catalyst using a Hewlett-Packard (HP) gas chromatograph (GC) model 5890 Series II, integrated with a thermal conductivity detector (TCD) and a HP integrator model 3395. The GC contained a temperature-controlled oven where a packed column was installed. The column was a 2 metre long 1/8 inch diameter Molesieve 5Å (MS5A) for the H<sub>2</sub> separation. Certified span gas 30% H<sub>2</sub> in N<sub>2</sub> was applied for GC calibration. Higher TCD sensitivity to hydrogen was achieved by using argon as the carrier gas since argon's thermal conductivity (0.024 W/(m·K)) is less similar to that of hydrogen (0.223 W/(m·K)) compared with other typical carrier gases such as helium (0.17 W/(m·K)) and nitrogen (0.0312 W/(m·K)).

## **3.4 Experimental Conditions**

The gaseous reactant compositions at the inlet of the reactor was 2000-4000 ppm total hydrocarbon (THC), 200-600 ppm NO, 12% O<sub>2</sub>, 0% H<sub>2</sub>O, 0% CO<sub>2</sub>, 0 ppm CO and N<sub>2</sub> (balance) at 15 litre/minute (~80000 h<sup>-1</sup> space velocity). All of the tests were performed with 600 ppm hydrogen addition. The exhaust temperature at the inlet of the reactor was kept in the range of 250-370 °C (controlled by the furnace). All experimental conditions are detailed in Table 3.3.

**Table 3.3:** Experimental conditions used in the optimisation and validation of the model.

Experimental condition	Inlet temperature (°C)	Inlet THC (ppm C <sub>1</sub> )	Inlet NO (ppm)
1	250	1758	200
2	250	2111	418
3	250	2116	601
4	250	4135	202
5	250	4287	395
6	250	4253	604
7	290	1719	198
8	290	1841	399
9	290	1892	626
10	290	3934	209
11	290	3982	403
12	290	4027	603
13	370	2146	197
14	370	2104	413
15	370	2250	597
16	370	4007	199
17	370	3912	416
18	370	3911	605

## CHAPTER 4

### GOVERNING EQUATIONS AND NUMERICAL METHOD

In this chapter, the assumptions used in this research in order to mathematically simplify the modelling of the catalytic reduction of  $\text{NO}_x$  are given. The governing equations as well as boundary conditions are outlined. The method employed to numerically solve the mentioned governing equations is presented.

#### 4.1 Assumptions

A monolith type of automotive catalytic converter consists of hundreds of parallel channels, as shown in Figure 4.1. Each channel within the monolith shares the same behaviours such as transport and chemical properties, velocity, temperature and concentration profiles; so a single channel can be assumed to be representative of the entire monolith. While the square cross-section channel is rounded by the washcoat at corners of channel, the single channel can be modelled in two dimensions by considering the channel as tubular. Due to no temperature gradient between individual channels, the single channel is considered to be under adiabatic condition. Usually, the automotive monolith is made from low heat conduction material, ceramic in general; as a result thermal conduction in walls is negligible. In aftertreatment application, since temperature is moderately high and small residence times of the exhaust gas within the monolith for common operating conditions, a homogeneous gas phase reaction is neglected. The engine exhaust is assumed to be an ideal gas because it is not only moderately high temperature but also low pressure, mostly atmospheric. Normally, Reynolds number based on channel diameter and inlet flow

condition in aftertreatment system does not exceed 2300; thus flow is classified as laminar flow.

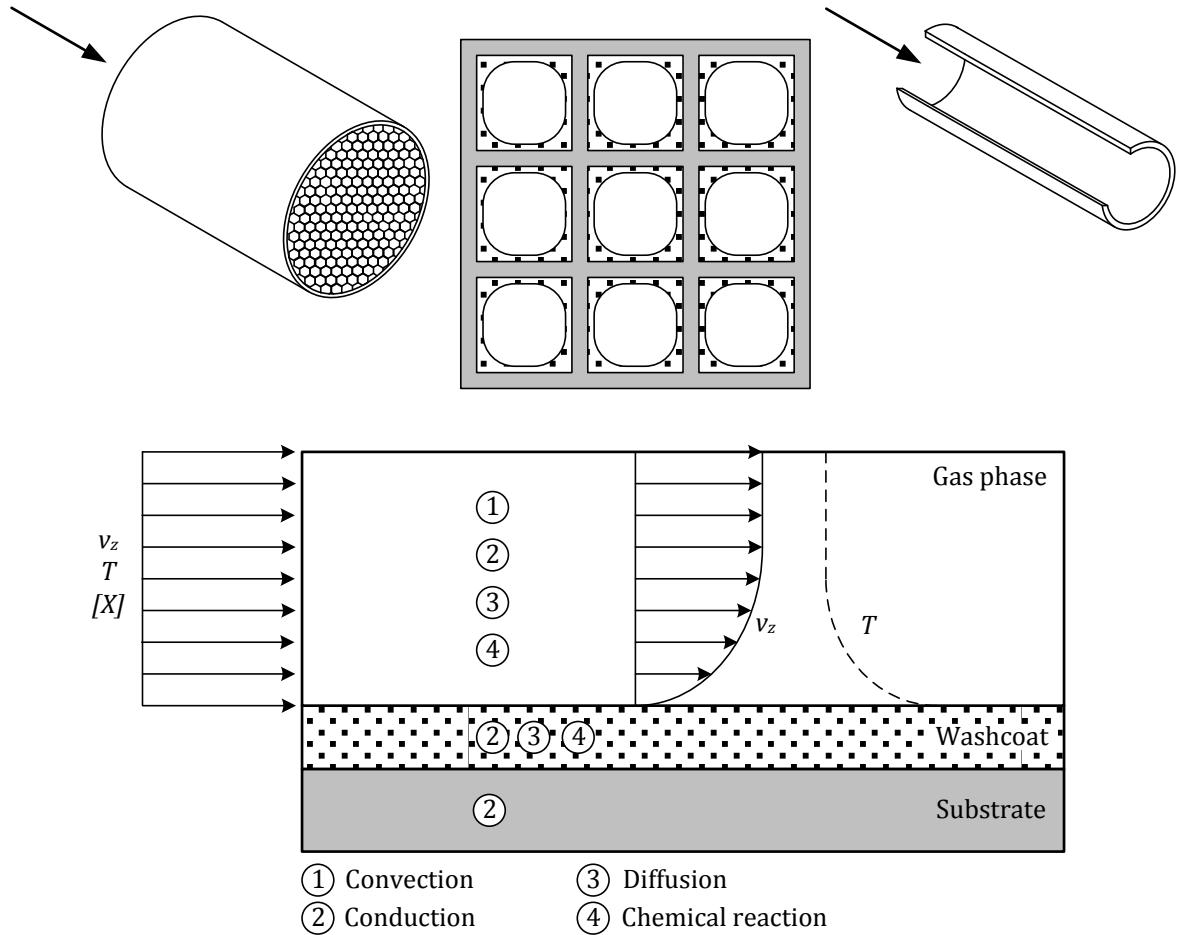


**Figure 4.1:** Illustration of the structure of the monolithic catalyst and the transport and catalysis phenomena occurring inside a channel.

## 4.2 Governing Equations

In this thesis, the two-dimensional Navier-Stokes model established from the conservation laws is selected as the model in order to simulate  $C_3H_8$ -SCR of  $NO_x$ . The mass continuity equation, Equation (4.1), is used to ensure that the mass going into the channel is equal to the mass going out of the channel. Axial and radial momentum equations, as illustrated in Equation (4.2) and (4.3), that are formulated based on the

conservation of momentum, are employed to calculate velocities in axial,  $v_z$ , and radial,  $v_r$ , directions. The concentration of gas-phase species  $i$ ,  $Y_i$ , is determined by using the species continuity equation. This equation, as presented in Equation (4.4), is established from the conservation of species. Developed based on the conservation of energy, the thermal energy equation, as shown in Equation (4.5), is applied to uncover the profile of temperature,  $T$ , inside the channel. The diffusive mass flux ( $J_{i,z}$  and  $J_{i,r}$ ) as demonstrated in Equation (4.6), represents the flux goes from regions of high concentration to regions of low concentration. Density,  $\rho$ , is calculated via the ideal gas law, called equation of state, as illustrated in Equation (4.7).

*Mass Continuity Equation*

$$\frac{\partial}{\partial z}(\rho v_z) + \frac{1}{r} \frac{\partial}{\partial r}(r \rho v_r) = 0 \quad (4.1)$$

*Axial Momentum Equation*

$$\begin{aligned} \rho v_z \frac{\partial v_z}{\partial z} + \rho v_r \frac{\partial v_z}{\partial r} \\ = -\frac{\partial P}{\partial z} + \frac{\partial}{\partial z} \left[ 2\mu \frac{\partial v_z}{\partial z} - \frac{2}{3}\mu \left( \frac{\partial v_z}{\partial z} + \frac{1}{r} \frac{\partial (r v_r)}{\partial r} \right) \right] \\ + \frac{1}{r} \frac{\partial}{\partial r} \left[ \mu r \left( \frac{\partial v_r}{\partial z} + \frac{\partial v_z}{\partial r} \right) \right] \end{aligned} \quad (4.2)$$

*Radial Momentum Equation*

$$\begin{aligned}
 \rho v_z \frac{\partial v_r}{\partial z} + \rho v_r \frac{\partial v_r}{\partial r} &= -\frac{\partial P}{\partial r} + \frac{\partial}{\partial z} \left[ \mu \left( \frac{\partial v_r}{\partial z} + \frac{\partial v_z}{\partial r} \right) \right] \\
 &+ \frac{\partial}{\partial r} \left[ 2\mu \frac{\partial v_r}{\partial r} - \frac{2}{3}\mu \left( \frac{\partial v_z}{\partial z} + \frac{1}{r} \frac{\partial (rv_r)}{\partial r} \right) \right] + \frac{2\mu}{r} \left[ \frac{\partial v_r}{\partial r} - \frac{v_r}{r} \right]
 \end{aligned} \tag{4.3}$$

*Species Continuity Equation*

$$\rho v_z \frac{\partial Y_i}{\partial z} + \rho v_r \frac{\partial Y_i}{\partial r} = \frac{\partial J_{i,z}}{\partial z} + \frac{1}{r} \frac{\partial (rJ_{i,r})}{\partial r} + R_i, \quad (i = 1, \dots, N_g) \tag{4.4}$$

*Thermal Energy Equation*

$$\begin{aligned}
 \rho C_P \left( v_z \frac{\partial T}{\partial z} + v_r \frac{\partial T}{\partial r} \right) &= \left( v_z \frac{\partial P}{\partial z} + v_r \frac{\partial P}{\partial r} \right) + \frac{\partial}{\partial z} \left( \lambda \frac{\partial T}{\partial z} \right) + \frac{\partial}{\partial r} \left( r\lambda \frac{\partial T}{\partial r} \right) \\
 &- \sum_{i=1}^{N_g} C_{P,i} \left( J_{i,z} \frac{\partial T}{\partial z} + J_{i,r} \frac{\partial T}{\partial r} \right) - \sum_{i=1}^{N_g} h_i R_i
 \end{aligned} \tag{4.5}$$

*Diffusive Mass Flux*

$$\begin{aligned}
 J_{i,z} &= -\rho D_{i,B} \frac{\partial Y_i}{\partial z} \\
 J_{i,r} &= -\rho D_{i,B} \frac{\partial Y_i}{\partial r}
 \end{aligned} \tag{4.6}$$

*Equation of State*

$$P = \frac{\rho RT}{M} \tag{4.7}$$

### Diffusion Coefficient

The molecular diffusion coefficient of species  $i$  diffusing in the mixture of  $i$  and  $B$ ,  $D_{i,B}$ , are estimated by the method of Fuller, Schettler and Giddings (Reid et al., 1977) for binary gas systems at low pressure. The empirical correlation suggested is explained in Equation (4.8).

$$D_{i,B} = \frac{10^{-7} T^{1.75} [(M_i + M_B) / M_i M_B]^{0.5}}{P [(\Sigma v)_i^{1/3} + (\Sigma v)_B^{1/3}]^2} \quad (4.8)$$

The temperature is in the unit of Kelvin and pressure is in the unit of atmosphere. The diffusion volumes,  $\Sigma v$ , for simple molecules and diffusion-volume increments,  $v$ , used to calculate diffusion volumes are listed in Table A.3 and A.2, respectively. In aftertreatment application, the main gas component in the exhaust gas is nitrogen. Therefore nitrogen is assumed to be species  $B$  appearing in the above equation. The polynomial function with temperature for molecular diffusion coefficient of species  $i$  diffusing in the mixture of  $i$  and nitrogen,  $D_{i,N_2}$ , are listed in Table A.4.

### Viscosity and Thermal Conductivity

The viscosity,  $\mu$ , and thermal conductivity,  $\lambda$ , of the mixture are computed by using the kinetic theory of gas (Fluent Inc., 2006), as shown in Equation (4.9) and (4.10).

$$\mu = 2.67 \times 10^{-6} \frac{\sqrt{MT}}{\sigma^2 \Omega_\mu} \quad (4.9)$$

$$\lambda = \frac{15 R}{4 M} \mu \left[ \frac{4 C_p M}{15 R} + \frac{1}{3} \right] \quad (4.10)$$

where

$$\Omega_\mu = \Omega_\mu(T^*)$$

$$T^* = \frac{T}{(\epsilon/k_B)}$$

The Lennard-Jones potential parameters,  $\sigma$  and  $\epsilon/k_B$ , are listed in Table A.1.

### *Specific Heat Capacity*

The specific heat capacity at constant pressure,  $C_p$ , of each species is fitted as a polynomial function of temperature, listed in Table A.5.

## **4.3 Boundary Conditions**

The boundary condition at a reactive wall is the most important part in the application of heterogeneous combustion simulation. A detailed multi-step reaction mechanism based on microkinetic analysis as shown later in Table 5.1 is applied as the reacting wall boundary in order to model the surface chemistry occurring on the catalyst surface. The diffusive mass flux of gas-phase species  $i$  at the reactive wall,  $J_{i,r=R}$  is calculated through the net rate of production/depletion of species  $i$ ,  $\dot{s}_i$ :

$$J_{i,r=R} = \dot{s}_i M_i \quad (4.11)$$

The net rate of production/depletion of species  $i$  used in the above equation is computed from Equation (5.1). For other boundary conditions, the flow enters the computational domain with known velocities, gas compositions and temperatures. A uniform axial velocity of 0.6 m/s and a zero radial velocity are specified at the inlet boundary. At the exit of the computational domain, an outlet boundary is set by atmospheric pressure. At the channel centreline, a symmetry boundary condition is applied.

#### 4.4 Numerical Method

The computational domain was created by using mesh generation software, GAMBIT. In the axial direction, the geometry was uniformly divided into 400 control volumes. In the radial direction, the domain was separated into 20 uneven control volumes. With the purpose of capturing the high gradient region, these control volumes were forced to be fine near to the reacting wall boundary. The computational domain used in this thesis is shown in Figure 4.2.

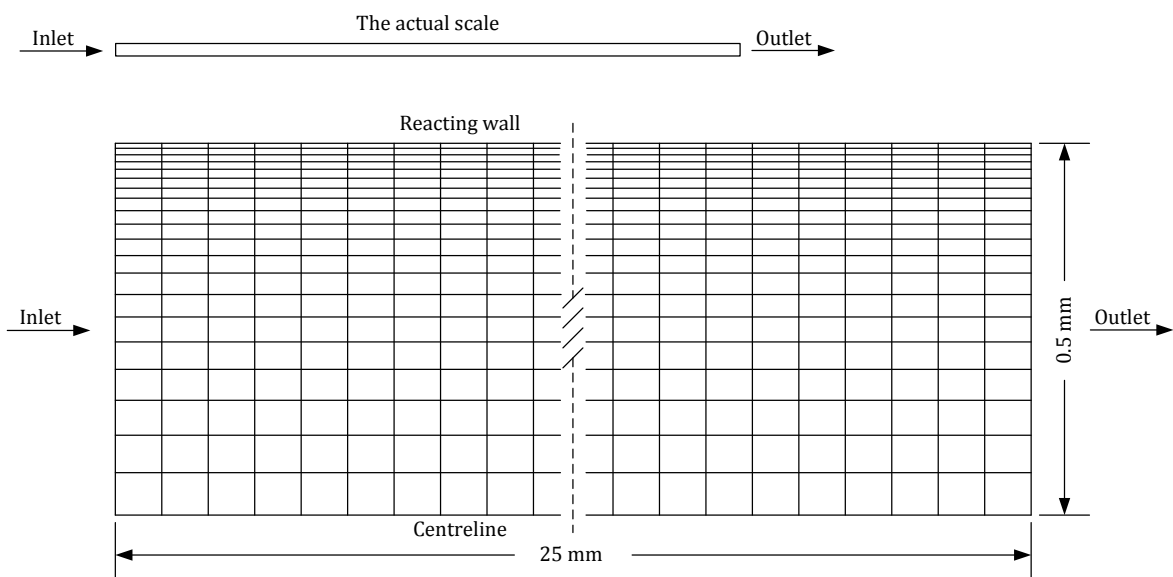


**Figure 4.2:** The actual scale and rectangular structured grids of the single channel.

The governing equations that cannot be analytically solved are numerically solved by FLUENT version 6.3. FLUENT is a commercial numerical method software which is developed based on a finite volume approach in order to solve a system of partial differential equations especially in fluid dynamic problems. The second order upwind is used as the numerical scheme for the convection term in order not only to identify flow direction but also maintain second order accuracy. The SIMPLE is selected as an algorithm for the calculation of pressure. It was originally developed by

Patankar to couple velocities and pressure together; then a guess-and-correct procedure is imposed to iteratively compute the right pressure (Patankar, 1980). The acronym SIMPLE stands for Semi-implicit method for pressure-linked equations. The detailed reaction mechanism is enforced into FLUENT by using the built-in surface reaction module.

## CHAPTER 5

### MICROKINETIC MODELLING

In this chapter, the fundamentals of the microkinetic modelling applied in this work are provided. The procedure to construct the detailed reactions mechanism is described. The methodologies to estimate reaction rate constants and activation energies are also explained.

A microkinetic mechanism of  $C_3H_8$ -SCR on a silver catalyst is constructed based on the hierarchical multiscale approach which was originally developed by the Vlachos research group (Aghalayam et al., 2000, Mhadeshwar and Vlachos, 2005b), outlined in Figure 5.1. A chemically mechanistic understanding of HC-SCR such as intermediate surface species is taken from the literature; then, all possible elementary reaction steps are formed. Reaction rate constants for the adsorption process are computed by using the knowledge about surface science such as sticking coefficient. For desorption processes or surface reactions, rate constants are estimated by using an order of magnitude obtained from transition state theory (TST). Activation energies and heats of reaction are determined through heats of adsorption that can be calculated by using the theory of Unity Bond Index-Quadratic Exponential Potential (UBI-QEP), the theory originally established by Shustorovich et al. (Shustorovich and Sellers, 1998, Sellers and Shustorovich, 2002, Shustorovich and Zeigarnik, 2003). The initial surface reaction mechanism is used as the reacting wall boundary condition in a CFD solver to initially predict different types of experimental data. Sensitivity analysis (SA), then, is applied in order to identify the important elementary reaction steps for different operating conditions. Finally, preexponential

factors of these crucial reaction steps are optimised by using the solution mapping method with the purpose of fitting simulated results with data from experiments.

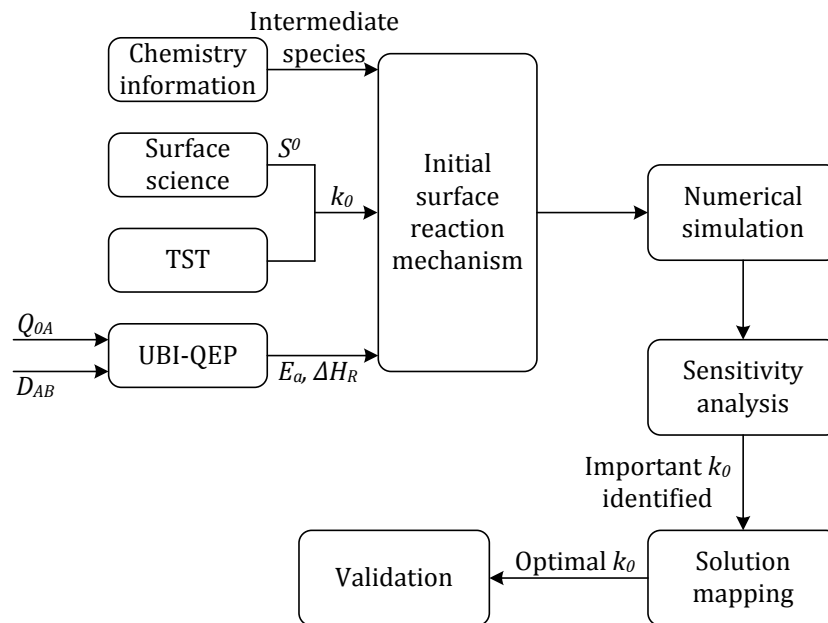


**Figure 5.1:** Methodology for microkinetic analysis development of propane-SCR on a silver catalyst. (Adapted from reference (Aghalayam et al., 2000).)

## 5.1 C<sub>3</sub>H<sub>8</sub>-SCR Microkinetic Mechanism Development

Numerical simulation of complex reactive flow requires as an input a valid chemical reaction model, or a reaction mechanism. The reaction mechanism is a sequence of elementary steps that attempt to explain, at a molecular level, the chemical behaviour in which the catalytic reaction takes place. The validity of an elementary step in the mechanism often contributes to the number of chemical bonds broken and formed. Usually the elementary reaction and its rate parameters are collected from literature. Due to a lack of information about primary intermediates derived from hydrocarbon of HC-SCR on a silver catalyst, this information is taken from the literature which relates to the reaction pathway for the catalytic oxidation of

propane. In the partial oxidation of propane and propylene on mixed metal oxide catalysts, as described in a review work by Bettahar et al. (Bettahar et al., 1996), i-propanol ( $C_3H_7OH$ ), also known as 2-propanol, could be formed from the partial oxidation of propane. In addition, i-propanol was found as the initial intermediate produced from propane by many researchers (Lin et al., 2000, Luo et al., 2001, Yi et al., 2007).

Acetaldehyde ( $CH_3CHO$ ) was usually found as the intermediate species in the selective reduction of  $NO_x$  by using oxygenate fuels as a reducing agent. (Chafik et al., 1998, Yu et al., 2003, Yu et al., 2004, Yeom et al., 2004, Yeom et al., 2006, Yeom et al., 2007, Yeom et al., 2008). Furthermore, acetaldehyde was also observed in the  $C_3H_6$ -SCR with the promotion of hydrogen on an  $Ag/Al_2O_3$  catalyst (Zhang et al., 2007). Moreover, acetaldehyde was also created by the reaction of ethanol with  $O_2$  and/or  $NO_2$ ; then oxidised to form acetate (Yeom et al., 2007).

Produced via the partial oxidation of hydrocarbons, acetate ( $CH_3COO$ ) is generally considered as the key intermediate surface species in the selective reduction of  $NO_x$  over silver/alumina catalysts (Shimizu et al., 1999, Shimizu et al., 2001b, Burch et al., 2002, Shimizu and Satsuma, 2006, Yu et al., 2007). Nevertheless, acetate is rarely activated by  $NO$  or  $O_2$  but easily consumed in a  $NO + O_2$  mixture, probably nitrates (Shimizu et al., 2001b). Shimizu et al. found that the consumption rate of acetate in a mixture of  $NO$  and  $O_2$  showed the same order of magnitude as the conversion rate of  $NO$  to  $N_2$ . Therefore, they summarised that acetate was active as a reductant and took part in the  $N_2$  formation through the reaction with a  $NO + O_2$  mixture, possibly nitrates (Shimizu et al., 1999). Later, Shibata et al., after studying some experiments of HC-SCR on silver/alumina catalyst, suggested that the formation

of surface acetate which was derived from partial oxidation of various hydrocarbons by oxygen was the rate-determining step, regardless of the promoting effect by hydrogen (Shibata et al., 2003).

Nitrates ( $\text{NO}_3$ ) are considered as one of the most crucial intermediates in the initial stage of the HC-SCR reaction. The accumulation on the catalyst surface of nitrates proceeds by NO oxidation to  $\text{NO}_2$  then adsorption of  $\text{NO}_2$  on surface oxygen species (Shimizu and Satsuma, 2006). Monodentate, bidentate and bridging are general types of nitrate which are found as a surface species during HC-SCR processes. Kameoka et al. studied the role of surface nitrates by in situ diffuse reflectance infrared Fourier transform (DRIFT) spectroscopy and temperature-programmed desorption (TPD) techniques. They reported that the reactivity with organic nitro compounds to form surface isocyanate species of the monodentate nitrate was higher than that of the bidentate and bridging nitrate (Kameoka et al., 2000). Furthermore, they also found that adsorbed NO and  $\text{NO}_2$  were hardly observed on the surface of catalyst. At high NO concentration or low temperature, nitrates act like inhibitor in  $\text{NO}_x$  reduction activity by strongly adsorbing on the catalyst surface (Shimizu et al., 2001b).

In the selective catalytic reduction of  $\text{NO}_x$ , isocyanate (NCO) and cyanide (CN) are widely accepted as key intermediates in HC-SCR (Kameoka et al., 1998, Shimizu et al., 2001b, Burch et al., 2002, Bion et al., 2003, Tamm et al., 2008). The creation of isocyanate species is believed to form from stored surface N-containing species (probably nitrate) and stored surface C-containing species (probably acetate) (Shimizu et al., 2001b, Tamm et al., 2008). Moreover, Bion et al. studied the formation of isocyanate from the reaction between isotope  $\text{C}^{18}\text{O}$  and  $\text{N}^{16}\text{O}$  and concluded that on

Ag/Al<sub>2</sub>O<sub>3</sub> isocyanate species were not formed by a linkage of CO molecules to surface nitrogen species due to the dissociation of NO (Bion et al., 2003). In terms of the consumption, surface isocyanate species are consumed by (1) O<sub>2</sub> (Kameoka et al., 1998, Shimizu et al., 2001b), (2) a mixture of NO and O<sub>2</sub> (Kameoka et al., 1998, Shimizu et al., 2001b) and (3) water via the hydrolysis process (Bion et al., 2003, Tamm et al., 2008). Furthermore, Kameoka et al. investigated the effect on the conversion of NO<sub>x</sub> to N<sub>2</sub> of the quantity of silver coated on the Ag/Al<sub>2</sub>O<sub>3</sub> catalysts (Kameoka et al., 1998). They proposed that the reactivity of surface isocyanate with O<sub>2</sub> proceeded only in the presence of silver, while that with a mixture of NO and O<sub>2</sub> (possibly NO<sub>2</sub>) carried on both in the presence and absence of silver. Interestingly, on the catalysts exposed by silver, the total amount of N<sub>2</sub> formation almost equalled the summation of the N<sub>2</sub> formation from two surface reactions; (1) the reaction between surface isocyanate and O<sub>2</sub> occurring on silver sites and (2) the reaction of surface isocyanate with NO + O<sub>2</sub> happening on Al<sub>2</sub>O<sub>3</sub> sites. In addition, the reaction rate of the former was higher than the latter; this indicated that on most of the surface isocyanate species were consumed by O<sub>2</sub> on the silver sites. On the other hand, surface isocyanate species are rapidly consumed by water, to produce gas-phase ammonia (NH<sub>3</sub>) and CO<sub>2</sub>. Ammonia, then, reacts rapidly with gas-phase NO<sub>x</sub> or surface nitrates (and nitrites) to produce N<sub>2</sub> (Tamm et al., 2008, Bion et al., 2003). Yeom et al. studied ethanol-SCR of NO<sub>x</sub> over various silver based catalysts. Using an isotropic experimental technique, they found that most of the carbon atoms in the isocyanate came from the methyl carbon of ethanol (Yeom et al., 2007).

In terms of surface cyanide species, Bion et al. have concluded that cyanide species are the precursor of isocyanate. Cyanide species are derived from

hydrocarbon, ethanol in this case, then isomerised to surface isocyanides after that reacted by oxygen to form surface isocyanate (Bion et al., 2003). Cyanide is also quickly converted to isocyanate after reacting with water on a silver/ $\gamma$ - $\text{Al}_2\text{O}_3$  catalyst (Yeom et al., 2007).

Mhadeshwar et al. proposed the mechanism of HC-SCR by using both intermediate species and reaction pathways based on ethanol-SCR; first, all types of hydrocarbons are oxidised to ethoxy radical. Then, ethoxy radical is split into two major pathways; one oxidise to acetaldehyde and another one to ethylene. Ethylene is oxidised to carbon dioxide; however, acetaldehyde is used as a reducing agent in order to convert NO to  $\text{N}_2$  (Mhadeshwar et al., 2009). In this thesis, the pathway of the  $\text{C}_3\text{H}_8$ -SCR on a silver based catalyst is shown in Figure 5.2. The main chemical reaction pathways of HC-SCR are complete oxidation of hydrocarbons and selective reduction of  $\text{NO}_x$  by oxygenated species that are produced from the hydrocarbons. On the basis of complete oxidation pathway, methoxy radical which is variously derived from i-propoxy radical, acetate and acetyl radical is the essential intermediate species for this process. Methoxy radical can be oxidised by oxygen to generate water vapour directly. Along with water vapour formation, carbon dioxide is indirectly produced from methoxy radical via formyl radical. In terms of the selective reduction of  $\text{NO}_x$  route, nitromethane is the first intermediate which contains both carbon and nitrogen species. Nitromethane is created by either the reaction between surface acetate and nitrogen dioxide or the reaction of surface acetylene radical and nitrate. Both surface acetate and acetylene radical are derivative products generated from the same source, acetaldehyde. Acetaldehyde appears as the surface intermediate species which is produced from propane by oxidation processes via i-propanol and i-propoxy

radical species. Once nitromethane is formed, it is further chemically converted to nitrogen through nitromethylene, formaldiminoxy, nitrile N-oxide, cyanide and isocyanate respectively. The detailed elementary reaction mechanism for C<sub>3</sub>H<sub>8</sub>-SCR on the silver catalyst is presented in Table 5.1.

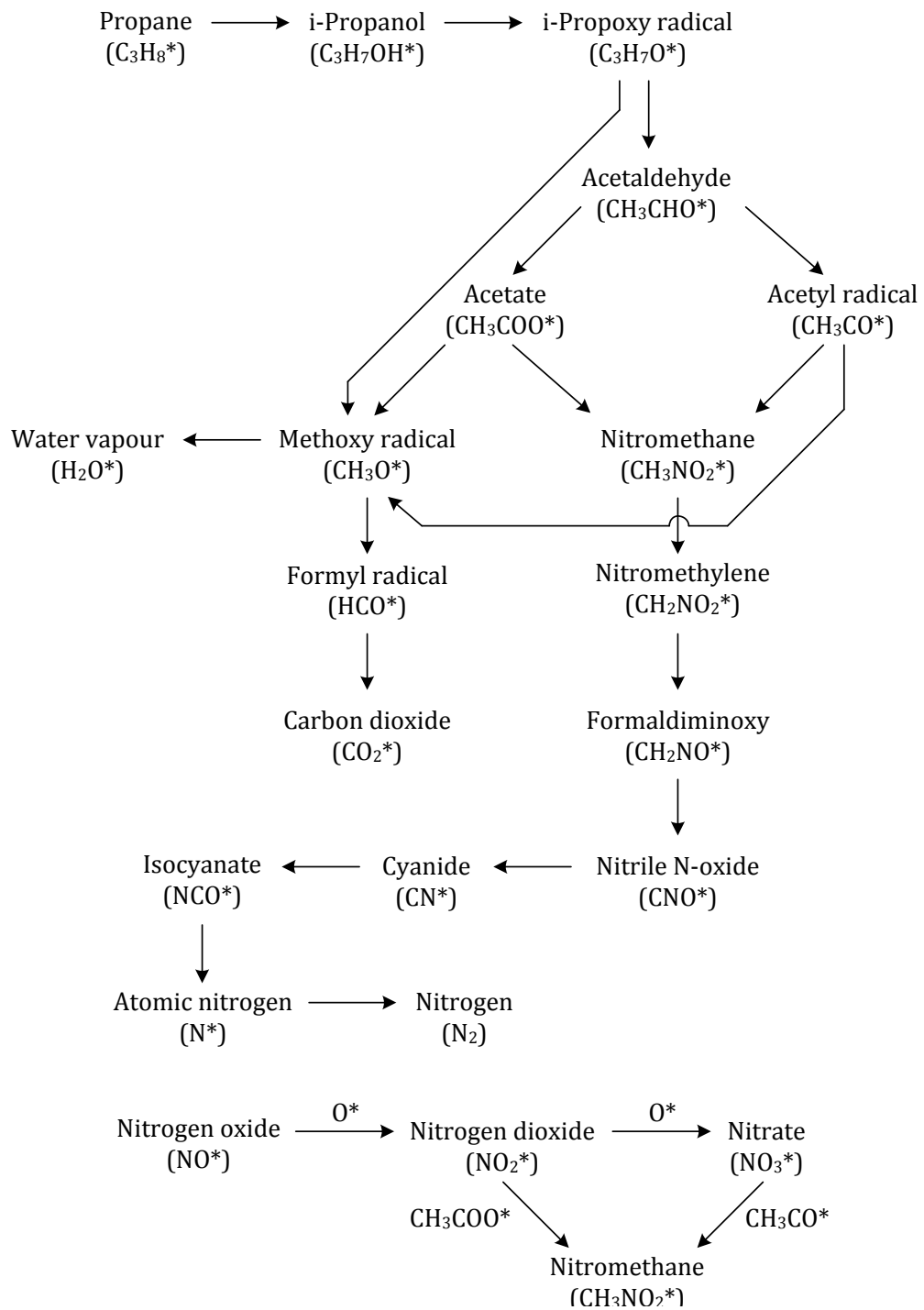


**Figure 5.2:** Kinetic reaction pathway of selective catalytic reduction of  $NO_x$  by propane.

**Table 5.1:** Detailed reaction mechanism for C<sub>3</sub>H<sub>8</sub>-SCR on a silver catalyst with standard enthalpy of reaction, initial values of sticking coefficients or preexponential factors and activation energies.

Reaction	$\Delta H_{298.15}^0$ (kJ/mol)	S <sup>0</sup> or A <sup>#</sup>	E <sub>a</sub> (kJ/mol)
R(1) CH <sub>3</sub> CHO + * → CH <sub>3</sub> CHO*	-43.25	1.0	0.00
R(2) CH <sub>3</sub> CHO* → CH <sub>3</sub> CHO + *	43.25	1.0 × 10 <sup>13</sup>	43.25
R(3) CO <sub>2</sub> + * → CO <sub>2</sub> *	-13.47	0.0	0.00
R(4) CO <sub>2</sub> * → CO <sub>2</sub> + *	13.47	1.0 × 10 <sup>13</sup>	13.47
R(5) H <sub>2</sub> O + * → H <sub>2</sub> O*	-35.76	1.0	0.00
R(6) H <sub>2</sub> O* → H <sub>2</sub> O + *	35.76	1.0 × 10 <sup>13</sup>	35.76
R(7) O <sub>2</sub> + 2* → 2O*	-171.06	1.0	0.00
R(8) 2O* → O <sub>2</sub> + 2*	171.06	1.0 × 10 <sup>8</sup>	39.55
R(9) H <sub>2</sub> + 2* → 2H*	0.86	1.0	0.00
R(10) 2H* → H <sub>2</sub> + 2*	-0.86	1.0 × 10 <sup>13</sup>	19.77
R(11) C <sub>3</sub> H <sub>8</sub> + * → C <sub>3</sub> H <sub>8</sub> *	-41.02	1.0	0.00
R(12) C <sub>3</sub> H <sub>8</sub> * → C <sub>3</sub> H <sub>8</sub> + *	41.02	1.0 × 10 <sup>13</sup>	41.02
R(13) N <sub>2</sub> + 2* → 2N*	108.50	0.0	0.00
R(14) 2N* → N <sub>2</sub> + 2*	-108.50	1.0 × 10 <sup>13</sup>	34.12
R(15) NO + * → NO*	-71.40	1.0	0.00
R(16) NO* → NO + *	71.40	1.0 × 10 <sup>13</sup>	71.40
R(17) NO <sub>2</sub> + * → NO <sub>2</sub> *	-79.38	1.0	0.00
R(18) NO <sub>2</sub> * → NO <sub>2</sub> + *	79.38	1.0 × 10 <sup>13</sup>	79.38
R(19) NO <sub>3</sub> + * → NO <sub>3</sub> *	-206.15	1.0	0.00
R(20) NO <sub>3</sub> * → NO <sub>3</sub> + *	206.15	1.0 × 10 <sup>13</sup>	206.15
R(21) CH <sub>3</sub> CO + * → CH <sub>3</sub> CO*	-98.80	1.0	0.00
R(22) CH <sub>3</sub> CO* → CH <sub>3</sub> CO + *	98.80	1.0 × 10 <sup>13</sup>	98.80
R(23) CH <sub>3</sub> COO + * → CH <sub>3</sub> COO*	-148.72	1.0	0.00
R(24) CH <sub>3</sub> COO* → CH <sub>3</sub> COO + *	148.72	1.0 × 10 <sup>13</sup>	148.72
R(25) OH + * → OH*	-251.46	1.0	0.00
R(26) OH* → OH + *	251.46	1.0 × 10 <sup>13</sup>	251.46
R(27) CO + * → CO*	-56.69	1.0	0.00
R(28) CO* → CO + *	56.69	1.0 × 10 <sup>13</sup>	56.69
R(29) C <sub>3</sub> H <sub>7</sub> O + * → C <sub>3</sub> H <sub>7</sub> O*	-155.54	1.0	0.00
R(30) C <sub>3</sub> H <sub>7</sub> O* → C <sub>3</sub> H <sub>7</sub> O + *	155.54	1.0 × 10 <sup>13</sup>	155.54
R(31) CH <sub>3</sub> O + * → CH <sub>3</sub> O*	-149.87	1.0	0.00
R(32) CH <sub>3</sub> O* → CH <sub>3</sub> O + *	149.87	1.0 × 10 <sup>13</sup>	149.87
R(33) HCO + * → HCO*	-104.16	1.0	0.00
R(34) HCO* → HCO + *	104.16	1.0 × 10 <sup>13</sup>	104.16
R(35) C <sub>3</sub> H <sub>7</sub> OH + * → C <sub>3</sub> H <sub>7</sub> OH*	-39.22	1.0	0.00
R(36) C <sub>3</sub> H <sub>7</sub> OH* → C <sub>3</sub> H <sub>7</sub> OH + *	39.22	1.0 × 10 <sup>13</sup>	39.22
R(37) CH <sub>3</sub> NO <sub>2</sub> + * → CH <sub>3</sub> NO <sub>2</sub> *	-43.71	1.0	0.00
R(38) CH <sub>3</sub> NO <sub>2</sub> * → CH <sub>3</sub> NO <sub>2</sub> + *	43.71	1.0 × 10 <sup>13</sup>	43.71
R(39) CH <sub>2</sub> NO <sub>2</sub> + * → CH <sub>2</sub> NO <sub>2</sub> *	-102.51	1.0	0.00
R(40) CH <sub>2</sub> NO <sub>2</sub> * → CH <sub>2</sub> NO <sub>2</sub> + *	102.51	1.0 × 10 <sup>13</sup>	102.51
R(41) CH <sub>2</sub> NO + * → CH <sub>2</sub> NO*	-101.33	1.0	0.00
R(42) CH <sub>2</sub> NO* → CH <sub>2</sub> NO + *	101.33	1.0 × 10 <sup>13</sup>	101.33

Reaction	$\Delta H_{298.15}^{\circ}$ (kJ/mol)	S <sup>0</sup> or A <sup>#</sup>	E <sub>a</sub> (kJ/mol)
R(43) CN + * → CN*	-175.88	1.0	0.00
R(44) CN* → CN + *	175.88	1.0 × 10 <sup>13</sup>	175.88
R(45) CNO + * → CNO*	-199.16	1.0	0.00
R(46) CNO* → CNO + *	199.16	1.0 × 10 <sup>13</sup>	199.16
R(47) NCO + * → NCO*	-196.23	1.0	0.00
R(48) NCO* → NCO + *	196.23	1.0 × 10 <sup>13</sup>	196.23
R(49) NO* + O* → NO <sub>2</sub> * + *	19.45	1.0 × 10 <sup>11</sup>	39.15
R(50) NO <sub>2</sub> * + * → NO + O*	-19.45	1.0 × 10 <sup>11</sup>	19.70
R(51) NO <sub>2</sub> * + O* → NO <sub>3</sub> * + *	-0.81	1.0 × 10 <sup>11</sup>	31.68
R(52) NO <sub>3</sub> * + * → NO <sub>2</sub> + O*	0.81	1.0 × 10 <sup>11</sup>	32.48
R(53) C <sub>3</sub> H <sub>8</sub> * + O* → C <sub>3</sub> H <sub>7</sub> OH* + *	-81.42	1.0 × 10 <sup>11</sup>	0.00
R(54) C <sub>3</sub> H <sub>7</sub> OH* + * → C <sub>3</sub> H <sub>8</sub> * + O*	81.42	1.0 × 10 <sup>11</sup>	81.42
R(55) C <sub>3</sub> H <sub>7</sub> OH* + O* → C <sub>3</sub> H <sub>7</sub> O* + OH*	-20.91	1.0 × 10 <sup>11</sup>	37.60
R(56) C <sub>3</sub> H <sub>7</sub> O* + OH* → C <sub>3</sub> H <sub>7</sub> OH* + O*	20.91	1.0 × 10 <sup>11</sup>	58.50
R(57) C <sub>3</sub> H <sub>7</sub> O* + O* → CH <sub>3</sub> CHO* + CH <sub>3</sub> O*	-86.70	1.0 × 10 <sup>11</sup>	9.75
R(58) CH <sub>3</sub> CHO* + CH <sub>3</sub> O* → C <sub>3</sub> H <sub>7</sub> O* + O*	86.70	1.0 × 10 <sup>11</sup>	96.45
R(59) CH <sub>3</sub> CHO* + O* → CH <sub>3</sub> CO* + OH*	-28.46	1.0 × 10 <sup>11</sup>	4.92
R(60) CH <sub>3</sub> CO* + OH* → CH <sub>3</sub> CHO* + O*	28.46	1.0 × 10 <sup>11</sup>	33.38
R(61) CH <sub>3</sub> CO* + O* → CH <sub>3</sub> O* + CO*	-139.28	1.0 × 10 <sup>11</sup>	0.00
R(62) CH <sub>3</sub> O* + CO* → CH <sub>3</sub> CO* + O*	139.28	1.0 × 10 <sup>11</sup>	139.28
R(63) CH <sub>3</sub> O* + O* → HCO* + H <sub>2</sub> O*	-86.68	1.0 × 10 <sup>11</sup>	8.42
R(64) HCO* + H <sub>2</sub> O* → CH <sub>3</sub> O* + O*	86.68	1.0 × 10 <sup>11</sup>	95.10
R(65) HCO* + O* → CO <sub>2</sub> * + H*	-259.57	1.0 × 10 <sup>11</sup>	0.00
R(66) CO <sub>2</sub> * + H* → HCO* + O*	259.57	1.0 × 10 <sup>11</sup>	259.57
R(67) CO* + OH* → CO <sub>2</sub> * + H*	-25.17	1.0 × 10 <sup>11</sup>	10.53
R(68) CO <sub>2</sub> * + H* → CO* + OH*	25.17	1.0 × 10 <sup>11</sup>	35.72
R(69) OH* + H* → H <sub>2</sub> O* + *	-63.83	1.0 × 10 <sup>11</sup>	26.40
R(70) H <sub>2</sub> O* + * → OH* + H*	63.83	1.0 × 10 <sup>11</sup>	90.24
R(71) OH* + OH* → H <sub>2</sub> O* + O*	65.25	1.0 × 10 <sup>11</sup>	95.49
R(72) H <sub>2</sub> O* + O* → OH* + OH*	-65.25	1.0 × 10 <sup>11</sup>	30.24
R(73) CH <sub>3</sub> CHO* + O* → CH <sub>3</sub> COO* + H*	-33.21	1.0 × 10 <sup>11</sup>	2.54
R(74) CH <sub>3</sub> COO* + H* → CH <sub>3</sub> CHO* + O*	33.21	1.0 × 10 <sup>11</sup>	35.76
R(75) CH <sub>3</sub> COO* + * → CH <sub>3</sub> O* + CO*	-5.44	1.0 × 10 <sup>11</sup>	17.84
R(76) CH <sub>3</sub> O* + CO* → CH <sub>3</sub> COO* + *	5.44	1.0 × 10 <sup>11</sup>	23.29
R(77) CH <sub>3</sub> COO* + NO <sub>2</sub> * → CH <sub>3</sub> NO <sub>2</sub> * + CO <sub>2</sub> *	-150.22	1.0 × 10 <sup>11</sup>	0.00
R(78) CH <sub>3</sub> NO <sub>2</sub> * + CO <sub>2</sub> * → CH <sub>3</sub> COO* + NO <sub>2</sub> *	150.22	1.0 × 10 <sup>11</sup>	150.22
R(79) CH <sub>3</sub> CO* + NO <sub>3</sub> * → CH <sub>3</sub> NO <sub>2</sub> * + CO <sub>2</sub> *	-283.25	1.0 × 10 <sup>11</sup>	0.00
R(80) CH <sub>3</sub> NO <sub>2</sub> * + CO <sub>2</sub> * → CH <sub>3</sub> CO* + NO <sub>3</sub> *	283.25	1.0 × 10 <sup>11</sup>	283.25
R(81) CH <sub>3</sub> NO <sub>2</sub> * + O* → CH <sub>2</sub> NO <sub>2</sub> * + OH*	1.91	1.0 × 10 <sup>11</sup>	20.29
R(82) CH <sub>2</sub> NO <sub>2</sub> * + OH* → CH <sub>3</sub> NO <sub>2</sub> * + O*	-1.91	1.0 × 10 <sup>11</sup>	18.37
R(83) CH <sub>2</sub> NO <sub>2</sub> * + * → CH <sub>2</sub> NO* + O*	-42.51	1.0 × 10 <sup>11</sup>	17.64
R(84) CH <sub>2</sub> NO* + O* → CH <sub>2</sub> NO <sub>2</sub> * + *	42.51	1.0 × 10 <sup>11</sup>	60.14
R(85) CH <sub>2</sub> NO* + O* → CNO* + H <sub>2</sub> O*	-123.78	1.0 × 10 <sup>11</sup>	0.00
R(86) CNO* + H <sub>2</sub> O* → CH <sub>2</sub> NO* + O*	123.78	1.0 × 10 <sup>11</sup>	123.78
R(87) CNO* + * → CN* + O*	54.06	1.0 × 10 <sup>11</sup>	84.68

Reaction	$\Delta H_{298.15}^o$ (kJ/mol)	$S^0$ or $A^\#$	$E_a$ (kJ/mol)
R(88) $CN^* + O^* \rightarrow CNO^* + ^*$	-54.06	$1.0 \times 10^{11}$	30.62
R(89) $CN^* + O^* \rightarrow NCO^* + ^*$	-242.34	$1.0 \times 10^{11}$	0.00
R(80) $NCO^* + ^* \rightarrow CN^* + O^*$	242.34	$1.0 \times 10^{11}$	242.34
R(91) $NCO^* + O^* \rightarrow N^* + CO_2^*$	-202.80	$1.0 \times 10^{11}$	0.00
R(92) $N^* + CO_2^* \rightarrow NCO^* + O^*$	202.80	$1.0 \times 10^{11}$	202.80
R(93) $NCO^* + ^* \rightarrow N^* + CO^*$	-48.53	$1.0 \times 10^{11}$	0.69
R(94) $N^* + CO^* \rightarrow NCO^* + ^*$	48.53	$1.0 \times 10^{11}$	49.23

#  $S^0$  is the sticking coefficient (dimensionless) and  $A$  is the preexponential factor ( $s^{-1}$ )

## 5.2 Reaction Rate Constant Estimation

The kinetic parameter estimation plays an important role in the use of microkinetic analysis. Theoretical concepts, such as collision and transition-state theories, are applied to provide estimates of reaction rate constants that cannot be inferred from available experimental data. The net rate of production/depletion of individual species  $i$  in Table 5.1 can be defined in a general form:

$$\dot{s}_i = \sum_{k=1}^{K_s} (\nu''_{i,k} - \nu'_{i,k}) k_k \prod_{j=1}^{N_g+N_s} c_j^{\nu'_{j,k}}, \quad (i = 1, \dots, N_g + N_s) \quad (5.1)$$

Here,  $\dot{s}_i$  is the net rate of production/depletion of species  $i$ ,  $K_s$  is the number of elementary reactions,  $\nu''$  (products) and  $\nu'$  (reactants) are the stoichiometric coefficients,  $N_g$  and  $N_s$  are the number of gas-phase and surface species, respectively and  $c_j$  is the molecular concentration of species  $j$ . The rate constant of elementary reaction  $k$ ,  $k_k$  for adsorption process which is established based on collision theory can be written in the form of:

$$k_k = \frac{S_i^0}{\Gamma^n} \sqrt{\frac{RT}{2\pi M_i}} T^{\beta_k} e^{-\left(\frac{E_{a_k}}{RT}\right)} \quad (5.2)$$

Usually, under most cases the adsorption process is considered to be non-activated. Thus all activation energies for all adsorption reactions are set by the value of zero. For the desorption process or surface reaction, the rate constant of elementary reaction  $k$  which is set up rooted in transition state theory is defined as an Arrhenius expression:

$$k_k = \frac{A_k}{\Gamma^{n-1}} T^{\beta_k} e^{-\left(\frac{E_{a_k}}{RT}\right)} \quad (5.3)$$

At this point,  $A_k$ ,  $\beta_k$  and  $E_{a_k}$  are preexponential factor, temperature exponent and activation energy for elementary reaction  $k$ , respectively.  $S_i^0$  is sticking coefficient at vanishing coverage of species  $i$ ,  $\Gamma$  is site density and  $n$  is reaction order. A typical solid surface has a site density of approximately  $10^{15}$  sites/cm<sup>2</sup> (Dumesic et al., 1993, Mhadeshwar et al., 2009).

Nitrogen is an inert gas at low temperature; so the sticking coefficient in the adsorption of nitrogen, R(13), is set equal to zero. Recently, Mhadeshwar et al. (Mhadeshwar et al., 2009) concluded that CO<sub>2</sub> does not promote or inhibit NO<sub>x</sub> conversion in the SCR process. Accordingly, the value of zero is applied for the sticking coefficient in the adsorption of carbon dioxide, R(3). Unity is initially assumed for all remaining sticking coefficients in adsorption processes.

In case of desorption processes and surface reactions, transition state theory is employed to estimate their preexponential factors. The theory is used primarily to understand qualitatively, how chemical reactions take place. Different from collision theory, transition state theory allow details of molecular structure to be incorporated into rate constant calculation. The theory assumes that equilibrium (quasi-equilibrium) is defined between the reactants and an activated complex, which is a

reactive chemical species that is in transition between reactants and products (Cortright and Dumesic, 2001). First, the standard enthalpy of activation, the standard entropy of activation and the standard Gibbs energy of activation are computed using transition state theory. Then, the preexponential factor is calculated via these preceding values. According to Dumesic et al., general order-of-magnitude estimates for preexponential factors under various conditions of surface mobility are summarised in Table 5.2 (Dumesic et al., 1993).

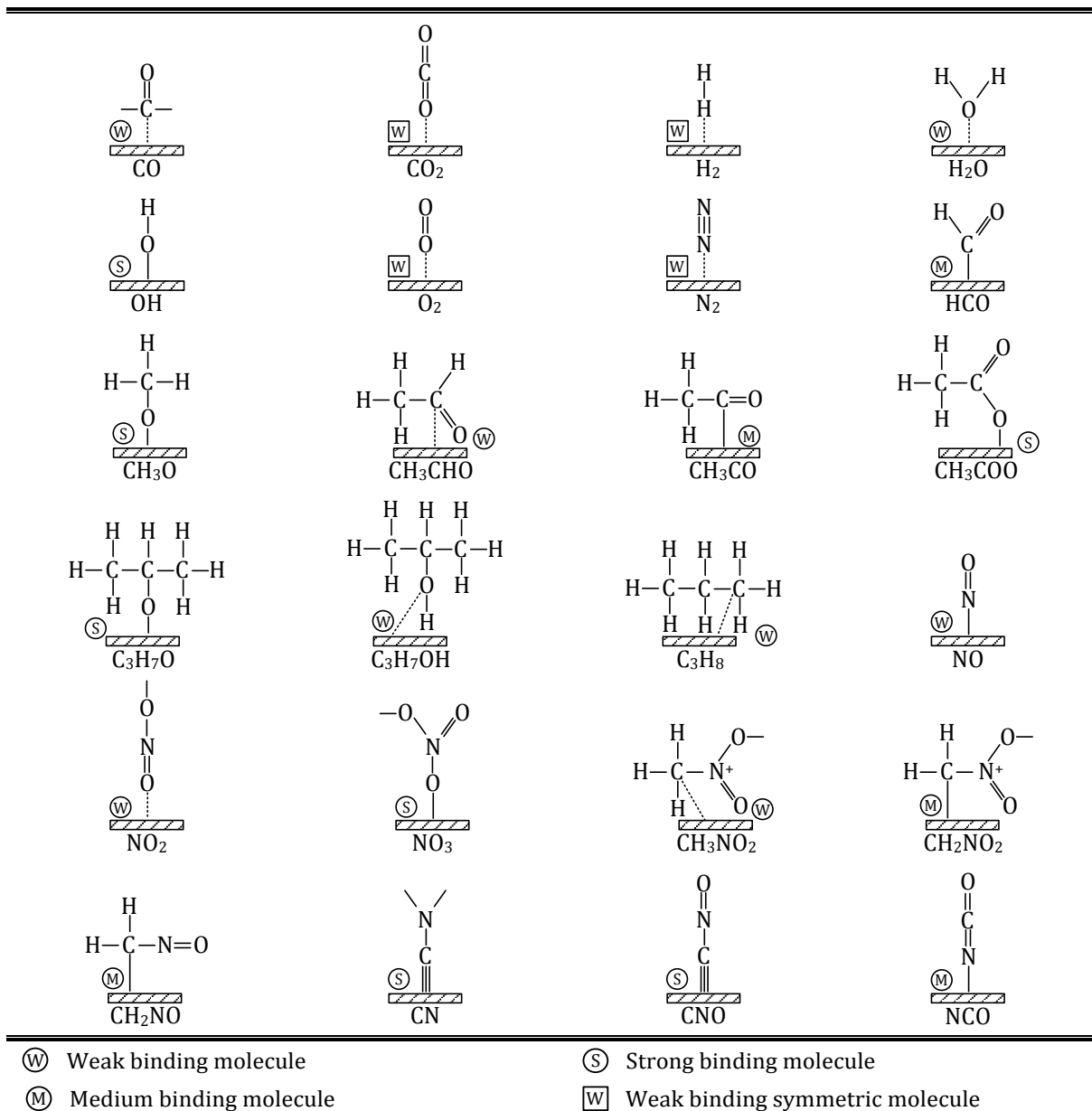
**Table 5.2:** Transition state theory estimates of preexponential factor.

Reaction and conditions	Preexponential factor value (s <sup>-1</sup> )
Langmuir-Hinshelwood reaction	
$A^* + B^* \rightarrow C^* + D^*$	
Mobile surface species with rotation	$A = 10^8$
Mobile surface species without rotation	$A = 10^{11}$
Immobile surface species without rotation	$A = 10^{13}$
Molecular desorption	
$A^* \rightarrow A + *$	
Similar freedom for adsorbed and transition states	$A = 10^{13}$
More rotational and translational freedom for transition state	$A = 10^{16}$
Associative desorption	
$2A^* \rightarrow A_2 + 2^*$	
Mobile adsorbed and transition states with full rotational freedom	$A = 10^8$
Mobile adsorbed and transition states without rotation	$A = 10^{11}$
Immobile adsorbed and transition states	$A = 10^{13}$
Immobile species with more rotational and translational freedom for transition state	$A = 10^{16}$

### 5.3 Heat of Adsorption Calculation

To estimate the heat of adsorption of an atom or molecule, the following initial input parameters are required surface bonding geometry and bond-energy partitioning or total gas phase energies. These parameters are separately given in Table 5.3 and Table 5.5, respectively.

**Table 5.3:** Schematic illustration of possible adsorbing and binding geometry of surface species.



The heat of adsorption is then computed by using the UBI-QEP theory. Details for calculating the heat of adsorption for different molecular structures used in this research are provided below.

### 5.3.1 Metal-Atom Binding

Atomic heat of adsorption of atom  $A$  on the catalyst surface,  $Q_A$ , is calculated by Equation (5.4).  $Q_{0A}$  is the heat of adsorption of the atom  $A$  on the on-top site and  $n$  is the number of metal atoms to which  $A$  binds. For a three-fold fcc(111),  $n$  equals 3.

$$Q_{0A} = \frac{Q_A}{2 - 1/n} \quad (5.4)$$

Recommended UBI-QEP values of  $Q_{0A}$  obtained from experimental atomic binding energy on various fcc(111) surfaces are shown in the Table 5.4 (Shustorovich and Zeigarnik, 2003).

**Table 5.4:** Recommended UBI-QEP values of  $Q_{0A}$  for selected adatoms and metals.

Adatom	Cu	Ag	Au	Ni	Pd	Pt
H	140.58	130.54	115.48	158.16	155.64	153.13
O	258.57	200.83	188.28	288.70	218.82	213.38
N	288.70	251.04	243.51	338.90	326.35	291.21
C	301.25	276.98	271.96	429.28	401.66	376.56

Unit: (kJ/mol)

### 5.3.2 Weak Binding Molecule

Closed shell molecules, such as, CO, H<sub>2</sub>, H<sub>2</sub>O, CH<sub>4</sub>, CH<sub>3</sub>OH, CH<sub>3</sub>CHO, CH<sub>2</sub>CO and CH<sub>3</sub>CH<sub>2</sub>OH, or radicals with strongly delocalised unpaired electrons, such as, O<sub>2</sub> or NO, are typically considered as weak binding molecules (Shustorovich and Sellers, 1998, Storsæter et al., 2006). For the  $AB$  molecule with the  $A$  atom group as the surface contact atom and the  $B$  atom group directed away from the surface,  $\eta^1\mu_n$  coordination, the UBI-QEP heat of adsorption is

$$Q_{AB,n} = \frac{Q_{0A}^2}{Q_{0A}/n + \mathcal{D}_{AB}} \quad (5.5)$$

Bond-energy partitioning,  $\mathcal{D}_{AB}$ , is the energy required for separating the  $A$  atom group from the  $B$  atom group in the gas phase. Bond-energy partitioning of the  $AB$  molecule bounded to the surface is calculated by the sum of bond energies between the atom group that bind to the surface, the  $A$  atom group, and the rest of the molecule, the  $B$  atom group. An explanation of a bond-energy partitioning calculation is provided in Appendix B. The value of 1 is specified to  $n$  in Equation (5.5) for all weak binding molecules to represent the on-top binding site.

### 5.3.3 Strong Binding Molecule

Molecular radicals with considerable localised, unpaired electrons, such as, OH, CH, CH<sub>2</sub>, CH<sub>3</sub>O, CCH<sub>3</sub>, CHCH<sub>3</sub>, CHCHO and CH<sub>3</sub>CH<sub>2</sub>O, are classified as strong binding molecules. Heat of adsorption of the strong binding molecule  $AB$  which the  $A$  atom group ends down to the catalyst surface,  $\eta^1\mu_n$  coordination, is estimated by Equation (5.6).

$$Q_{AB} = \frac{Q_A^2}{Q_A + \mathcal{D}_{AB}} \quad (5.6)$$

### 5.3.4 Medium Binding Molecule

Molecules bounded to the surface with monovalent radical or tetravalent carbon, for example, CH<sub>3</sub>, HCO, CH<sub>3</sub>CO, CH<sub>2</sub>CHO and CH<sub>2</sub>CH<sub>3</sub>, are medium binding molecules. Heat of adsorption of the medium binding molecule  $AB$  which the  $A$  atom group connects to the catalyst surface,  $\eta^1\mu_n$  coordination, is determined by Equation (5.7).

$$Q_{AB} = \frac{1}{2} \left[ \frac{Q_{0A}^2}{Q_{0A}/n + \mathcal{D}_{AB}} + \frac{Q_A^2}{Q_A + \mathcal{D}_{AB}} \right] \quad (5.7)$$

Since the calculation of bond-energy partitioning in polyatomic molecules was based on the intuitive chemical reasoning resulting in no physical explanation, Shustorovich and Zeigarnik presented a new UBI-QEP formalism to compute heat of adsorption of polyatomic molecules without bond-energy partitioning (Shustorovich and Zeigarnik, 2003). The new formulae are shown in Equation (5.8) and (5.9) and are used to calculate heat of adsorption of the medium binding molecule  $AB$  which both the  $A$  atom group and  $B$  atom group bound to the surface,  $\eta^2 \mu_n$  coordination. The total gas phase energy,  $\tilde{\mathcal{D}}_{AB}$ , which is a uniquely defined and observable thermodynamic quantity is applied instead of bond-energy partitioning.

$$Q_{AB} = \frac{ab(a+b) + \tilde{\mathcal{D}}_{AB}(a-b)^2}{ab + \tilde{\mathcal{D}}_{AB}(a+b)} \quad (5.8)$$

$$a = Q_{0A}^2 \frac{Q_{0A} + 2Q_{0B}}{(Q_{0A} + Q_{0B})^2} \quad (5.9)$$

$$b = Q_{0B}^2 \frac{Q_{0B} + 2Q_{0A}}{(Q_{0A} + Q_{0B})^2}$$

### 5.3.5 Weak Binding Symmetric Molecule

For symmetric molecules weakly bounded to the surface, for instance,  $O_2$ ,  $H_2$ ,  $N_2$  and  $CO_2$ , the heat of adsorption is calculated by Equation (5.10).

$$Q_{AB} = \frac{9}{2} \left( \frac{Q_{0A}^2}{3Q_{0A} + 8\tilde{\mathcal{D}}_{AB}} \right) \quad (5.10)$$

### 5.3.6 Weak Binding Diatomic Molecule

The heat of adsorption of diatomic molecules (both symmetric and non-symmetric) which are bound weakly through two atoms to the surface,  $M_{(1)} - X_m A - BY_m - M_{(2)}$  coordination, is estimated by Equation (5.11) and (5.12) according to the new UBI-QEP formalism by Shustorovich and Zeigarnik (Shustorovich and Zeigarnik, 2003).

$$Q_{AB} = \frac{ab(a+b) + \tilde{D}_{AB}(a-b)^2}{ab + \tilde{D}_{AB}(a+b)} \quad (5.11)$$

$$a = Q_{0A} \left[ 1 - \left( \frac{mQ_{0X}}{mQ_{0A} + Q_{0X}} \right)^2 \right] \quad (5.12)$$

$$b = Q_{0B} \left[ 1 - \left( \frac{m'Q_{0Y}}{m'Q_{0B} + Q_{0Y}} \right)^2 \right]$$

Examples of weak binding diatomic molecules are CHCH, CH<sub>2</sub>CH<sub>2</sub>, CH<sub>3</sub>CH<sub>3</sub>, CCH, CCH<sub>2</sub>, CHCH<sub>2</sub>, CHCO and CH<sub>2</sub>CO.

**Table 5.5:** Heats of adsorption, binding type, bond-energy partitioning or total gas phase energies used to calculate heat of adsorption.

Chemical formula <sup>a</sup>	Binding type	Equation used	$\mathcal{D}_{AB}$ or $\tilde{\mathcal{D}}_{AB}$ (kJ/mol)	$Q_{AB}$ (kJ/mol)
H	Metal-atom	(5.4)	-	217.57
O	Metal-atom	(5.4)	-	334.72
<b>CO</b>	Weak	(5.5)	1076.38	56.69
<b>CO<sub>2</sub></b>	Weak symmetric	(5.10)	1608.58	13.47
H <sub>2</sub>	Weak symmetric	(5.10)	435.78	19.77
<b>H<sub>2</sub>O</b>	Weak	(5.5)	927.01	35.76
OH	-	-	-	251.46 <sup>b</sup>
O <sub>2</sub>	Weak symmetric	(5.10)	498.36	39.55
N <sub>2</sub>	Weak symmetric	(5.10)	944.84	34.12
<b>HCO</b>	Medium	(5.7)	1048.77	104.16
<b>CH<sub>3</sub>O</b>	Strong	(5.6)	412.87	149.87
<b>CH<sub>3</sub>CHO</b>	Weak	(5.5)	1496.76	43.25
<b>CH<sub>3</sub>CO</b>	Medium	(5.7)	1123.02	98.80
<b>CH<sub>3</sub>COO</b>	Strong	(5.6)	418.64	148.72
<b>C<sub>3</sub>H<sub>7</sub>O</b>	Strong	(5.6)	385.59	155.54
<b>C<sub>3</sub>H<sub>7</sub>OH</b>	Weak	(5.5)	827.65	39.22
<b>C<sub>3</sub>H<sub>8</sub></b>	Weak	(5.5)	1593.36	41.02
<b>NO</b>	Weak	(5.5)	631.62	71.40
<b>NO<sub>2</sub></b>	Weak	(5.5)	307.29	79.38
<b>NO<sub>3</sub></b>	Strong	(5.6)	208.75	206.15
<b>CH<sub>3</sub>NO<sub>2</sub></b>	Weak	(5.5)	1478.18	43.71
<b>CH<sub>2</sub>NO<sub>2</sub></b>	Medium	(5.7)	1070.82	102.51
<b>CH<sub>2</sub>NO</b>	Medium	(5.7)	1087.08	101.33
<b>CN</b>	Strong	(5.6)	750.01	175.88
CNO	-	-	-	199.16 <sup>b</sup>
NCO	-	-	-	196.23 <sup>b</sup>
<b>N</b>	Metal-atom	(5.4)	-	418.40

<sup>a</sup> boldface = bond with catalyst surface

<sup>b</sup> source: (Mhadeshwar et al., 2009)

## 5.4 Activation Energy Estimation

The activation energy is subsequently calculated from the heats of adsorption computed previously. Storsæter et al. clearly explained the using of UBI-QEP theory to find heats of adsorption and activation energies (Storsæter et al., 2006).

For the desorption process of a surface species  $A$ ,  $A^* \rightarrow A + *$ , Equation (5.13) is used to find the forward activation energy. It should be noted that the letters emerged in this section, such as  $A$ ,  $B$  and  $AB$ , are not the same meaning with those that appeared in the previous section.

$$E_{a,f} = Q_A \quad (5.13)$$

To compute the forward activation energy for the dissociation of an adsorbed species  $AB$  to surface species  $A$  and  $B$ ,  $AB^* + * \rightarrow A^* + B^*$ , Equation (5.14) and (5.15) are employed. The surface reaction enthalpy,  $\Delta H$ , is the energy which is released or consumed as the result of the surface reaction. The bond dissociation energy,  $D_{AB}$ , is the energy required for separating the  $A$  atom group from the  $B$  atom group in the gas phase. It should be noted that although the bond dissociation energy,  $D_{AB}$ , and the bond-energy partitioning,  $\mathcal{D}_{AB}$ , presented in the last section have the same definition, the in values are often different depending on the form of the atom group  $A$  and  $B$ .

$$E_{a,f} = \frac{1}{2} \left( \Delta H + \frac{Q_A Q_B}{Q_A + Q_B} \right) \quad (5.14)$$

$$\Delta H = Q_{AB} + D_{AB} - Q_A - Q_B \quad (5.15)$$

The forward activation energy for recombination of surface species  $A$  and  $B$  to an adsorbed  $AB$ ,  $A^* + B^* \rightarrow AB^* + *$ , the reverse of dissociation reaction as mentioned above, can be calculated by Equation (5.16) and (5.17).

$$E_{a,f} = \frac{1}{2} \left( -\Delta H + \frac{Q_A Q_B}{Q_A + Q_B} \right) \quad (5.16)$$

$$\Delta H = Q_{AB} + D_{AB} - Q_A - Q_B \quad (5.17)$$

For the reaction between the adsorbed  $A$  and  $BC$  to produce the adsorbed  $AB$  and  $C$ , called the disproportionation reaction,  $A^* + BC^* \rightarrow AB^* + C^*$ , the forward activation energy can be estimated by Equation (5.18) and (5.19).

$$E_{a,f} = \frac{1}{2} \left( \Delta H + \frac{Q_{AB} Q_C}{Q_{AB} + Q_C} \right) \quad (5.18)$$

$$\Delta H = Q_A + Q_{BC} + D_{BC} - D_{AB} - Q_{AB} - Q_C \quad (5.19)$$

With awareness, to define the forward direction of the disproportionation reaction, the bond dissociation energy of the reactant  $BC$  ( $D_{BC}$ ) has to be greater than that of the product  $AB$  ( $D_{AB}$ ). The direction of the reaction is defined so that  $D_{BC}$  is always greater than  $D_{AB}$ . Sometime when the  $D_{BC}$  is lower than  $D_{AB}$ , the direction of original disproportionation reaction is reversed and the labels of initial reactants and products are swapped to specify the inverse one reverse direction.

The reverse activation energy of each reaction can be simply calculated from a combination of the forward activation energy and the enthalpy of the surface reaction which are computed formerly. This combination which is demonstrated in Equation (5.20) is established based on the law of energy conservation (Shustorovich and Sellers, 1998).

$$\Delta H = E_{a,f} - E_{a,r} \quad (5.20)$$

Nevertheless, the UBI-QEP theory provides formally the negative value of activation energy which is physically meaningless. Consequently, to assign a physical meaning when the activation energy is a negative value it is set to zero; and to satisfy the law of conservation of energy, its reverse activation energy is equal to the surface

reaction enthalpy. The explanation of the calculations of activation energies and related variables are given in Appendix B.

## 5.5 Heat of Reaction

The heat of reaction,  $\Delta H_{R,T}$ , is the change in enthalpy at temperature  $T$  during a chemical reaction. If the chemical reaction releases heat then the reaction is called an exothermic reaction, and the heat of reaction is negative. If the change in enthalpy is positive the reaction is endothermic and heat is absorbed. The heat of reaction can be calculated from the standard heat of reaction via the standard heat of formation. The standard heat of formation,  $\Delta H_f^o$ , is defined as the enthalpy change when one mole of a compound is formed from the elements at the standard state (one atmosphere pressure and the temperature of 298.15 K). The standard heat of reaction,  $\Delta H_R^o$ , is the heat of reaction at the standard state. The value of the standard heat of reaction is the sum of the standard heats of formation of the products minus the sum of the standard heats of formation of the reactants (Hayes and Kolaczkowski, 1997), as shown in Equation (5.22). The heat of reaction is a function of both temperature and pressure. The dependence of the heat of reaction on pressure is neglected because of the ideal gas assumption; therefore at the temperature  $T$ , the heat of reaction is equal to the standard heat of reaction ( $\Delta H_{R,T} = \Delta H_{R,T}^o$ ). Equation (5.21) and (5.22) are used in order to find the heat of reaction per mole of species  $k$ . Stoichiometric coefficients of reactants and products are represented by  $\nu$ .

$$\begin{aligned}
 \Delta H_{R,T} &= \Delta H_{R,T}^0 \\
 &= \frac{1}{\nu_k} \left[ \sum_{\text{reactant } i} \int_T^{298.15} \nu_i C_p dT \right] + \Delta H_{R,298.15}^0 \\
 &\quad + \frac{1}{\nu_k} \left[ \sum_{\text{product } j} \int_{298.15}^T \nu_j C_p dT \right]
 \end{aligned} \tag{5.21}$$

$$\Delta H_{R,298.15}^0 = \frac{1}{\nu_k} \left[ \sum_{\text{product } j} \nu_j \Delta H_{f,298.15}^0 - \sum_{\text{reactant } i} \nu_i \Delta H_{f,298.15}^0 \right] \tag{5.22}$$

# CHAPTER 6

## MODEL OPTIMISATION

In this chapter, chemical reaction parameters (i.e. sticking coefficients and preexponential factors) that have initially been estimated for each elementary reaction in Chapter 5 will be carefully optimised in order to best-fit some results from experiments (called optimisation targets). Firstly, the important parameters (called active parameters) are identified by a method of sensitivity analysis. Only these active parameters need to be considered for optimisation. Then the optimization is carried out by minimising errors between simulation results and optimisation targets.

### 6.1 Sensitivity Analysis

Since not all rate constants equally affect the corresponding change in optimisation targets, a sensitivity analysis is applied to identify these rate constants that have strong effects on the optimisation targets. Due to the simplicity for measuring from experiments, the conversions of propane as well as  $\text{NO}_x$  and the ratio of  $\text{CO}_2$  to  $\text{CO}$  are selected as the optimisation targets. To cover the broad range of operating conditions (temperatures and THC to  $\text{NO}$  ratios), nine sets of experimental conditions out of those reported in Table 3.3 of Chapter 3 are chosen for optimisation. These experimental conditions are 2, 3 and 4 for exhaust gas temperature 250 °C; 7, 8 and 11 for 290 °C; 13, 17 and 18 for 370 °C. Each rate constant (sticking coefficient or preexponential factor) of each elementary reaction is perturbed by an increase or decrease of one order of magnitude from their nominal (initial) values. Results from

the sensitivity analysis are summarised in the form of the sensitivity coefficient which is defined as (Aghalayam et al., 2000):

$$\frac{y(\vartheta_{\text{perturbed}}) - y(\vartheta_{\text{nominal}})}{y(\vartheta_{\text{nominal}})} \quad (6.1)$$

where  $y$  is the optimisation targets and  $\vartheta$  is the reaction parameters (sticking coefficients or preexponential factors). The sensitivity coefficients that are presented in Figure 6.1 clearly illustrate that the conversion of propane is markedly influenced by the desorption of surface NO, R(16) in Table 5.1, and the Langmuir-Hinshelwood reaction between surface i-propanol and atomic oxygen, R(55), (this produces a surface i-propoxy radical and hydroxyl species). On the subject of the NO<sub>x</sub> conversion, the primary objective, this optimisation target is mainly controlled by both the adsorption process and Langmuir-Hinshelwood reactions. The adsorption process is the adsorption of gaseous NO, R(15). The Langmuir-Hinshelwood reactions are: (1) the reaction between surface acetaldehyde and atomic oxygen to produce acetyl radical and hydroxyl, R(59); (2) the surface reaction of adsorbed acetaldehyde and atomic oxygen to generate acetate and atomic hydrogen, R(73); (3) the dissociative reaction of acetate to form methoxy radical and carbon monoxide, R(75) and (4) the surface reaction of adsorbed acetate and nitrogen dioxide to create surface nitromethane and carbon dioxide, R(77). Interestingly, the formation of acetate is considered as a rate-determining step, confirmed by Shibata et al. (Shibata et al., 2003). Regarding the ratio of CO<sub>2</sub> to CO, the last optimisation target, this ratio is primarily affected by the Langmuir-Hinshelwood reaction between adsorbed carbon monoxide and hydroxyl to produce surface carbon dioxide and atomic hydrogen, R(67), and the reaction of adsorbed isocyanate and atomic oxygen to form surface

atomic nitrogen and carbon dioxide, R(91). As a result, the active parameters are identified as 9 from 94 elementary reactions.

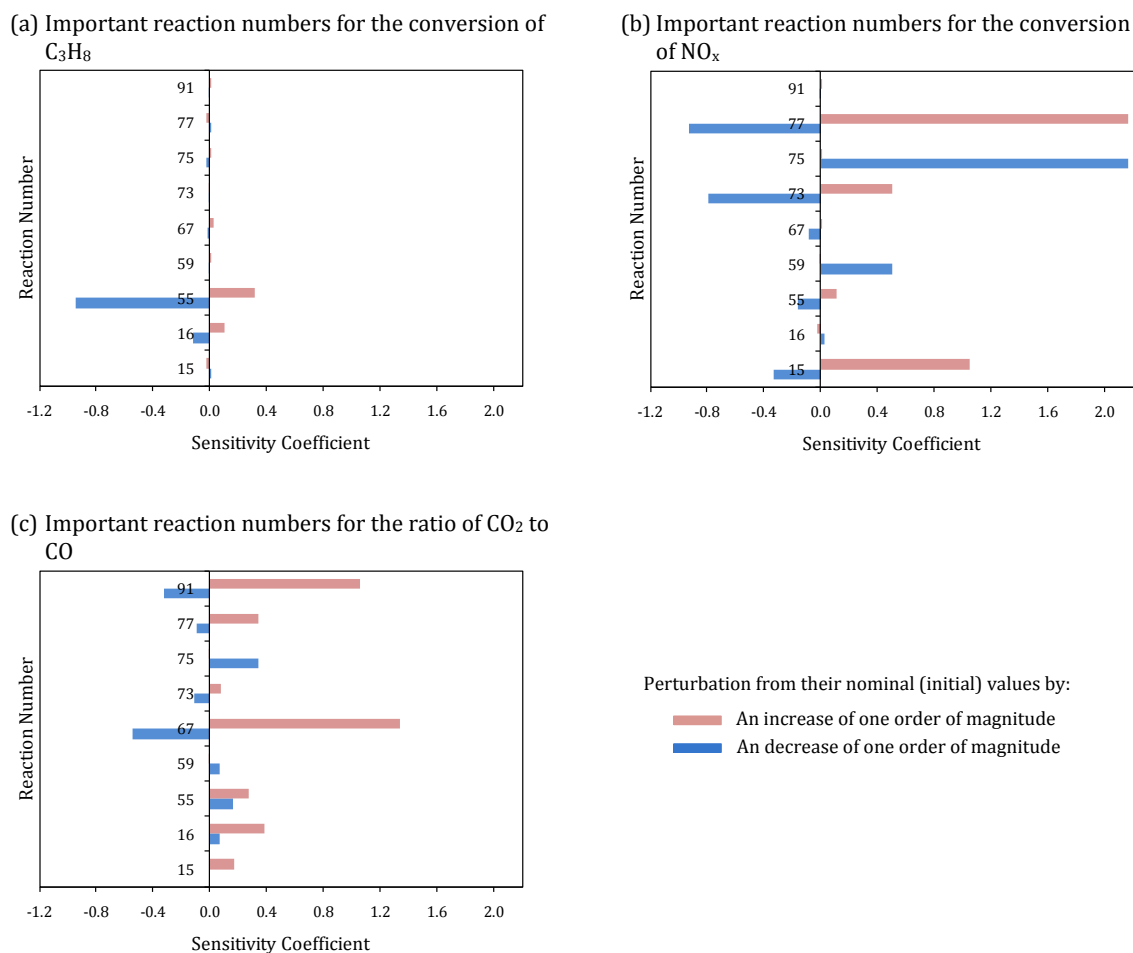


**Figure 6.1:** Sensitivity analysis.

## 6.2 Solution-Mapping Method

Solution-mapping method (also referred to as response surface method) is one of the techniques used to determine an optimum set of parameters for multi-parameter multi-data-set optimisation. This method has been used by Frenklach et al. to form optimised parameters for a methane combustion mechanism (Frenklach et al., 1992). The active parameters that were previously identified by using the

sensitivity analysis as explained in Section 6.1 are scaled in order to avoid the difference in value by many orders of magnitude (e.g. sticking coefficients and preexponential factors). These scaled parameters are called factorial variables and are defined by the following Equation (6.2) (Aghalayam et al., 2000)

$$X = \frac{\ln\left(\frac{k^2}{k_{\min} k_{\max}}\right)}{\ln\left(\frac{k_{\max}}{k_{\min}}\right)} \quad (6.2)$$

where a sticking coefficient or preexponential factor  $k$  in the interval  $[k_{\min}, k_{\max}]$  is mapped to  $X$  in the same range of values  $[-1, 1]$ . Values of the sticking coefficients and preexponential factors that are used to calculate factorial variables are shown in Table 6.1.

**Table 6.1:** Minimum and maximum values of sticking coefficient and preexponential factors used to calculate factorial variables.

Factorial variables	$k_{\min}$	$k_{\max}$
X <sub>15</sub>	0.518	1.00
X <sub>16</sub>	$1.00 \times 10^{12}$	$1.00 \times 10^{13}$
X <sub>55</sub>	$1.00 \times 10^{10}$	$1.00 \times 10^{11}$
X <sub>59</sub>	$1.00 \times 10^{10}$	$1.00 \times 10^{11}$
X <sub>67</sub>	$1.00 \times 10^6$	$1.00 \times 10^7$
X <sub>73</sub>	$1.00 \times 10^{11}$	$1.00 \times 10^{12}$
X <sub>75</sub>	$5.00 \times 10^{10}$	$1.00 \times 10^{11}$
X <sub>77</sub>	$1.00 \times 10^{11}$	$1.50 \times 10^{12}$
X <sub>91</sub>	$1.00 \times 10^9$	$1.00 \times 10^{10}$

By using the computer experiment technique (Frenklach et al., 1992) which is developed based on the factorial design technique (Box et al., 1978), model responses to several values of factorial variable are systematically constructed. These model responses for all optimisation targets (i.e. C<sub>3</sub>H<sub>8</sub> conversion, NO<sub>x</sub> conversion and CO<sub>2</sub> to CO ratio), for example, at the operating condition 370 °C, 2000 ppm THC and 200

ppm NO (experimental condition 13), are shown in Table 6.2, 6.3 and 6.4. According to the factorial design method, a problem in  $m$  dimensions, that is, involving  $m$  operation parameters ( $k$ 's in this case), there are  $2^m$  sample points needed. Apart from the  $2^m$  sample points determined by factorial design, additional ones have been incorporated into the model in order to improve the polynomial fits.

**Table 6.2:** Factorial design table for the conversion of  $C_3H_8$  (experimental condition 13).

No.	Factorial variables		Model response <sup>a</sup>
	$X_{16}$	$X_{55}$	
1	1.00	0.25	97.86
2	1.50	0.25	97.44
3	2.00	0.25	96.88
4	1.00	0.10	93.18
5	1.50	0.10	92.66
6	2.00	0.10	91.93
7	1.00	0.00	89.50
8	1.50	0.00	88.75
9	2.00	0.00	87.87

<sup>a</sup> Model response is  $C_3H_8$  conversion (%).

**Table 6.3:** Factorial design table for the conversion of  $NO_x$  (experimental condition 13).

No.	Factorial variables					Model response <sup>a</sup>
	$X_{15}$	$X_{59}$	$X_{73}$	$X_{75}$	$X_{77}$	
1	0.65	3.00	0.50	-2.50	-1.00	13.96
2	0.65	3.00	0.50	-2.50	0.00	33.73
3	0.65	3.00	0.50	-3.50	-1.00	36.57
4	0.65	3.00	0.50	-3.50	0.00	65.19
5	0.95	3.00	0.50	-2.50	-1.00	14.95
6	0.95	3.00	0.50	-2.50	0.00	35.64
7	0.95	3.00	0.50	-3.50	-1.00	38.54
8	0.95	3.00	0.50	-3.50	0.00	67.19
9	0.65	3.00	1.50	-2.50	-1.00	19.95
10	0.65	3.00	1.50	-2.50	0.00	47.66
11	0.65	3.00	1.50	-3.50	-1.00	51.33
12	0.65	3.00	1.50	-3.50	0.00	85.20
13	0.95	3.00	1.50	-2.50	-1.00	21.43
14	0.95	3.00	1.50	-2.50	0.00	50.20
15	0.95	3.00	1.50	-3.50	-1.00	54.00
16	0.95	3.00	1.50	-3.50	0.00	87.20

No.	Factorial variables					Model response <sup>a</sup>
	X <sub>15</sub>	X <sub>59</sub>	X <sub>73</sub>	X <sub>75</sub>	X <sub>77</sub>	
17	0.65	1.00	0.50	-2.50	-1.00	23.41
18	0.65	1.00	0.50	-2.50	0.00	54.83
19	0.65	1.00	0.50	-3.50	-1.00	58.88
20	0.65	1.00	0.50	-3.50	0.00	91.83
21	0.95	1.00	0.50	-2.50	-1.00	25.15
22	0.95	1.00	0.50	-2.50	0.00	57.67
23	0.95	1.00	0.50	-3.50	-1.00	61.69
24	0.95	1.00	0.50	-3.50	0.00	93.40
25	0.65	1.00	1.50	-2.50	-1.00	24.80
26	0.65	1.00	1.50	-2.50	0.00	57.52
27	0.65	1.00	1.50	-3.50	-1.00	61.66
28	0.65	1.00	1.50	-3.50	0.00	93.69
29	0.95	1.00	1.50	-2.50	-1.00	26.63
30	0.95	1.00	1.50	-2.50	0.00	60.43
31	0.95	1.00	1.50	-3.50	-1.00	64.59
32	0.95	1.00	1.50	-3.50	0.00	95.08
33	0.75	2.30	0.80	-2.80	-0.70	36.40
34	0.75	2.30	0.80	-2.80	-0.30	49.61
35	0.75	2.30	0.80	-3.20	-0.70	51.08
36	0.75	2.30	0.80	-3.20	-0.30	65.45
37	0.85	2.30	0.80	-2.80	-0.70	37.14
38	0.85	2.30	0.80	-2.80	-0.30	50.47
39	0.85	2.30	0.80	-3.20	-0.70	52.00
40	0.85	2.30	0.80	-3.20	-0.30	66.39
41	0.75	2.30	1.20	-2.80	-0.70	39.39
42	0.75	2.30	1.20	-2.80	-0.30	53.37
43	0.75	2.30	1.20	-3.20	-0.70	54.90
44	0.75	2.30	1.20	-3.20	-0.30	69.72
45	0.85	2.30	1.20	-2.80	-0.70	40.18
46	0.85	2.30	1.20	-2.80	-0.30	54.26
47	0.85	2.30	1.20	-3.20	-0.70	55.80
48	0.85	2.30	1.20	-3.20	-0.30	70.61
49	0.75	1.70	0.80	-2.80	-0.70	40.55
50	0.75	1.70	0.80	-2.80	-0.30	54.80
51	0.75	1.70	0.80	-3.20	-0.70	56.35
52	0.75	1.70	0.80	-3.20	-0.30	71.29
53	0.85	1.70	0.80	-2.80	-0.70	41.36
54	0.85	1.70	0.80	-2.80	-0.30	55.71
55	0.85	1.70	0.80	-3.20	-0.70	57.33
56	0.85	1.70	0.80	-3.20	-0.30	72.18
57	0.75	1.70	1.20	-2.80	-0.70	42.33
58	0.75	1.70	1.20	-2.80	-0.30	56.96
59	0.75	1.70	1.20	-3.20	-0.70	58.61
60	0.75	1.70	1.20	-3.20	-0.30	73.69
61	0.85	1.70	1.20	-2.80	-0.70	43.22

No.	Factorial variables					Model response <sup>a</sup>
	X <sub>15</sub>	X <sub>59</sub>	X <sub>73</sub>	X <sub>75</sub>	X <sub>77</sub>	
62	0.85	1.70	1.20	-2.80	-0.30	57.96
63	0.85	1.70	1.20	-3.20	-0.70	59.55
64	0.85	1.70	1.20	-3.20	-0.30	74.58

<sup>a</sup> Model response is NO<sub>x</sub> conversion (%).

**Table 6.4:** Factorial design table for the ratio of CO<sub>2</sub> to CO (experimental condition 13).

No.	Factorial variables		Model response <sup>a</sup>
	X <sub>67</sub>	X <sub>91</sub>	
1	0.50	-0.50	4.59
2	0.50	0.00	4.69
3	0.50	0.50	4.82
4	0.75	-0.50	5.55
5	0.75	0.00	5.67
6	0.75	0.50	5.82
7	1.00	-0.50	7.03
8	1.00	0.00	7.18
9	1.00	0.50	7.35
10	1.25	-0.50	9.37
11	1.25	0.00	9.56
12	1.25	0.50	9.77
13	1.50	-0.50	13.18
14	1.50	0.00	13.42
15	1.50	0.50	13.70

<sup>a</sup> Model response is CO<sub>2</sub> to CO ratio.

For each optimisation target and operating condition, a relationship between model responses and factorial variables is written as a second order polynomial. These polynomial forms for experimental condition 13, for instance, are:

#### *C<sub>3</sub>H<sub>8</sub> Conversion*

$$y_{C_3H_8}^{\#13} = 96.06 - 7.41X_{16} + 20X_{55} + 9.12X_{16}X_{55} + 1.67X_{16}^2 + 3.92X_{55}^2 \quad (6.3)$$

*NO<sub>x</sub> Conversion*

$$\begin{aligned}
y_{NO_x}^{\#13} = & 25.7 - 0.4X_{15} + 2.76X_{59} - 3.07X_{73} + 10.45X_{75} + 6.52X_{77} \\
& - 1.41X_{15}X_{59} + 1.67X_{15}X_{73} - 1.47X_{15}X_{75} + 2X_{15}X_{77} \\
& + 4.89X_{59}X_{73} + 5.42X_{59}X_{75} - 5.09X_{59}X_{77} - 7.01X_{73}X_{75} \\
& + 6.99X_{73}X_{77} - 6.18X_{75}X_{77} + 3.34X_{15}^2 - 0.14X_{59}^2 \\
& - 8.61X_{73}^2 + 8.8X_{75}^2 - 9.22X_{77}^2
\end{aligned} \tag{6.4}$$

*CO<sub>2</sub> to CO Ratio*

$$y_{CO_2/CO}^{\#13} = 5.92 - 6.15X_{67} + 0.14X_{91} + 0.17X_{67}X_{91} + 7.41X_{67}^2 + 0.04X_{91}^2 \tag{6.5}$$

**6.3 Optimisation of the Surface Reaction Mechanism**

To capture the state of the catalytic surface along the reacting wall which varies with operating conditions, Koop and Deutschmann employed dependence of rate coefficients on the operating condition in the form of a modified Arrhenius expression (Koop and Deutschmann, 2009). This expression takes a coverage dependence of a reaction rate through a coverage-dependent activation energy parameter and coverage-dependent reaction order parameter. Similarly, to consider the substantial change of activation energies with varying operating conditions, Mhadeshwar and Vlachos incorporated temperature and coverage dependences of activation energy into the calculations of the heat of chemisorption (Mhadeshwar and Vlachos, 2005a). In this work, to realise the effect of operating conditions, the active parameters are optimised and written as a function of temperatures and/or inlet concentrations of C<sub>3</sub>H<sub>8</sub> and NO<sub>x</sub>. To determine the optimised value of active

parameters, an objective function for each experimental condition is formulated as (e.g. experimental condition 13):

$$\Phi^{\#13} = \left( \frac{y_{C_3H_8}^{\#13} - Expt_{C_3H_8}^{\#13}}{Expt_{C_3H_8}^{\#13}} \right)^2 + \left( \frac{y_{NO_x}^{\#13} - Expt_{NO_x}^{\#13}}{Expt_{NO_x}^{\#13}} \right)^2 + \left( \frac{y_{CO_2/CO}^{\#13} - Expt_{CO_2/CO}^{\#13}}{Expt_{CO_2/CO}^{\#13}} \right)^2 \quad (6.6)$$

where  $y_{C_3H_8}^{\#13}$ ,  $y_{NO_x}^{\#13}$  and  $y_{CO_2/CO}^{\#13}$  are the model predictions for the conversion of  $C_3H_8$ , and  $NO_x$ , and the ratio of  $CO_2$  to  $CO$ . These values are polynomially formed with the factorial variables according to Equation (6.3), (6.4) and (6.5), respectively.  $Expt_{C_3H_8}^{\#13}$ ,  $Expt_{NO_x}^{\#13}$  and  $Expt_{CO_2/CO}^{\#13}$  are the experimental results for the conversion of  $C_3H_8$  and  $NO_x$ , and the ratio of  $CO_2$  to  $CO$ , respectively. The #13 stands for experimental condition 13 (cf. Table 3.3). Linear regression analysis is then adopted to calculate the values of the factorial variables,  $X$ , in order to minimise the objective function in Equation (6.6). Therefore, the optimised values of the factorial variables for experimental condition 13 are determined. However, these optimised values for the remaining experimental conditions (#2, 3, 4, 7, 8, 11, 17 and 18) can be approximated in the same way. Then, when all optimised factorial variables for all experimental conditions are established, the active parameters,  $k$ , can be reversely calculated from optimised  $X$  values by using Equation (6.2). Finally, these active parameters are mathematically formed as a function of inlet temperatures and/or concentrations of  $C_3H_8$  and  $NO_x$ . The optimised sticking coefficient and preexponential factors as a function of inlet conditions are listed in Table 6.5.

**Table 6.5:** Optimised values of active parameters for C<sub>3</sub>H<sub>8</sub>-SCR mechanism on a silver catalyst.

Active parameter	Sticking coefficient or preexponential factor (s <sup>-1</sup> ) value
$S_{15}^0$	0.9837
$A_{16}$	$3.16 \times 10^{14}$
$A_{55}$	$-3.98 \times 10^{12}T_s + 7.58 \times 10^{12}$ when $T_{in} \leq 563.15$ K $-2.34 \times 10^{11}T_s + 5.39 \times 10^{11}$ when $T_{in} > 563.15$ K
$A_{59}$	$9.13 \times 10^3 e^{8.63T_s}$
$A_{67}$	$9.46 \times 10^5 T_s^2 + 3.63 \times 10^5 THC_s^2 - 2.27 \times 10^4 NO_s^2 + 2.32 \times 10^4 T_s THC_s + 8.35 \times 10^5 T_s NO_s + 5.48 \times 10^4 THC_s NO_s - 5.23 \times 10^5 T_s - 1.39 \times 10^6 THC_s - 1.35 \times 10^6 NO_s + 5 \times 10^5$
$A_{73}$	$5.88 \times 10^{15} e^{-4.32T_s}$
$A_{75}$	$6.84 \times 10^{11} T_s^{-9.7702} e^{-0.0545 \left(\frac{THC}{NO}\right)_{in}}$
$A_{77}$	$2.53 \times 10^{11} T_s^2 - 1.31 \times 10^{12} T_s + 1.85 \times 10^{12}$
$A_{91}$	$-2.88 \times 10^9 T_s^2 + 2.08 \times 10^{10} T_s - 2.57 \times 10^{10}$

$S^0$  is the sticking coefficient and  $A$  is the preexponential factor.

$$T_s = \frac{T_{inlet}}{300}, \quad THC_s = \frac{THC_{inlet}}{1000}, \quad NO_s = \frac{NO_{inlet}}{100}$$

$T_{inlet}$  in the unit of Kelvin,  $THC_{inlet}$  and  $NO_{inlet}$  in the unit of ppm

## CHAPTER 7

### RESULTS AND DISCUSSION

The numerical simulation for selective catalytic reduction of NO<sub>x</sub> by propane (C<sub>3</sub>H<sub>8</sub>-SCR) on a silver based catalyst is validated in this chapter against the experimental data measured defined in Chapter 3. The model governing equations are formed and solved by the numerical method as presented in Chapter 4, while the catalytic reaction mechanism is developed and optimised as described in Chapters 5 and 6, respectively. Finally, the model was used to predict the effect on the NO<sub>x</sub> conversion at different operating conditions of the engine, for instance, inlet concentration of C<sub>3</sub>H<sub>8</sub> and NO<sub>x</sub> and inlet temperature.

#### 7.1 Model Validation

The validations between model predictions and experimental data are presented in Figure 7.1, 7.2 and 7.3. The conversions of C<sub>3</sub>H<sub>8</sub> and NO<sub>x</sub> are defined as:

$$C_3H_8 \text{ Conversion (\%)} = \frac{[CO]_{outlet} + [CO_2]_{outlet}}{[THC]_{inlet}} \times 100$$

$$NO_x \text{ Conversion (\%)} = \frac{([NO] + [NO_2])_{inlet} - ([NO] + [NO_2])_{outlet}}{([NO] + [NO_2])_{inlet}} \times 100$$

The experimental conditions appearing in the figures are given in Table 3.3 (Chapter 3).

The predicted C<sub>3</sub>H<sub>8</sub> conversion is in good agreement with the experimental data (Figure 7.1). As expected, propane conversion over the Ag/Al<sub>2</sub>O<sub>3</sub> catalyst increases with temperature. Interestingly, at relatively low temperatures of

approximately 250 °C, the C<sub>3</sub>H<sub>8</sub> conversion was decreased as the concentration of input NO was increased (conditions 1-3 and 4-6). In contrast, at relatively medium and high temperatures, 290 and 370 °C, the quantities of input NO have only a slight effect on the C<sub>3</sub>H<sub>8</sub> conversions.

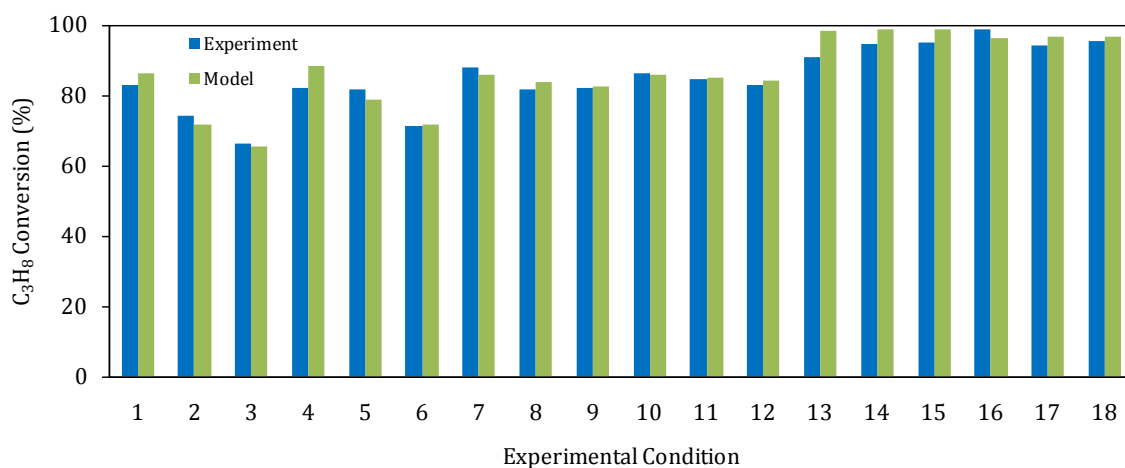


**Figure 7.1:** Comparisons between model predictions and experimental data for the conversion of C<sub>3</sub>H<sub>8</sub> at various operating conditions.

Figure 7.2 demonstrates that the conversion of NO<sub>x</sub> is influenced by three sources; input concentration of NO and C<sub>3</sub>H<sub>8</sub> and the inlet temperature. At constant input temperature and C<sub>3</sub>H<sub>8</sub> concentration (experimental condition 1-3 for 250 °C and 2000 ppm THC, 4-6 for 250 °C and 4000 ppm THC, 7-9 for 290 °C and 2000 ppm THC, 10-12 for 290 °C and 4000 ppm THC, 13-15 for 370 °C and 2000 ppm THC and 16-18 for 370 °C and 4000 ppm THC), NO<sub>x</sub> conversion declined noticeably when the input NO are increased. This decline was more noticeable at relatively low C<sub>3</sub>H<sub>8</sub> concentration of 2000 ppm THC (experimental condition 1-3, 7-9 and 13-15). These can be explained by the fact that in HC-SCR the input hydrocarbon is competitively consumed by two chemical pathways: complete oxidation with oxygen and selective reduction of NO<sub>x</sub>. When the input NO are increased or hydrocarbon additions

reduced, there is insufficient hydrocarbon and active sites for the SCR process to maintain good  $\text{NO}_x$  reduction efficiency. Increases in  $\text{C}_3\text{H}_8$  concentration improve the  $\text{Ag}/\text{Al}_2\text{O}_3$  efficiency in reducing  $\text{NO}_x$  emissions. This is a result of the i) more reducing agent, ii) improved probability of  $\text{NO}_x$  – HC – active site interaction and iii) increased gas temperature.

At constant concentration of  $\text{NO}$  and  $\text{C}_3\text{H}_8$  (experimental condition (1,7,13), (2,8,14), (3,9,15), (4,10,16), (5,11,17) and (6,12,18), the conversions of  $\text{NO}_x$  decrease as the temperature is increased. Interestingly, Figure 7.2 shows a remarkable decline in the conversions of  $\text{NO}_x$  at relative high temperature of 370 °C. These results indicate that at this temperature range, hydrocarbons are mainly used in complete oxidation rather than to selectively reduce  $\text{NO}_x$  emissions.

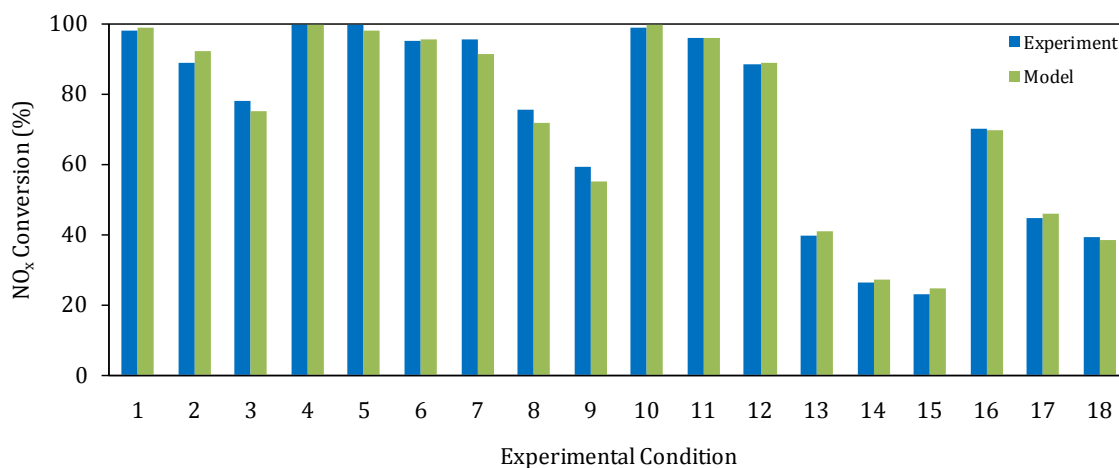


**Figure 7.2:** Comparisons between model predictions and experimental data for the conversion of  $\text{NO}_x$  at various operating conditions.

Model validations displayed in Figure 7.3, shown the predicted  $\text{CO}_2$  to  $\text{CO}$  ratios from a range of experimental conditions. At the same input  $\text{C}_3\text{H}_8$  concentration and temperature (experimental condition 1-3, 4-6, 7-9, 10-12, 13-15 and 16-18),  $\text{CO}_2$  to  $\text{CO}$  ratios increase as more  $\text{NO}$  is added to the mixture. This implies that the

production of CO<sub>2</sub> relates kinetically to the input concentration of NO. From Table 5.1, species derived from NO, such as NO<sub>2</sub>, NO<sub>3</sub> and NCO, can be linked to CO<sub>2</sub> through R(77), R(79) and R(91), respectively. Due to low activation energy, these elementary reactions can occur easily to produce CO<sub>2</sub>.

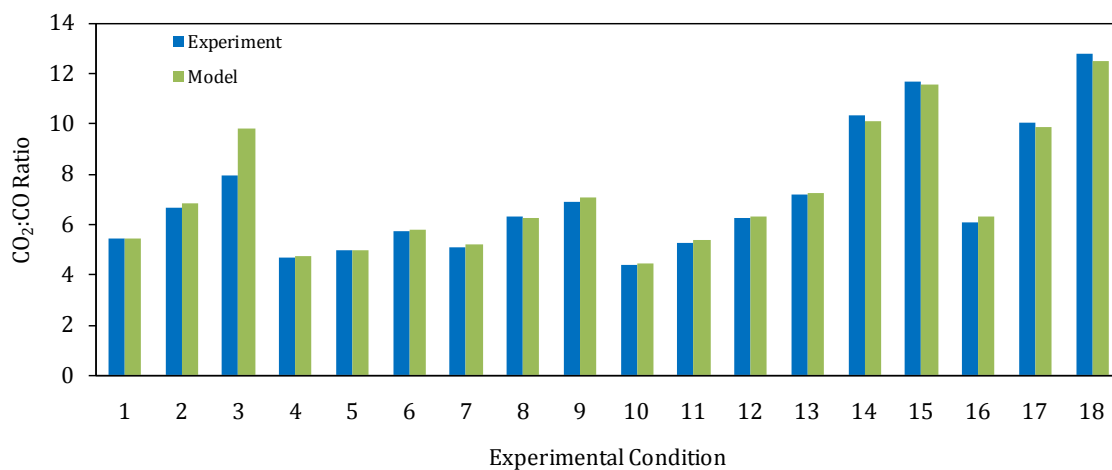


**Figure 7.3:** Comparisons between model predictions and experimental data for the ratio of CO<sub>2</sub> to CO at various operating conditions.

## 7.2 Simulations of C<sub>3</sub>H<sub>8</sub>-SCR on the Silver Catalyst

The effect of operating conditions on NO<sub>x</sub> conversion activity is present in Figure 7.4. The figure can be utilised to suggest a suitable quantity of propane to reduce NO<sub>x</sub> when the other operating conditions (i.e. temperature and NO<sub>x</sub> concentration) are known. For example, at temperatures of 400 °C, the NO<sub>x</sub> conversion is higher than 40% only when THC is higher than 25 times the NO (5000, 6000, 7000 and 8000 ppm THC in Figure 7.4a and 8000 ppm THC in Figure 7.4b).

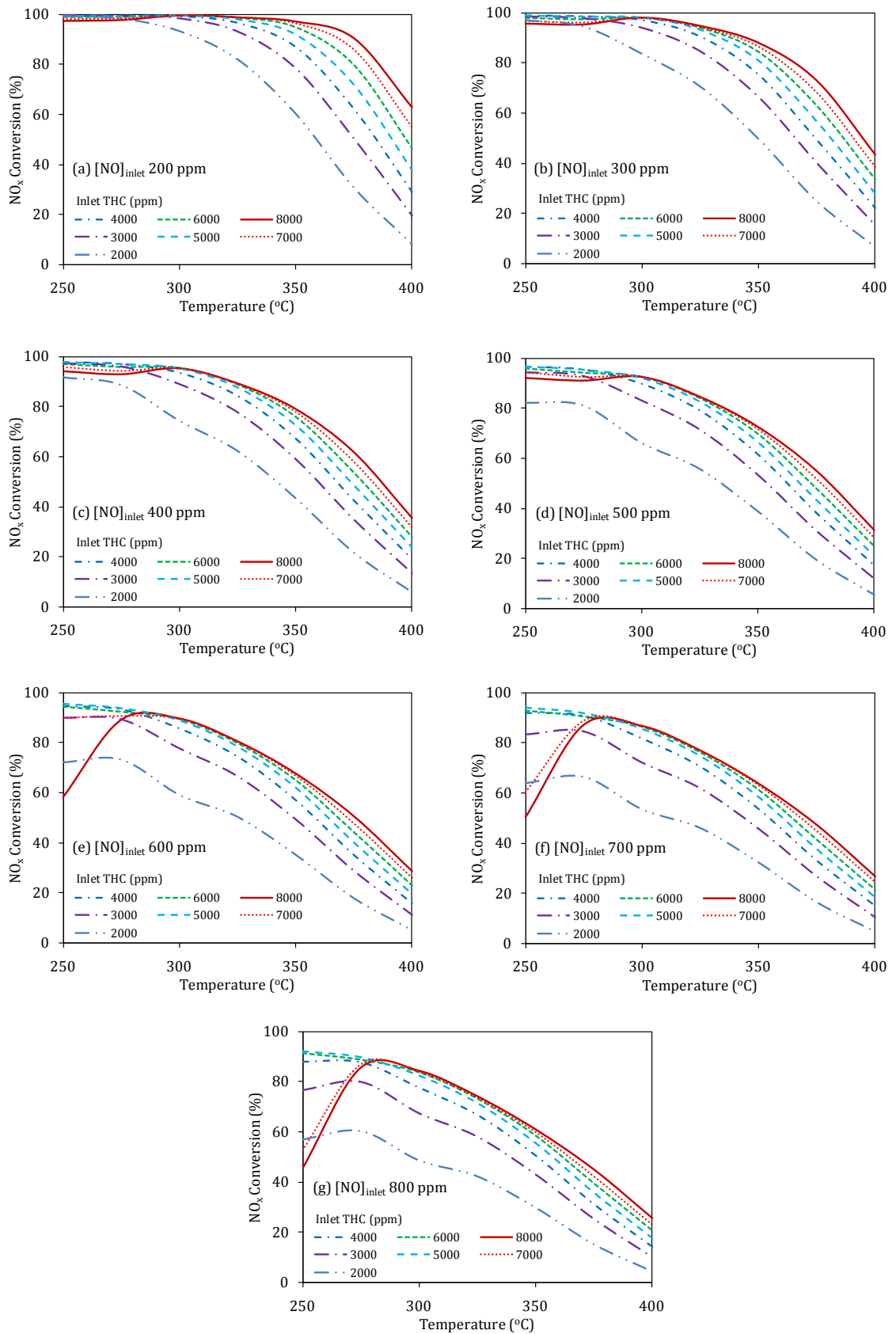


**Figure 7.4:** Model prediction of  $\text{NO}_x$  conversion as a function of temperature at different inlet concentration of  $\text{C}_3\text{H}_8$  and  $\text{NO}$ .

Wall and axial gas temperature profiles at different inlet temperatures and concentrations of  $C_3H_8$  are presented in Figure 7.5. The wall temperatures are predicted to be higher than the axial temperatures for all operating conditions; consequently, the  $C_3H_8$ -SCR process can be reasonably defined as an exothermic reaction. When the concentration of the input propane is increased, there are more hydrocarbons to react with oxygen (complete oxidation) and  $NO_x$  (selective reduction); so both wall and axial temperatures increase. In contrast, a change of the inlet  $NO$  concentration slightly affects both wall and axial temperatures (the results are not shown). Interestingly, at 250 °C inlet temperature (Figure 7.5a), wall and axial temperatures rise gradually by approximately 25 °C at the first 15 mm before sharply increasing. This trend suggests that the  $C_3H_8$ -SCR based on a silver catalyst initiates at approximately 270-280 °C. This starting temperature is a result of the oxidation of part of  $C_3H_8$  in the first 15 mm along the catalyst. This means that the first approximately 15 mm part of the catalyst is not used for  $C_3H_8$ -SCR of  $NO_x$ , and can be called an inactive length. The inadequate catalytic surface (as a result of the inactive length) on  $NO_x$  conversions can be seen especially at operating conditions where more active surface is required to convert  $NO_x$  (low temperatures and high inlet concentrations of  $C_3H_8$  and  $NO$ , Figure 7.4e-g). Accordingly, at these operating conditions,  $NO_x$  conversion is obviously low.

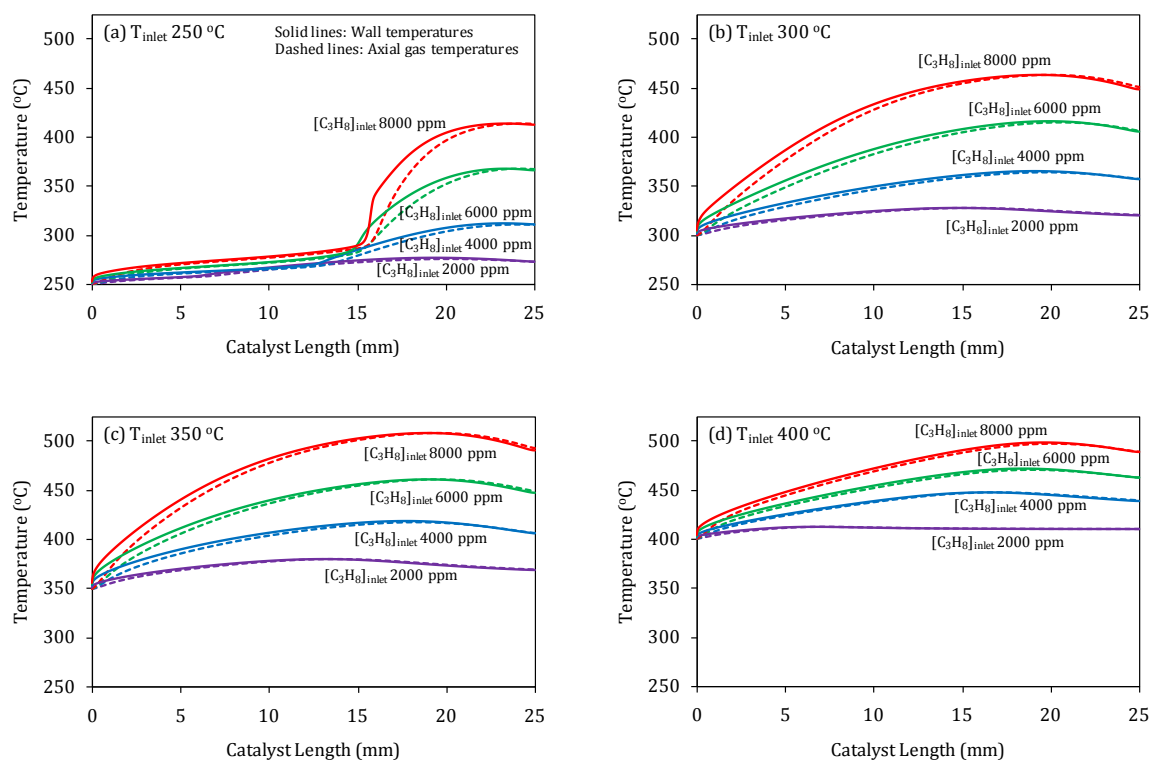


**Figure 7.5:** Wall and axial gas temperature profiles at different inlet temperatures. The inlet concentration of NO is 400 ppm.

Catalyst surface coverage by major species (i.e. atomic oxygen, hydroxyl, methoxy radical, acetate, nitrate and nitrile N-oxide), is presented in Figure 7.6. The reason for the inactive catalyst length at relatively low temperature of 250 °C, as mentioned earlier, can be explained by using Figure 7.6f; almost the entire catalyst surface is covered by adsorbed nitrile N-oxide (CNO). As a result, there is not enough active site for other gas species to adsorb onto it. From R(87) in Table 5.1, the relatively high activation energy, 84.68 kJ/mol, is required to transform surface nitrile N-oxide to surface cyanide and atomic oxygen. Thus it can be concluded that at relatively low temperature, 250 °C, the transformation of surface nitrile N-oxide to surface cyanide is the rate determining step and the surface nitrile N-oxide is the most abundant reaction intermediate. After the temperature at which SCR of NO<sub>x</sub>

processes are initiated, approximately 270-280 °C, surface nitrile N-oxide decrease rapidly. Accordingly, active sites not occupied by nitrile N-oxide are more available to activate other chemical reaction processes. These reactions include the formations of surface atomic oxygen, hydroxyl, methoxy radical and acetate as the sudden increases of these surface species are obviously observed. At temperature from 300 to 400 °C, the main surface species are atomic oxygen and hydroxyl. These abundant surface intermediates are in agreement with the recent paper published by Mhadeshwar et al. (Mhadeshwar et al., 2009). From Table 5.1, relatively high activation energies are required for the desorption of surface hydroxyl, 251.46 kJ/mol in R(26), and the formation of surface water from surface hydroxyls, 95.49 kJ/mol in R(71). These explain why the surface hydroxyl still remains a major species on the catalyst surface. The large amount of oxygen (usually found in exhaust from diesel engines) as well as a medium activation energy for its desorption process, 39.55 kJ/mol in R(8), make atomic oxygen the main surface species as well.

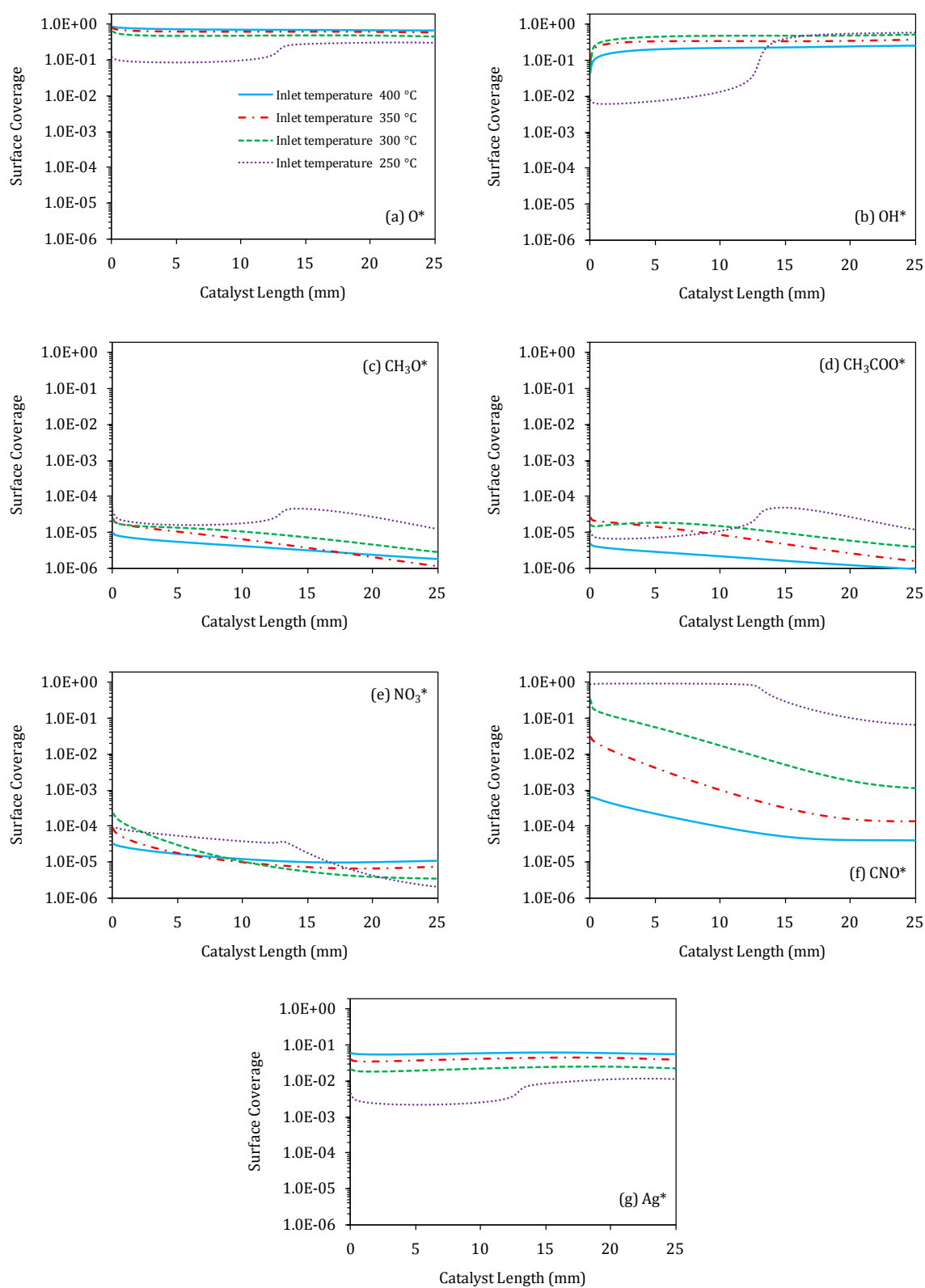


**Figure 7.6:** Simulated surface coverage profiles of surface species, O, OH, CH<sub>3</sub>O, CH<sub>3</sub>COO, NO<sub>3</sub>, CNO and Ag. Operating condition: 4000 ppm THC of C<sub>3</sub>H<sub>8</sub> and 400 ppm of NO.

The effect of temperatures on the surface coverage of the main species is demonstrated in Figure 7.7. Values of surface coverage are taken at the outlet of the channel. The figure shows that atomic oxygen and hydroxyl are the most abundant reaction intermediates throughout the range of inlet temperatures. The surface hydroxyl tends to decrease gradually when the inlet temperature rises. According to R(26) and R(71), activation energies of the depletion of surface hydroxyl are relatively high. This indicates that the migration of surface hydroxyl requires high temperatures. So, the removal of hydroxyl from the catalyst surface is promoted by temperatures. In contrast with the surface hydroxyl, surface atomic oxygen increases steadily as a function of inlet temperatures. An excessive amount of oxygen makes the atomic oxygen the principal species depositing on the surface of catalyst. A growth in surface coverage of adsorbed NO, NO<sub>2</sub> and NO<sub>3</sub> with temperature is the result of the insufficiency of hydrocarbon to selectively reduce these surface species at high temperature conditions. Vacant sites, Ag\*, increase with temperature as a result from less occupation on active sites of surface species, especially hydroxyl. Moreover, the surface coverage of NO<sub>3</sub> is obviously higher than that of NO and NO<sub>2</sub>. This simulation result coincides with the study by Kameoka et al. (Kameoka et al., 2000) as previously mentioned that adsorbed NO and NO<sub>2</sub> were hardly observed on the surface of catalyst.

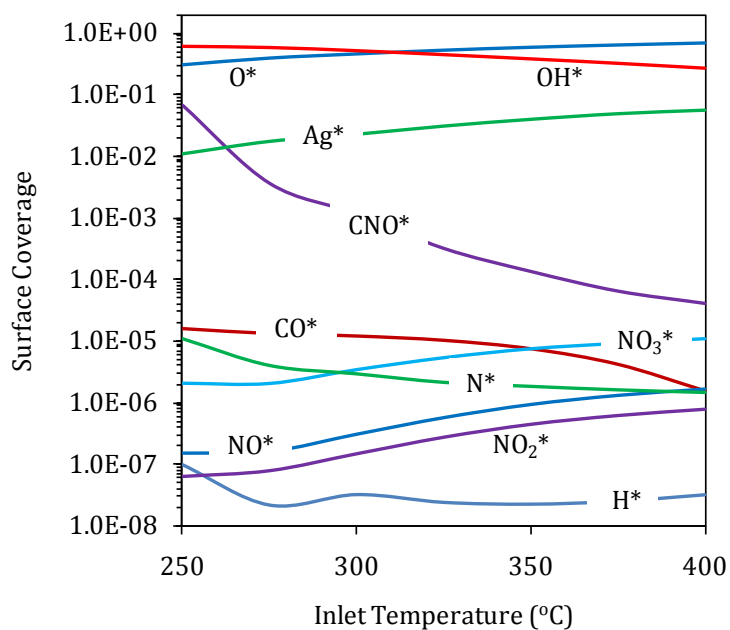


**Figure 7.7:** Simulated surface coverage of different surface species as a function of inlet temperature.  
Operating condition: 4000 ppm THC of  $C_3H_8$  and 400 ppm of NO.

# CHAPTER 8

## CONCLUSIONS

In this final chapter, the conclusions together with final remarks for the research are discussed. Future work is presented on the associated topic of catalytic reduction of  $\text{NO}_x$  in diesel engine exhaust gas.

### 8.1 Concluding Remarks

A numerical simulation for hydrocarbon selective catalytic reduction (HC-SCR) on a silver based catalyst of nitrogen oxides ( $\text{NO}_x$ ) in diesel engine exhaust gas has been systematically developed in this thesis. An in-depth understanding in terms of both physical and chemical phenomena has been effectively accomplished by using a computerised simulation rooted in computational fluid dynamics (CFD) and a detailed elementary reaction mechanism.

In terms of surface chemistry, a surface-reaction mechanism for SCR of  $\text{NO}_x$  by propane ( $\text{C}_3\text{H}_8$ -SCR) was logically constructed. Firstly, information on kinetic processes of HC-SCR on silver based catalysts, such as intermediate species and reaction pathways, was carefully taken from available literature. Secondly, microkinetic analysis was methodically applied in order to elucidate the chemical phenomena that took place on the catalyst surface. Finally, instead of fitting from experimental data, rate parameters appearing in the detailed elementary reactions were initially estimated by using theories of chemical bonding, for example, transition state theory (TST) and unity bond index-quadratic exponential potential (UBI-QEP).

Some rate parameters that significantly affect the C<sub>3</sub>H<sub>8</sub>-SCR process were identified by a method of sensitivity analysis. These important parameters were optimised using the solution-mapping method. In order to realise the influence of states of the catalytic surface, these optimised parameters were formed as a function of operating conditions.

A whole monolithic automotive catalytic converter was mathematically simplified to a single circular channel. The two-dimensional Navier-Stokes equations coupled with the surface-reaction mechanism as a reacting wall boundary condition were applied to model the C<sub>3</sub>H<sub>8</sub>-SCR process. The governing equations were numerically solved by using numerical method software, FLUENT version 6.3.

Validation was done by comparing modelling results with experimental data in a range of operating conditions (e.g. inlet concentrations of C<sub>3</sub>H<sub>8</sub> and NO<sub>x</sub> and inlet temperatures). The simulated results showed good agreements with data from experiments in many aspects, for instance, C<sub>3</sub>H<sub>8</sub> and NO<sub>x</sub> conversions and the ratio of produced CO<sub>2</sub> to CO. Moreover, due to the small scale of the physical domain, numerical simulation could provide both physical and chemical details that were difficult or impractical to measure, for example, concentration and temperature profiles, wall temperatures and occupations of surface species. Furthermore, the numerical simulation could predict the effect of operating conditions on NO<sub>x</sub> reduction. These predictions showed that at relative high temperatures, propane was predominantly preferable to completely oxidise with oxygen rather than selectively reduce with NO<sub>x</sub>. In terms of the temperature profile inside the channel of monolith, the simulation revealed that in a C<sub>3</sub>H<sub>8</sub>-SCR on the silver catalyst with the promotion of hydrogen, the starting point of temperature for SCR process was around 270-280

°C. In addition, at operating condition: low temperature and high inlet concentration of  $C_3H_8$  and  $NO_x$ , the modelling explained the causes of extremely low  $NO_x$  conversion through an “inactive length” of the catalyst’s active surface. In cases of surface species, the simulation indicated that atomic oxygen (O) and hydroxyl (OH) were the main components sticking on the catalyst surface. The modelling also showed that at relatively low temperature, the depletion of adsorbed nitrile N-oxide (CNO) to form surface cyanide (CN) was the rate determining step.

## **8.2 Future Work**

This thesis has shown the potential of the physical, chemical as well as mathematical modelling for SCR of  $NO_x$  on a silver based catalyst using propane as the reductant. The numerical simulations have revealed the computerised ability that can be used as an effective tool to assist in the development of an aftertreatment system. In order to abide by stringent automotive emission standards and be appropriate for practical uses, however, there is still a lot of work needed not only in areas of SCR of  $NO_x$  but also other related subjects.

### **8.2.1 Surface-Reaction Mechanisms for SCR of $NO_x$ by Using Different Types of Hydrocarbon as a Reducing Agent**

Many kinds of hydrocarbon have been found in exhaust gas from a diesel engine, for example,  $C_2$ - $C_{15}$  hydrocarbon (Caplain et al., 2006); methane, ethylene, propylene and toluene (Yamada et al., 2011). Nevertheless, these hydrocarbons have different physical and chemical properties. Moreover, the catalytically kinetic mechanism for each hydrocarbon is diverse. Subsequently, the surface-reaction

mechanism for many hydrocarbons is required to simulate the actual diesel-SCR. The finding of mechanistic chemistry can start from uncomplicated hydrocarbon such as propane (presented in this thesis). Then, the catalytic combustion mechanism for complex hydrocarbon can be built based on that simple mechanism.

### **8.2.2 The Effect of Water Vapour on a HC-SCR Process**

Water vapour is an inherent product from all internal combustion engines. Normally, water vapour has been considered as an inhibitor because its inactive behaviour competitively occupies active catalyst surface. However, recently Shimizu et al. reported that water vapour prevents the unselective oxidation of hydrocarbons, therefore promoting catalyst  $\text{NO}_x$  reduction activity (Shimizu et al., 2000b). Furthermore, He and Yu proposed that water vapour promote ethanol-SCR by suppressing the formation of acetate but supporting the creation of enolic species (He and Yu, 2005). Accordingly, the mechanistic activities of water vapour have to be studied in order to understand its effect on HC-SCR. To achieve this, though, equipment for controlling and measuring water vapour is required.

### **8.2.3 The Effect of Hydrogen on a HC-SCR Process**

Hydrogen has been widely accepted as an ideal co-feeder gas in active mode HC-SCR operation in order to decrease the minimum temperature needed to drive the  $\text{NO}_x$ -reducing reactions. However, the kinetic mechanism of hydrogen for reducing the catalyst activity window to lower temperatures is not fully understood yet. Theinnoi has reported that the differences of hydrogen concentration can make a huge variation on the  $\text{NO}_x$  conversion performance (Theinnoi, 2008). For that reason, the mechanistic effect of hydrogen concentration on HC-SCR has to be investigated

with the aim of finding the optimum amount of hydrogen required to be added to the NO<sub>x</sub> reduction process.

#### **8.2.4 Deactivation of a HC-SCR Catalyst**

There is no evidence of catalyst deactivation with/without hydrogen addition if a single-component hydrocarbon (n-octane, n-decane and n-dodecane) is used as a reducing agent. However, when long chain multi-component fuels (i.e. conventional and synthetic diesel) are obtained, the presence of hydrogen does not prevent catalyst coking at high THC:NO<sub>x</sub> ratios (Houel et al., 2007). Sawatmongkhon et al. have shown that the different configurations of a powdered catalyst can prevent the catalyst from deactivation (Sawatmongkhon et al., 2010). To kinetically understand the catalyst deactivation, laboratory scale experimental rigs and numerical modelling for unsteady state condition are essential. The deactivation procedures are modelled in the mathematical and chemical forms; then are solved using numerical methods. This knowledge can be used as an alternative tool to monitor, control and limit catalyst deactivation.

#### **8.2.5 Exhaust Gas Fuel Reforming**

To maintain the advantage of hydrogen for the HC-SCR of NO<sub>x</sub>, fuel reforming could be practically utilised as the on-board source for the required hydrogen. Tsolakis has shown the feasibility for producing hydrogen from exhaust gas reforming by incorporating a mini reformer in the exhaust system of a diesel engine (Tsolakis, 2004). In order to fully complete the HC-SCR of NO<sub>x</sub> system, the modelling of exhaust gas fuel reforming is necessary. Physical and chemical details as well as catalytic mechanisms for fuel reforming processes, such as partial oxidation, stream

reforming, dry reforming, autothermal reforming and water-gas shift, need to be simultaneously formulated.

## APPENDIX A

### TRANSPORT AND CHEMICAL PROPERTIES

**Table A.1:** Chemical formulas, names, molecular weights, standard enthalpies of formation and Lennard-Jones potential parameters.

Chemical formula	Name	Molecular weight, $M$ (kg/kmol)	Standard enthalpy of formation, $\Delta H_f^\circ$ (kJ/mol)	Lennard-Jones characteristic length, $\sigma$ (angstrom)	Lennard-Jones energy parameter, $\epsilon/k_B$ (K)
H	Atomic hydrogen	1.008	218.00	2.050	145.00
O	Atomic oxygen	15.999	249.19	2.750	80.00
CO	Carbon monoxide	28.010	-110.53	3.650	98.10
CO <sub>2</sub>	Carbon dioxide	44.010	-393.52	3.763	244.00
H <sub>2</sub>	Hydrogen	2.016	0.00	2.920	38.00
H <sub>2</sub> O	Water vapour	18.015	-241.82	2.605	572.40
OH	Hydroxyl	17.007	37.28	2.750	80.00
O <sub>2</sub>	Oxygen	31.999	0.00	3.458	107.40
N <sub>2</sub>	Nitrogen	28.013	0.00	3.621	97.53
HCO	Formyl	29.018	42.68	3.590	498.00
CH <sub>3</sub> O	Methoxy radical	31.034	-16.99	3.690	417.00
CH <sub>3</sub> CHO	Acetaldehyde	44.053	-166.20	3.970	436.00
CH <sub>3</sub> CO	Acetyl radical	43.045	-10.46	3.970	436.00
CH <sub>3</sub> COO	Acetate	59.044	-179.91	3.970	436.00
C <sub>3</sub> H <sub>7</sub> O	i-Propoxy radical	59.088	-48.53	5.574	481.24
C <sub>3</sub> H <sub>7</sub> OH	i-Propanol	60.096	-272.60	4.549	576.70
C <sub>3</sub> H <sub>8</sub>	Propane	44.096	-103.85	4.982	266.80
NO	Nitric oxide	30.006	91.30	3.621	97.53
NO <sub>2</sub>	Nitrogen dioxide	46.006	33.20	3.500	200.00
NO <sub>3</sub>	Nitrate	62.005	73.64	3.500	200.00
CH <sub>3</sub> NO <sub>2</sub>	Nitromethane	61.040	-74.30	4.913	499.85
CH <sub>2</sub> NO <sub>2</sub>	Nitromethylene	60.032	115.06	4.913	499.85
CH <sub>2</sub> NO	Formaldiminoxy	44.033	156.90	4.913	499.85
CN	Cyanide	26.018	439.32	3.856	75.00
CNO	Nitrile N-oxide	42.017	323.00	3.828	232.40
NCO	Isocyanate	42.017	131.80	3.828	232.40
N	Atomic nitrogen	14.007	472.65	3.298	71.40

**Table A.2:** Atomic and structural diffusion-volume increments.

Atom/structure	$v$
C	16.50
H	1.98
O	5.48
N	5.69
Cl	19.50
S	17.00
Aromatic ring	-20.20
Heterocyclic ring	-20.20

**Table A.3:** Diffusion volumes for simple molecules.

Molecule	$\Sigma v$
H <sub>2</sub>	7.07
D <sub>2</sub>	6.70
He	2.88
N <sub>2</sub>	17.90
O <sub>2</sub>	16.60
Air	20.10
Ar	16.10
Kr	22.80
Xe	37.90
CO	18.90
CO <sub>2</sub>	26.90
N <sub>2</sub> O	35.90
NH <sub>3</sub>	14.90
H <sub>2</sub> O	12.70
CCl <sub>2</sub> F <sub>2</sub>	114.80
SF <sub>6</sub>	69.70
Cl <sub>2</sub>	37.70
Br <sub>2</sub>	67.20
SO <sub>2</sub>	41.10

**Table A.4:** Polynomial coefficients for mass diffusion coefficient for species  $i$  in the mixture of  $i$  and nitrogen.

$$D_{i,N_2} = a_0 + a_1T + a_2T^2 + a_3T^3 + a_4T^4$$

Chemical formula	$a_0$	$a_1$	$a_2$	$a_3$	$a_4$
CO	-1.4027E-06	2.3327E-08	1.7909E-10	-3.9117E-14	8.5762E-18
CO <sub>2</sub>	-1.1229E-06	1.8674E-08	1.4336E-10	-3.1314E-14	6.8654E-18
H <sub>2</sub>	-5.1879E-06	8.6276E-08	6.6235E-10	-1.4467E-13	3.1719E-17
H <sub>2</sub> O	-1.8043E-06	3.0006E-08	2.3036E-10	-5.0315E-14	1.1031E-17
OH	-2.1539E-06	3.5820E-08	2.7500E-10	-6.0065E-14	1.3169E-17
O <sub>2</sub>	-1.4182E-06	2.3585E-08	1.8107E-10	-3.9549E-14	8.6710E-18
N <sub>2</sub>	-1.4284E-06	2.3755E-08	1.8237E-10	-3.9834E-14	8.7335E-18
HCO	-1.2818E-06	2.1317E-08	1.6365E-10	-3.5746E-14	7.8372E-18
CH <sub>3</sub> O	-1.1948E-06	1.9870E-08	1.5254E-10	-3.3318E-14	7.3049E-18
CH <sub>3</sub> CHO	-9.1714E-07	1.5252E-08	1.1709E-10	-2.5576E-14	5.6074E-18
CH <sub>3</sub> CO	-9.3688E-07	1.5581E-08	1.1961E-10	-2.6127E-14	5.7282E-18
CH <sub>3</sub> COO	-8.4649E-07	1.4077E-08	1.0807E-10	-2.3606E-14	5.1755E-18
C <sub>3</sub> H <sub>7</sub> O	-7.4457E-07	1.2382E-08	9.5061E-11	-2.0763E-14	4.5523E-18
C <sub>3</sub> H <sub>7</sub> OH	-7.3402E-07	1.2207E-08	9.3714E-11	-2.0469E-14	4.4878E-18
C <sub>3</sub> H <sub>8</sub>	-8.0099E-07	1.3321E-08	1.0226E-10	-2.2337E-14	4.8973E-18
NO	-1.6335E-06	2.7165E-08	2.0855E-10	-4.5552E-14	9.9871E-18
NO <sub>2</sub>	-1.3123E-06	2.1824E-08	1.6754E-10	-3.6595E-14	8.0233E-18
NO <sub>3</sub>	-1.1325E-06	1.8834E-08	1.4459E-10	-3.1582E-14	6.9242E-18
CH <sub>3</sub> NO <sub>2</sub>	-9.2459E-07	1.5376E-08	1.1805E-10	-2.5784E-14	5.6530E-18
CH <sub>2</sub> NO <sub>2</sub>	-9.4528E-07	1.5720E-08	1.2069E-10	-2.6361E-14	5.7795E-18
CH <sub>2</sub> NO	-1.0591E-06	1.7613E-08	1.3522E-10	-2.9535E-14	6.4754E-18
CN	-1.3532E-06	2.2505E-08	1.7277E-10	-3.7737E-14	8.2737E-18
CNO	-1.1219E-06	1.8657E-08	1.4323E-10	-3.1285E-14	6.8590E-18
NCO	-1.1219E-06	1.8657E-08	1.4323E-10	-3.1285E-14	6.8590E-18

The temperature is in the unit of Kelvin.

**Table A.5:** Polynomial coefficients for specific heat capacity.

$$C_p = a_0 + a_1T + a_2T^2 + a_3T^3 + a_4T^4$$

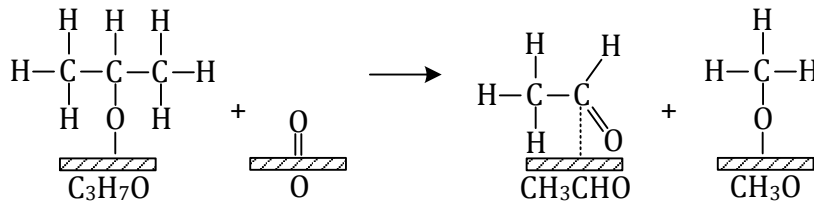
Chemical formula	$a_0$	$a_1$	$a_2$	$a_3$	$a_4$
H	Constant value of $C_p$ 20,609 J/kg·K				
O	1.5302E+03	-8.5074E-01	1.2573E-03	-8.3240E-07	2.0205E-10
CO	9.6778E+02	4.4850E-01	-1.1515E-03	1.6558E-06	-7.3417E-10
CO <sub>2</sub>	4.2965E+02	1.8732E+00	-1.9652E-03	1.2964E-06	-3.9973E-10
H <sub>2</sub>	1.3594E+04	3.4002E+00	-3.3563E-03	-3.9055E-07	1.7043E-09
H <sub>2</sub> O	1.5621E+03	1.6027E+00	-2.9309E-03	3.2141E-06	-1.1561E-09
OH	1.7770E+03	9.0428E-02	-8.1890E-04	1.1663E-06	-4.1193E-10
O <sub>2</sub>	8.3428E+02	2.9277E-01	-1.4947E-04	3.4117E-07	-2.2769E-10
N <sub>2</sub>	9.7840E+02	4.1769E-01	-1.1755E-03	1.6733E-06	-7.2516E-10
HCO	8.2990E+02	1.7750E+00	-2.7554E-03	3.1206E-06	-1.3100E-09
CH <sub>3</sub> O	5.6391E+02	1.9321E+00	1.4293E-03	-1.9753E-06	5.5572E-10
CH <sub>3</sub> CHO	4.7260E+02	2.5217E+00	8.8119E-04	-2.1278E-06	8.0416E-10
CH <sub>3</sub> CO	6.0327E+02	1.8875E+00	8.7277E-04	-1.7391E-06	6.1648E-10
CH <sub>3</sub> COO	2.3694E+02	2.2806E+00	-1.3110E-04	-5.7363E-07	2.7105E-20
C <sub>3</sub> H <sub>7</sub> O	3.8258E+01	5.4470E+00	-2.8791E-03	5.3511E-07	1.3553E-20
C <sub>3</sub> H <sub>7</sub> OH	2.9290E+02	5.2688E+00	-2.8587E-03	6.0307E-07	-
C <sub>3</sub> H <sub>8</sub>	1.6900E+02	5.0291E+00	1.0234E-03	-4.0060E-06	1.7417E-09
NO	9.3499E+02	3.4698E-01	-9.1456E-04	1.4449E-06	-6.7739E-10
NO <sub>2</sub>	4.8233E+02	1.4157E+00	-1.4564E-03	1.1128E-06	-4.1904E-10
NO <sub>3</sub>	1.6363E+02	2.5177E+00	-1.8014E-03	1.7080E-07	1.8145E-10
CH <sub>3</sub> NO <sub>2</sub>	4.3896E+01	3.6279E+00	-2.6279E-03	1.0567E-06	-1.9040E-10
CH <sub>2</sub> NO <sub>2</sub>	1.0345E+02	3.3290E+00	-2.1383E-03	5.1199E-07	1.3553E-20
CH <sub>2</sub> NO	1.0345E+02	3.3290E+00	-2.1383E-03	5.1199E-07	1.3553E-20
CN	1.1699E+03	-3.6934E-01	6.9089E-04	5.9215E-08	-2.6234E-10
CNO	7.5538E+02	1.2688E+00	-1.0487E-03	4.5645E-07	-8.4171E-11
NCO	6.6436E+02	1.0665E+00	-1.6106E-04	-3.7827E-07	1.5497E-10
N	Constant value of $C_p$ 1,483 J/kg·K				

The temperature is in the unit of Kelvin.

## APPENDIX B

### EXAMPLES OF CALCULATION

**Example 1:** Consider the elementary reaction R(57) in Table 5.1:



As shown in Table 5.3 and 5.5,  $\text{C}_3\text{H}_7\text{O}$  binds strongly on the catalyst surface.

Therefore, heat of adsorption of  $\text{C}_3\text{H}_7\text{O}$  can be estimated by using Equation (5.6).

$$Q_{AB} = \frac{Q_A^2}{Q_A + \mathcal{D}_{AB}} \quad (5.6)$$

The alphabet  $A$  is molecular oxygen due to  $\text{C}_3\text{H}_7\text{O}$  molecule binding with the catalyst surface via it. To calculate  $Q_A$ , Equation (5.4) is applied.

$$Q_{0A} = \frac{Q_A}{2 - 1/n} \quad (5.4)$$

From Table 5.4, the value of  $Q_{0A}$  for oxygen adatom on silver is 200.83 kJ/mol. By substituting the value of 3 for  $n$ , therefore,  $Q_A$  can be computed, 334.72 kJ/mol. Bond-energy partitioning,  $\mathcal{D}_{AB}$ , for  $\text{C}_3\text{H}_7\text{O}$  in this example, is the energy required for separating surface bonding molecule (molecular oxygen) from  $\text{C}_3\text{H}_7\text{O}$  in the gas phase which can be calculated by:

$$\mathcal{D}_{AB} = -\Delta H_{f,\text{C}_3\text{H}_7\text{O}}^0 + \Delta H_{f,\text{C}_3\text{H}_7}^0 + \Delta H_{f,\text{O}}^0$$

From Table A.1, the standard enthalpy of formation for C<sub>3</sub>H<sub>7</sub>O and molecular oxygen are -48.53 and 249.19 kJ/mol respectively. The standard enthalpy of formation for C<sub>3</sub>H<sub>7</sub> is taken from literature (Luo, 2007), 87.86 kJ/mol. So, bond energy partitioning of C<sub>3</sub>H<sub>7</sub>O is estimated, 385.59 kJ/mol. Thus heat of adsorption,  $Q_{AB}$ , of C<sub>3</sub>H<sub>7</sub>O can be computed. The necessary parameters for estimating the activation energy are shown below.

	C <sub>3</sub> H <sub>7</sub> O	O	CH <sub>3</sub> CHO	CH <sub>3</sub> O
$Q_{OA}$	200.83	200.83	276.98	200.83
$Q_A$	334.72	334.72	461.63	334.72
$D_{AB}$	385.59	0.00	1496.76	412.87
$Q_{AB}$	155.54	334.72	43.25	149.87
$D$	29.04	0.00	0.00	412.88

All values are in the unit of kJ/mol.

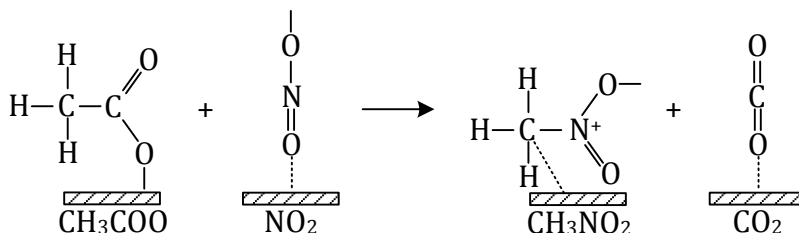
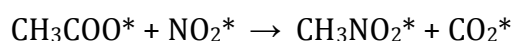
The activation energy of the disproportionation reaction,  $A^* + BC^* \rightarrow AB^* + C^*$ , can be calculated by using Equation (5.18) and (5.19).

$$E_{a,f} = \frac{1}{2} \left( \Delta H + \frac{Q_{AB} Q_C}{Q_{AB} + Q_C} \right) \quad (5.18)$$

$$\Delta H = Q_A + Q_{BC} + D_{BC} - D_{AB} - Q_{AB} - Q_C \quad (5.19)$$

The forward direction of the disproportionation reaction is defined as the bond dissociation energy of the reactant  $BC$  ( $D_{BC}$ ) has to be greater than that of the product  $AB$  ( $D_{AB}$ ). The value of the bond dissociation energy of CH<sub>3</sub>O is higher than that of C<sub>3</sub>H<sub>7</sub>O; accordingly, the alphabet  $A$ ,  $BC$ ,  $AB$  and  $C$  represent CH<sub>3</sub>CHO, CH<sub>3</sub>O, C<sub>3</sub>H<sub>7</sub>O and O respectively. Calculated by using Equation (5.18) and (5.19), the activation energy of R(57) in Table 5.1 is 9.75 kJ/mol.

**Example 2:** Consider the elementary reaction R(77) in Table 5.1:



The required variables used to calculate the activation energy are shown below.

	CH <sub>3</sub> COO	NO <sub>2</sub>	CH <sub>3</sub> NO <sub>2</sub>	CO <sub>2</sub>
$Q_{0A}$	200.83	200.83	276.98	200.83
$Q_A$	334.72	334.72	461.63	334.72
$\mathcal{D}_{AB}$	418.64	307.29	1478.18	1608.58
$Q_{AB}$	148.72	79.38	43.71	13.47
$D$	52.38	307.27	148.62	532.21

All values are in the unit of kJ/mol.

Calculated by using Equation (5.18) and (5.19), the activation energy is the negative value. To be physical meaning, consequently, the activation energy is forced to be the value of zero.

## **APPENDIX C**

### **AUTHOR'S PUBLICATIONS**

Sawatmongkhon, B., Tsolakis, A., Sitshebo, S., Rodríguez-Fernández, J., Ahmadinejad, M., Collier, J. & Rajaram, R. R. 2010. Understanding the Ag/Al<sub>2</sub>O<sub>3</sub> hydrocarbon-SCR catalyst deactivation through TG/DT analyses of different configurations. *Applied Catalysis B: Environmental*, 97, 373-380.

Sawatmongkhon, B., Tsolakis, A., York, A. P. E. & Theinnoi, K. 2011. Microkinetic modelling for propane oxidation in channel flows of a silver-based automotive catalytic converter. *SAE*, Paper No. 2011-01-2094.

Sawatmongkhon, B., Tsolakis, A., Theinnoi, K., York, A. P. E., Millington, P. J. & Rajaram, R. R. 2012. Microkinetic modelling for selective catalytic reduction (SCR) of NO<sub>x</sub> by propane in a silver-based automotive catalytic converter. *Applied Catalysis B: Environmental*, 111-112, 165-177.

## LIST OF REFERENCES

- Aghalayam, P., Park, Y. K., Fernandes, N., Papavassiliou, V., Mhadeshwar, A. B. & Vlachos, D. G. 2003. A C1 mechanism for methane oxidation on platinum. *Journal of Catalysis*, 213, 23-38.
- Aghalayam, P., Park, Y. K. & Vlachos, D. G. 2000. Construction and optimization of complex surface-reaction mechanism. *AIChE Journal*, 46, 2017-2029.
- Ansell, G. P., Bennett, P. S., Cox, J. P., Frost, J. C., Gray, P. G., Jones, A. M., Rajaram, R. R., Walker, A. P., Litorell, M. & Smedler, G. 1996. The development of a model capable of predicting diesel lean NO<sub>x</sub> catalyst performance under transient conditions. *Applied Catalysis B: Environmental*, 10, 183-201.
- Bettahar, M. M., Costentin, G., Savary, L. & Lavalley, J. C. 1996. On the partial oxidation of propane and propylene on mixed metal oxide catalysts. *Applied Catalysis A: General*, 145, 1-48.
- Bion, N., Saussey, J., Haneda, M. & Daturi, M. 2003. Study by in situ FTIR spectroscopy of the SCR of NO<sub>x</sub> by ethanol on Ag/Al<sub>2</sub>O<sub>3</sub>--Evidence of the role of isocyanate species. *Journal of Catalysis*, 217, 47-58.
- Blakeman, P. G., Andersen, P. J., Chen, H.-Y., Jonsson, J. D., Phillips, P. R. & Twigg, M. V. 2003. Performance of NO<sub>x</sub> adsorber emissions control systems for diesel engines. *SAE*, Paper No. 2003-01-0045.
- Box, G. E. P., Hunter, W. G. & Hunter, S. 1978. *Statistics for Experimenters: An Introduction to Design, Data Analysis and Model Building*, John Wiley & Sons.
- Burch, R., Breen, J. P. & Meunier, F. C. 2002. A review of the selective reduction of NO<sub>x</sub> with hydrocarbons under lean-burn conditions with non-zeolitic oxide and platinum group metal catalysts. *Applied Catalysis B: Environmental*, 39, 283-303.
- Burch, R. & Millington, P. J. 1995. Selective reduction of nitrogen oxides by hydrocarbons under lean-burn conditions using supported platinum group metal catalysts. *Catalysis Today*, 26, 185-206.
- Burch, R. & Ottery, D. 1997. The selective reduction of nitrogen oxides by higher hydrocarbons on Pt catalysts under lean-burn conditions. *Applied Catalysis B: Environmental*, 13, 105-111.
- Canu, P. & Vecchi, S. 2002. CFD simulation of reactive flows: Catalytic combustion in a monolith. *AIChE Journal*, 48, 2921 - 2935.
- Čapek, L., Novoveská, K., Sobalík, Z., Wichterlová, B., Cider, L. & Jobson, E. 2005. Cu-ZSM-5 zeolite highly active in reduction of NO with decane under water vapor presence: Comparison of decane, propane and propene by in situ FTIR. *Applied Catalysis B: Environmental*, 60, 201-210.

- Caplain, I., Cazier, F., Nouali, H., Mercier, A., Déchaux, J.-C., Nollet, V., Joumard, R., André, J.-M. & Vidon, R. 2006. Emissions of unregulated pollutants from European gasoline and diesel passenger cars. *Atmospheric Environment*, 40, 5954-5966.
- Chafik, T., Kameoka, S., Ukisu, Y. & Miyadera, T. 1998. In situ diffuse reflectance infrared Fourier transform spectroscopy study of surface species involved in NO<sub>x</sub> reduction by ethanol over alumina-supported silver catalyst. *Journal of Molecular Catalysis A: Chemical*, 136, 203-211.
- Chatterjee, D., Deutschmann, O. & Warnatz, J. 2001. Detailed surface reaction mechanism in a three-way catalyst. *Faraday Discussions*, 119, 371-384.
- Chatterjee, S., Walker, A. P. & Blakeman, P. G. 2008. Emission control options to achieve Euro IV and Euro V on heavy-duty diesel engines. *SAE*, Paper No. 2008-28-0021.
- Cortright, R. D. & Dumesic, J. A. 2001. Kinetics of heterogeneous catalytic reactions: Analysis of reaction schemes. *Advances in Catalysis*. Academic Press.
- Creaser, D., Kannisto, H., Sjöblom, J. & Ingelsten, H. H. 2009. Kinetic modeling of selective catalytic reduction of NO<sub>x</sub> with octane over Ag-Al<sub>2</sub>O<sub>3</sub>. *Applied Catalysis B: Environmental*, 90, 18-28.
- Dalle Nogare, D., Degenstein, N. J., Horn, R., Canu, P. & Schmidt, L. D. 2008. Modeling spatially resolved profiles of methane partial oxidation on a Rh foam catalyst with detailed chemistry. *Journal of Catalysis*, 258, 131-142.
- Deutschmann, O., Maier, L. I., Riedel, U., Stroemman, A. H. & Dibble, R. W. 2000. Hydrogen assisted catalytic combustion of methane on platinum. *Catalysis Today*, 59, 141-150.
- DieselNet. 2008. *Diesel Emissions* [Online]. Available: [www.DieselNet.com](http://www.DieselNet.com) [Accessed].
- Dumesic, J. A., Rudd, D. F., Aparicio, L. M., Rekoske, J. E. & Treviño, A. A. 1993. *The Microkinetics of Heterogeneous Catalysis*, Washington DC, American Chemical Society.
- Fluent Inc. 2006. *FLUENT 6.3 User's Guide*, Lebanon, Fluent Inc.
- Fogler, H. S. 2006. *Elements of Chemical Reaction Engineering*, Massachusetts, Prentice Hall.
- Frenklach, M., Wang, H. & Rabinowitz, M. J. 1992. Optimization and analysis of large chemical kinetic mechanisms using the solution mapping method--combustion of methane. *Progress in Energy and Combustion Science*, 18, 47-73.
- Hartmann, M., Maier, L., Minh, H. D. & Deutschmann, O. 2010. Catalytic partial oxidation of iso-octane over rhodium catalysts: An experimental, modeling, and simulation study. *Combustion and Flame*, 157, 1771-1782.
- Hayes, R. E. & Kolaczkowski, S. T. 1997. *Introduction to Catalytic Combustion*, CRC Press.

- Hayes, R. E. & Kolaczkowski, S. T. 1999. A study of Nusselt and Sherwood numbers in a monolith reactor. *Catalysis Today*, 47, 295-303.
- Hayes, R. E., Kolaczkowski, S. T., Li, P. K. C. & Awdry, S. 2001. The palladium catalysed oxidation of methane: reaction kinetics and the effect of diffusion barriers. *Chemical Engineering Science*, 56, 4815-4835.
- He, H. & Yu, Y. 2005. Selective catalytic reduction of NO<sub>x</sub> over Ag/Al<sub>2</sub>O<sub>3</sub> catalyst: from reaction mechanism to diesel engine test. *Catalysis Today*, 100, 37-47.
- He, H., Zhang, C. & Yu, Y. 2004. A comparative study of Ag/Al<sub>2</sub>O<sub>3</sub> and Cu/Al<sub>2</sub>O<sub>3</sub> catalysts for the selective catalytic reduction of NO by C<sub>3</sub>H<sub>6</sub>. *Catalysis Today*, 90, 191-197.
- Held, W., König, A., Richter, T. & Puppe, L. 1990. Catalytic NO<sub>x</sub> reduction in net oxidizing exhaust gas. *SAE*, Paper No. 900496.
- Heywood, J. B. 1988. *Internal Combustion Engine Fundamentals*, McGraw-Hill.
- Houel, V., James, D., Millington, P., Pollington, S., Poulston, S., Rajaram, R. & Torbati, R. 2005. A comparison of the activity and deactivation of Ag/Al<sub>2</sub>O<sub>3</sub> and Cu/ZSM-5 for HC-SCR under simulated diesel exhaust emission conditions. *Journal of Catalysis*, 230, 150-157.
- Houel, V., Millington, P., Rajaram, R. & Tsolakis, A. 2007. Promoting functions of H<sub>2</sub> in diesel-SCR over silver catalysts. *Applied Catalysis B: Environmental*, 77, 29-34.
- Iwamoto, M. 1990. Proceeding of the meeting on catalytic technology for the removal of nitrogen monoxide. *The Catalysis Society of Japan*, 17-22.
- Iwamoto, M., Yahiro, H., Shundo, S., Yu-u, Y. & Mizuno, N. 1991. Influence of sulfur dioxide on catalytic removal of nitric oxide over copper ion-exchanged ZSM-5 zeolite. *Applied Catalysis*, 69, L15-L19.
- Kameoka, S., Chafik, T., Ukisu, Y. & Miyadera, T. 1998. Reactivity of surface isocyanate species with NO, O<sub>2</sub> and NO+O<sub>2</sub> in selective reduction of NO over Ag/Al<sub>2</sub>O<sub>3</sub> and Al<sub>2</sub>O<sub>3</sub> catalysts. *Catalysis Letters*, 55, 211-215.
- Kameoka, S., Ukisu, Y. & Miyadera, T. 2000. Selective catalytic reduction of NO with CH<sub>3</sub>OH, C<sub>2</sub>H<sub>5</sub>OH and C<sub>3</sub>H<sub>6</sub> in the presence of O<sub>2</sub> over Ag/Al<sub>2</sub>O<sub>3</sub> catalyst: Role of surface nitrate species. *Physical Chemistry Chemical Physics*, 2, 367-372.
- Koebel, M., Elsener, M. & Kleemann, M. 2000. Urea-SCR: a promising technique to reduce NO<sub>x</sub> emissions from automotive diesel engines. *Catalysis Today*, 59, 335-345.
- Koebel, M., Elsener, M. & Madia, G. 2001. Recent advances in the development of urea-SCR for automotive applications. *SAE*, Paper No. 2001-01-3625.
- Koop, J. & Deutschmann, O. 2009. Detailed surface reaction mechanism for Pt-catalyzed abatement of automotive exhaust gases. *Applied Catalysis B: Environmental*, 91, 47-58.
- Lin, M., Desai, T. B., Kaiser, F. W. & Klugherz, P. D. 2000. Reaction pathways in the selective oxidation of propane over a mixed metal oxide catalyst. *Catalysis Today*, 61, 223-229.

- Lindfors, L. E., Eränen, K., Klingstedt, F. & Murzin, D. Y. 2004. Silver/alumina catalyst for selective catalytic reduction of NO<sub>x</sub> to N<sub>2</sub> by hydrocarbons in diesel powered vehicles. *Topics in Catalysis*, 28, 185-189.
- Lionta, G. D., Christoforou, S. C., Efthimiadis, E. A. & Vasalos, I. A. 1996. Selective catalytic reduction of NO with hydrocarbons: Experimental and simulation results. *Industrial & Engineering Chemistry Research*, 35, 2508-2515.
- Liu, B., Hayes, R. E., Yi, Y., Mmbaga, J., Checkel, M. D. & Zheng, M. 2007. Three dimensional modelling of methane ignition in a reverse flow catalytic converter. *Computers & Chemical Engineering*, 31, 292-306.
- Liu, Z. & Woo, S. I. 2006. Recent advances in catalytic DeNO<sub>x</sub> science and technology. *Catalysis Reviews*, 48, 43-89.
- Luo, L., Labinger, J. A. & Davis, M. E. 2001. Comparison of reaction pathways for the partial oxidation of propane over vanadyl ion-exchanged zeolite beta and Mo<sub>1</sub>V<sub>0.3</sub>Te<sub>0.23</sub>Nb<sub>0.12</sub>O<sub>x</sub>. *Journal of Catalysis*, 200, 222-231.
- Luo, Y.-R. 2007. *Comprehensive Handbook of Chemical Bond Energies*, CRC Press.
- Majewski, W. A. 2007. NO<sub>x</sub> Adsorbers [Online]. Available: [www.DieselNet.com](http://www.DieselNet.com) [Accessed].
- Matsumoto, S. 1996. DeNO<sub>x</sub> catalyst for automotive lean-burn engine. *Catalysis Today*, 29, 43-45.
- Meunier, F. C., Breen, J. P., Zuzaniuk, V., Olsson, M. & Ross, J. R. H. 1999. Mechanistic aspects of the selective reduction of NO by propene over alumina and silver-alumina catalysts. *Journal of Catalysis*, 187, 493-505.
- Meunier, F. C. & Ross, J. R. H. 2000. Effect of ex situ treatments with SO<sub>2</sub> on the activity of a low loading silver-alumina catalyst for the selective reduction of NO and NO<sub>2</sub> by propene. *Applied Catalysis B: Environmental*, 24, 23-32.
- Mhadeshwar, A. B., Aghalayam, P., Papavassiliou, V. & Vlachos, D. G. 2002. Surface reaction mechanism development for platinum-catalyzed oxidation of methane. *Proceedings of the Combustion Institute*, 29, 997-1004.
- Mhadeshwar, A. B. & Vlachos, D. G. 2005a. Hierarchical multiscale mechanism development for methane partial oxidation and reforming and for thermal decomposition of oxygenates on Rh. *The Journal of Physical Chemistry B (ACS Publications)*, 109, 16819-16835.
- Mhadeshwar, A. B. & Vlachos, D. G. 2005b. Hierarchical, multiscale surface reaction mechanism development: CO and H<sub>2</sub> oxidation, water-gas shift, and preferential oxidation of CO on Rh. *Journal of Catalysis*, 234, 48-63.
- Mhadeshwar, A. B. & Vlachos, D. G. 2005c. A thermodynamically consistent surface reaction mechanism for CO oxidation on Pt. *Combustion and Flame*, 142, 289-298.

- Mhadeshwar, A. B., Winkler, B. H., Eiteneer, B. & Hancu, D. 2009. Microkinetic modeling for hydrocarbon (HC)-based selective catalytic reduction (SCR) of  $\text{NO}_x$  on a silver-based catalyst. *Applied Catalysis B: Environmental*, 89, 229-238.
- Miyadera, T. 1993. Alumina-supported silver catalysts for the selective reduction of nitric oxide with propene and oxygen-containing organic compounds. *Applied Catalysis B: Environmental*, 2, 199-205.
- Miyadera, T. 1997. Selective reduction of nitric oxide with ethanol over an alumina-supported silver catalyst. *Applied Catalysis B: Environmental*, 13, 157-165.
- Mladenov, N., Koop, J., Tischer, S. & Deutschmann, O. 2010. Modeling of transport and chemistry in channel flows of automotive catalytic converters. *Chemical Engineering Science*, 65, 812-826.
- Park, Y. K., Aghalayam, P. & Vlachos, D. G. 1999. A generalized approach for predicting coverage-dependent reaction parameters of complex surface reactions: Application to  $\text{H}_2$  oxidation over platinum. *The Journal of Physical Chemistry A (ACS Publications)*, 103, 8101-8107.
- Patankar, S. V. 1980. *Numerical Heat Transfer and Fluid Flow*, New York, Taylor & Francis.
- Quiceno, R., Pérez-Ramírez, J., Warnatz, J. & Deutschmann, O. 2006. Modeling the high-temperature catalytic partial oxidation of methane over platinum gauze: Detailed gas-phase and surface chemistries coupled with 3D flow field simulations. *Applied Catalysis A: General*, 303, 166-176.
- Raja, L. L., Kee, R. J., Deutschmann, O., Warnatz, J. & Schmidt, L. 2000. A critical evaluation of Navier-Stokes, boundary-layer, and plug-flow models of the flow and chemistry in a catalytic-combustion monolith. *Catalysis Today*, 59, 47-60.
- Reid, R. C., Prausnitz, J. M. & Sherwood, T. K. 1977. *The Properties of Gases and Liquids*, McGraw-Hill.
- Rounce, P. L. 2011. *Engine Performance and Particulate Matter Speciation for Compression Ignition Engines Powered by a Range of Fossil and Biofuels*. Ph.D. thesis, University of Birmingham.
- Salomons, S., Hayes, R. E., Poirier, M. & Sapoundjiev, H. 2004. Modelling a reverse flow reactor for the catalytic combustion of fugitive methane emissions. *Computers & Chemical Engineering*, 28, 1599-1610.
- Santos, H. & Costa, M. 2009. Modelling transport phenomena and chemical reactions in automotive three-way catalytic converters. *Chemical Engineering Journal*, 148, 173-183.
- Satokawa, S., Shibata, J., Shimizu, K.-i., Satsuma, A. & Hattori, T. 2003. Promotion effect of  $\text{H}_2$  on the low temperature activity of the selective reduction of NO by light hydrocarbons over  $\text{Ag}/\text{Al}_2\text{O}_3$ . *Applied Catalysis B: Environmental*, 42, 179-186.
- Satokawa, S., Yamaseki, K.-i. & Uchida, H. 2001. Influence of low concentration of  $\text{SO}_2$  for selective reduction of NO by  $\text{C}_3\text{H}_8$  in lean-exhaust conditions on the activity of  $\text{Ag}/\text{Al}_2\text{O}_3$  catalyst. *Applied Catalysis B: Environmental*, 34, 299-306.

- Sawatmongkhon, B., Tsolakis, A., Sitshebo, S., Rodríguez-Fernández, J., Ahmadinejad, M., Collier, J. & Rajaram, R. R. 2010. Understanding the Ag/Al<sub>2</sub>O<sub>3</sub> hydrocarbon-SCR catalyst deactivation through TG/DT analyses of different configurations. *Applied Catalysis B: Environmental*, 97, 373-380.
- Sazama, P., Capek, L., Drobná, H., Sobalík, Z., Dedecek, J., Arve, K. & Wichterlová, B. 2005. Enhancement of decane-SCR-NO<sub>x</sub> over Ag/alumina by hydrogen. Reaction kinetics and in situ FTIR and UV-vis study. *Journal of Catalysis*, 232, 302-317.
- Schädel, B. T., Duisberg, M. & Deutschmann, O. 2009. Steam reforming of methane, ethane, propane, butane, and natural gas over a rhodium-based catalyst. *Catalysis Today*, 142, 42-51.
- Sellers, H. & Shustorovich, E. 2002. Intrinsic activation barriers and coadsorption effects for reactions on metal surfaces: unified formalism within the UBI-QEP approach. *Surface Science*, 504, 167-182.
- Shibata, J., Shimizu, K.-i., Satokawa, S., Satsuma, A. & Hattori, T. 2003. Promotion effect of hydrogen on surface steps in SCR of NO by propane over alumina-based silver catalyst as examined by transient FT-IR. *Physical Chemistry Chemical Physics*, 5, 2154-2160.
- Shimizu, K.-i., Higashimata, T., Tsuzuki, M. & Satsuma, A. 2006a. Effect of hydrogen addition on SO<sub>2</sub> tolerance of silver-alumina for SCR of NO with propane. *Journal of Catalysis*, 239, 117-124.
- Shimizu, K.-i., Kawabata, H., Maeshima, H., Satsuma, A. & Hattori, T. 2000a. Intermediates in the Selective Reduction of NO by Propene over Cu–Al<sub>2</sub>O<sub>3</sub> Catalysts: Transient in–Situ FTIR Study. *The Journal of Physical Chemistry B*, 104, 2885-2893.
- Shimizu, K.-i., Kawabata, H., Satsuma, A. & Hattori, T. 1999. Role of acetate and nitrates in the selective catalytic reduction of NO by propene over alumina catalyst as investigated by FTIR. *The Journal of Physical Chemistry B*, 103, 5240-5245.
- Shimizu, K.-i., Maeshima, H., Satsuma, A. & Hattori, T. 1998. Transition metal-aluminate catalysts for NO reduction by C<sub>3</sub>H<sub>6</sub>. *Applied Catalysis B: Environmental*, 18, 163-170.
- Shimizu, K.-i. & Satsuma, A. 2006. Selective catalytic reduction of NO over supported silver catalysts-practical and mechanistic aspects. *Physical Chemistry Chemical Physics*, 8, 2677-2695.
- Shimizu, K.-i., Satsuma, A. & Hattori, T. 2000b. Catalytic performance of Ag-Al<sub>2</sub>O<sub>3</sub> catalyst for the selective catalytic reduction of NO by higher hydrocarbons. *Applied Catalysis B: Environmental*, 25, 239-247.
- Shimizu, K.-i., Shibata, J. & Satsuma, A. 2006b. Kinetic and in situ infrared studies on SCR of NO with propane by silver-alumina catalyst: Role of H<sub>2</sub> on O<sub>2</sub> activation and retardation of nitrate poisoning. *Journal of Catalysis*, 239, 402-409.

- Shimizu, K.-i., Shibata, J., Satsuma, A. & Hattori, T. 2001a. Mechanistic causes of the hydrocarbon effect on the activity of Ag-Al<sub>2</sub>O<sub>3</sub> catalyst for the selective reduction of NO. *Physical Chemistry Chemical Physics*, 3, 880-884.
- Shimizu, K.-i., Shibata, J., Yoshida, H., Satsuma, A. & Hattori, T. 2001b. Silver-alumina catalysts for selective reduction of NO by higher hydrocarbons: structure of active sites and reaction mechanism. *Applied Catalysis B: Environmental*, 30, 151-162.
- Shimizu, K.-i., Tsuzuki, M., Kato, K., Yokota, S., Okumura, K. & Satsuma, A. 2007a. Reductive activation of O<sub>2</sub> with H<sub>2</sub>-reduced silver clusters as a key step in the H<sub>2</sub>-promoted selective catalytic reduction of NO with C<sub>3</sub>H<sub>8</sub> over Ag/Al<sub>2</sub>O<sub>3</sub>. *The Journal of Physical Chemistry C*, 111, 950-959.
- Shimizu, K.-i., Tsuzuki, M. & Satsuma, A. 2007b. Effects of hydrogen and oxygenated hydrocarbons on the activity and SO<sub>2</sub>-tolerance of Ag/Al<sub>2</sub>O<sub>3</sub> for selective reduction of NO. *Applied Catalysis B: Environmental*, 71, 80-84.
- Shustorovich, E. & Sellers, H. 1998. The UBI-QEP method: A practical theoretical approach to understanding chemistry on transition metal surfaces. *Surface Science Reports*, 31, 1-119.
- Shustorovich, E. & Zeigarnik, A. V. 2003. The UBI-QEP treatment of polyatomic molecules without bond-energy partitioning. *Surface Science*, 527, 137-148.
- Storsæter, S., Chen, D. & Holmen, A. 2006. Microkinetic modelling of the formation of C<sub>1</sub> and C<sub>2</sub> products in the Fischer-Tropsch synthesis over cobalt catalysts. *Surface Science*, 600, 2051-2063.
- Tamm, S., Ingelsten, H. H. & Palmqvist, A. E. C. 2008. On the different roles of isocyanate and cyanide species in propene-SCR over silver/alumina. *Journal of Catalysis*, 255, 304-312.
- Theinnoi, K. 2008. *The Impact of Diesel Fuel Properties and Diesel Engine Operating Conditions on Silver/Alumina Catalyst HC-SCR Activity for Reduced NO<sub>x</sub> Emissions*. Ph.D. thesis, University of Birmingham.
- Tronconi, E., Nova, I., Ciardelli, C., Chatterjee, D., Bandl-Konrad, B. & Burkhardt, T. 2005. Modelling of an SCR catalytic converter for diesel exhaust after treatment: Dynamic effects at low temperature. *Catalysis Today*, 105, 529-536.
- Tsolakis, A. 2004. *Exhaust gas fuel reforming for compression ignition engines fuelled by diesel and biodiesel*. Doctor of Philosophy, University of Birmingham.
- Tufano, V. & Turco, M. 1993. Kinetic modelling of nitric oxide reduction over a high-surface area V<sub>2</sub>O<sub>5</sub>-TiO<sub>2</sub> catalyst. *Applied Catalysis B: Environmental*, 2, 9-26.
- Voltz, S. E., Morgan, C. R., Liederman, D. & Jacob, S. M. 1973. Kinetic study of carbon monoxide and propylene oxidation on platinum catalysts. *Industrial Engineering Chemistry Production Research and Development*, 12, 294-301.
- Wanker, R., Raupenstrauch, H. & Staudinger, G. 2000. A fully distributed model for the simulation of a catalytic combustor. *Chemical Engineering Science*, 55, 4709-4718.

- Westerberg, B., Künkel, C. & Odenbrand, C. U. I. 2003. Transient modelling of a HC-SCR catalyst for diesel exhaust aftertreatment. *Chemical Engineering Journal*, 92, 27-39.
- Wichterlová, B., Sazama, P., Breen, J. P., Burch, R., Hill, C. J., Capek, L. & Sobalík, Z. 2005. An in situ UV-vis and FTIR spectroscopy study of the effect of H<sub>2</sub> and CO during the selective catalytic reduction of nitrogen oxides over a silver alumina catalyst. *Journal of Catalysis*, 235, 195-200.
- Wurzenberger, J. C. & Wanker, R. 2005. Multi-scale SCR modeling, 1D kinetic analysis and 3D system simulation. *SAE*, Paper No. 2005-01-0948.
- Yamada, H., Misawa, K., Suzuki, D., Tanaka, K., Matsumoto, J., Fujii, M. & Tanaka, K. 2011. Detailed analysis of diesel vehicle exhaust emissions: Nitrogen oxides, hydrocarbons and particulate size distributions. *Proceedings of the Combustion Institute*, 33, 2895-2902.
- Yeom, Y., Li, M., Savara, A., Sachtler, W. & Weitz, E. 2008. An overview of the mechanisms of NO<sub>x</sub> reduction with oxygenates over zeolite and  $\gamma$ -Al<sub>2</sub>O<sub>3</sub> catalysts. *Catalysis Today*, 136, 55-63.
- Yeom, Y. H., Li, M., Sachtler, W. M. H. & Weitz, E. 2006. A study of the mechanism for NO<sub>x</sub> reduction with ethanol on  $\gamma$ -alumina supported silver. *Journal of Catalysis*, 238, 100-110.
- Yeom, Y. H., Li, M., Sachtler, W. M. H. & Weitz, E. 2007. Low-temperature NO<sub>x</sub> reduction with ethanol over Ag/Y: A comparison with Ag/ $\gamma$ -Al<sub>2</sub>O<sub>3</sub> and BaNa/Y. *Journal of Catalysis*, 246, 413-427.
- Yeom, Y. H., Wen, B., Sachtler, W. M. H. & Weitz, E. 2004. NO<sub>x</sub> reduction from diesel emissions over a nontransition metal zeolite catalyst: A mechanistic study using FTIR spectroscopy. *The Journal of Physical Chemistry B*, 108, 5386-5404.
- Yi, X. D., Zhang, X. B., Weng, W. Z. & Wan, H. L. 2007. Studies on the reaction pathways for the selective oxidation of propane to acrolein over MoPO/SiO<sub>2</sub> catalyst by IR spectroscopy. *Journal of Molecular Catalysis A: Chemical*, 277, 202-209.
- Yu, Y., He, H. & Feng, Q. 2003. Novel enolic surface species formed during partial oxidation of CH<sub>3</sub>CHO, C<sub>2</sub>H<sub>5</sub>OH, and C<sub>3</sub>H<sub>6</sub> on Ag/Al<sub>2</sub>O<sub>3</sub>: An in situ DRIFTS study. *The Journal of Physical Chemistry B*, 107, 13090-13092.
- Yu, Y., He, H., Feng, Q., Gao, H. & Yang, X. 2004. Mechanism of the selective catalytic reduction of NO<sub>x</sub> by C<sub>2</sub>H<sub>5</sub>OH over Ag/Al<sub>2</sub>O<sub>3</sub>. *Applied Catalysis B: Environmental*, 49, 159-171.
- Yu, Y., Zhang, X. & He, H. 2007. Evidence for the formation, isomerization and decomposition of organo-nitrite and -nitro species during the NO<sub>x</sub> reduction by C<sub>3</sub>H<sub>6</sub> on Ag/Al<sub>2</sub>O<sub>3</sub>. *Applied Catalysis B: Environmental*, 75, 298-302.
- Zhang, X., Yu, Y. & He, H. 2007. Effect of hydrogen on reaction intermediates in the selective catalytic reduction of NO<sub>x</sub> by C<sub>3</sub>H<sub>6</sub>. *Applied Catalysis B: Environmental*, 76, 241-247.